CANADIAN THESES ON MICROFICHE

I.S.B.N.

THESES CANADIENNES SUR MICROFICHE

National Library of Canada
Collections Development Branch

Canadian Theses on
Microfiche Service

Ottawa, Canada
K1A 0N4

Bibliothèque nationale du Canada
Direction du développement des collections

Service des thèses canadiennes
sur microfiche

NOTICE

The quality of this microfiche is heavily dependent upon the quality of the original thesis submitted for microfilming. Every effort has been made to ensure the highest quality of reproduction possible.

If pages are missing, contact the university which granted the degree.

Some pages may have indistinct print especially if the original pages were typed with a poor typewriter ribbon or if the university sent us a poor photocopy.

Previously copyrighted materials (journal articles, published tests, etc.) are not filmed.

Reproduction in full or in part of this film is governed by the Canadian Copyright Act, R.S.C. 1970, c. C-30. Please read the authorization forms which accompany this thesis.

THIS DISSERTATION
HAS BEEN MICROFILMED
EXACTLY AS RECEIVED

AVIS

La qualité de cette microfiche dépend grandement de la qualité de la thèse soumise au microfilmage. Nous avons tout fait pour assurer une qualité supérieure de reproduction.

S'il manque des pages, veuillez communiquer avec l'université qui a conféré le grade.

La qualité d'impression de certaines pages peut laisser à désirer, surtout si les pages originales ont été dactylographiées à l'aide d'un ruban usé ou si l'université nous à fait parvenir une photocopie de mauvaise qualité.

Les documents qui font déjà l'objet d'un droit d'auteur (articles de revue, examens publiés, etc.) ne sont pas microfilmés.

La reproduction, même partielle, de ce microfilm est soumise à la Loi canadienne sur le droit d'auteur, SRC 1970, c. C-30. Veuillez prendre connaissance des formules d'autorisation qui accompagnent cette thèse.

LA THÈSE A ÉTÉ
MICROFILMÉE TELLE QUE
NOUS L'AVONS REÇUE

NL-339 (r. 82/08)

Canada

INTERACTIONS OF 72 GEV ARGON NUCLEI IN EMULSION

Claude Fortier

Thesis submitted to the School of Graduate Studies in partial fulfillment of the requirements for the degree of PhD in Physics

UNIVERSITY OF OTTAWA
OTTAWA CANADA 1984

UNIVERSITÉ D'OTTAWA
UNIVERSITY OF OTTAWA

TABLE OF CONTENTS

L I S T O F F I G U R E S

LIST OF TABLES

ABSTRACT

The interaction of relativistic Argon nuclei with emulsion nuclei has been investigated. General properties of the interactions have been determined, as well as correlations between them. Comparisons with several theoretical models has yielded insight into the collective behavior of nucleons in this type of interaction as well as the geometrical behavior of the nuclei as a whole.

Over 300 interactions were studied in great detail, from which the inelastic mean free path λ of 9.60 $\pm$ 0.52 cm. was obtained. The average numbers of tracks were determined for both the interactions as a whole and the interactions with projectile tracks removed. Values obtained for the former are $\langle N_s \rangle$ = 9.18 $\pm$ 0.44 for the shower particles, $\langle N_g \rangle$ = 7.12 $\pm$ 0.40 for the grey tracks, $\langle N_b \rangle$ = 6.20 $\pm$ 0.26 for the black tracks giving $\langle N_h \rangle$ = 13.31 $\pm$ 0.59 for the heavy tracks, while for the latter the corrected values obtained are $\langle N_s \rangle_c$ = 3.72 $\pm$ 0.26 representing the pions, $\langle N_g \rangle_c$ = 4.90 $\pm$ 0.36 and $\langle N_b \rangle_c$ = 5.38 $\pm$ 0.37 giving $\langle N_h \rangle_c$ = 10.28 $\pm$ 0.56 for target related black, grey and heavy tracks respectively. This separation of tracks allowed comparisons to be made between this nucleus-nucleus experiment and nucleon-nucleus experiments, while at the same time providing information on the Argon projectile breakup.

Secondary events were also studied to a lesser extent, such that comparisons between primary and secondary events could be made.

Angular distributions have been measured for over 1000 shower tracks, and compared to exclusive counter experiments.

From this overall view of the interactions, it has been possible to provide validation to certain aspects of both the thermodynamic models and the collective tube model.

ACKNOWLEDGMENTS

The author would like to express his gratitude to Prof. Jacques Hebert for his help, guidance and generosity throughout the course of this thesis.

Many thanks to Dr. C. J. D. Hebert for her encouragement and critical comment, as well as for her part in the gathering of data.

The author wishes to acknowledge several other persons for useful discussions, including Dr. E. Friedlander, Dr. Lokanathan. The theoretical calculations of Dr. DasGupta and his kind help are also very appreciated.

Special thanks are due to Dr. Harry Heckman for providing the emulsion plates, without which this thesis would not have been possible.

The financial support of I.P.P. and N.S.E.R.C grants is gratefully acknowledged.

INTRODUCTION

A new field of physics was opened with the construction of the Berkeley Bevatron. It has permitted physicists to obtain previously unavailable information on the dynamics of hadrons interacting in a collective system called the nucleus, at energies large enough for meson production. The experimental investigation of relativistic heavy ion interactions is no longer limited to balloon flight exposures of nuclear emulsion to the cosmic flux.

Beams of fully ionized heavy ions are now available for experimentation over almost the entire periodic table in an energy range of a few MeV per nucleon, and ions as heavy as ^{56}Fe are routinely available at an energy of 2 GeV per nucleon. Heavier relativistic nuclei are becoming available from existing facilities, and proposals for new facilities will provide nuclei as heavy as ^{238}U at energies upwards of 10 GeV per nucleon, possibly in a colliding beam configuration. Since the natural spectrum of the cosmic flux essentially vanishes above ^{56}Fe, it will be possible to produce nuclear densities never before possible, over larger and larger volumes.

Assuming that quarks and gluons exist, one must accept that it is practically impossible to isolate them. This has given rise to a new picture for the vacuum state, different

from the familiar perturbative vacuum in QED with its occasional electron-positron pair creation in an otherwise empty space. This perturbation type of picture is replaced in QCD by a state where certain fields are totally excluded, such as the colour field, in order that the colour carriers, quarks and gluons, be totally confined in the interior of hadrons. However, it has been predicted [1] that the physical vacuum may become unstable under the influence of high energy or matter density. In the large body of data available from p-p and p-nucleus collisions, one can see that when a hadron traverses a nucleus at high speed, only a small portion of its energy can be deposited in the nuclear volume. Indeed, the hadron passes through, making several collisions, with the forward products not fragmenting until they have left the nucleus [2], while the less forward products do fragment inside the nucleus, creating pions and the like. But the volume in which they are fragmenting is cold nuclear matter, where the creation of a few pion producing cascades is counterbalanced by pion absorption. Multiplicities are therefore only about 2 or 3 times that of p-p collisions, and it is not possible to heat up a volume sufficiently to perturb the vacuum.

Nucleus-nucleus collisions on the other hand offer the interesting possibility of two large relativistic nuclei stopping each other in a head-on collision, with a growth in

multiplicity which may be linear in A, the atomic number. Since a very large number of pions could be created in such an interaction, and assuming the two nuclei interpenetrate each other without an increase in volume, there will be no room in this volume for the normal volume assigned to each of the pions in the bag model [3]. (Normally, much of the space inside the nucleus is empty, since the hadrons only occupy a fraction of the available volume.) This might cause the space inside the nucleus which is usually a vacuum to become unstable [1], leading to conditions whereby the vacuum becomes perturbative and is filled with quarks and gluons. This large bag of quarks and gluons would come about from a deconfinement, with the normal liquid-like nuclear matter undergoing a phase transition to a state referred to as a quark-gluon plasma. A good guess [4] for the energy at which this might occur is at a temperature of 200 MeV spread out over a volume based on a scale of several fermi, with an energy density of 2 GeV/fm^3, or about 4 times that of the proton. Only relativistic nucleus-nucleus collisions seem to have the possibility of producing such conditions, and such a possibility may lead to exciting new physics.

Alternately, there may be the possibility of forming very heavy nuclei, located on an island of stability far removed from that of normal nuclei [5]. In fact if the right conditions may be achieved, producing a minimum in the

potential curve of nuclei when certain fields become large enough, nuclei with mass numbers upwards of 400 may become metastable, or even stable. This might have far reaching implications in the fields of astro and nuclear physics.

Some authors have also predicted the formation of pion condensates [6], or more specifically states in which the nucleons arrange themselves in layers of opposite spin alignment, under conditions of high density or pressure but of low temperature. This is a 'minimum' type of configuration, and has been thought to be a probable state of nuclear matter in the center of neutron stars. While at the moment it may be difficult to produce the necessary conditions in the lab for the type of stability of pion binding in dense nuclear matter which leads to pion condensation, one should be on the lookout for any signatures, such as anomalies in the transverse momentum spectra of collision fragments.

While these speculations warrant the study of both the high density state and the vacuum state of nuclear matter, some of the desired conditions are just short of those which can be produced with current accelerator facilities. In the meantime, there remains a wealth of data to be collected and analyzed, along with several competing theoretical models to be accepted, rejected, refined or best of all developed.

Early experiments on the interactions of heavy ions with target nuclei were originally concerned with interaction mean free paths and the production of nuclear fragments, as such data are most pertinent to the physics of cosmic rays. More recently, inclusive and exclusive type measurements have been carried out to obtain cross-sections and reaction rates. Often the geometry of the collision motivated the type of experiment, for in nucleus-nucleus collisions, one can classify the interactions into three broad classifications: central, peripheral and hybrid collisions. In central collisions, the two nuclei hit each other head-on, with an impact parameter less than 1 fermi. The agglomerate formed then disintegrates, with most of the projectile fragments thrown forward and the produced particles given large transverse momenta, whereby both the target and projectile are annihilated. Peripheral collisions are 'grazing' type of collisions where the participating nuclei barely overlap, and interact only slightly, and possibly only through Coulombic interaction. These types of collisions tend to leave the participants relatively intact. Hybrid collisions are in between, with the colliding nuclei at partial overlap, such that certain common regions undergo large excitation, while others remain relatively intact. This leads to the participant-spectator type of description for relativistic heavy ion interactions.

Such considerations recall certain important facts about the kinematics of these interactions. The use of such energetic projectile nuclei makes possible the study of fragmentation processes in two distinct regions: since the incident projectile has a very high velocity in the laboratory frame, and its fragments have low momenta relative to it, the projectile fragments and the projectile spectator will be highly collimated in the forward direction; the target related fragments will be slow and isotropically emitted in the laboratory frame. Thus the target and projectile fragments will be quite distinct, with products of the participant regions left to fill the gap.

Such large numbers of interacting nucleons in a single collision allow the use of very elegant statistical models for the description of these encounters. Much fine tuning of these models has occurred with the advent of new data, and the present investigation provides some insight into the applicability of these and other more dynamical models. Also of great interest are the hydrodynamical type of models, some of which provide for the existence of shock waves when the speed of sound in nuclear matter is exceeded during a collision. Certain measurements done in this experiment tend to exclude this phenomenon, but perhaps the proper conditions have not been achieved.

The possibility of engendering new phases of nuclear matter was one of the primary motivations for the present investigation. Although energy and particle densities were not high enough for true phase transitions, it was felt that a thorough investigation of interactions close to the 'threshold' might provide some clues of what could be expected in the future, and that certain correlations of data might provide guidance for future research. It is felt that while requiring meticulous data acquisition, an emulsion experiment with the then highest available mass nucleus as a projectile was able to provide an overall view of the collisions not easily obtainable with other detectors, albeit with low statistical accuracy. The investigation was done with the thought in mind of being able to compare data with other, different type of inclusive and exclusive experiments, and thus give a good starting point for the comparison with theoretical predictions.

1. CHAPTER 1. MEASUREMENTS IN EMULSION

1.1. Emulsion Techniques

1.1.1. Emulsion: The Detector

Nuclear emulsion has two basic constituents. It is composed of silver bromide crystals suspended in gelatine which is called the matrix or medium. It is the medium which localizes the AgBr crystals and prevents their movement. The gelatine is of animal origin and, with glycerin added is hygroscopic, with the actual quantity of water contained being a function of the environmental humidity. The humidity has a major influence on the thickness of an emulsion layer, by causing variable swelling. Thus the use of nuclear emulsion as a particle detector requires carefully controlled climactic conditions. The major elements contained in emulsion are divided into two groups: the light elements ^{1}H, ^{12}C, ^{14}N & ^{16}O and the heavy elements ^{108}Ag & ^{80}Br. There are also trace quantities of other substances which come from impurities in the gelatine or are added as sensitizing agents.

In an abbreviated fashion, one can describe how nuclear emulsion functions as a detector: a charged particle or photon upon passing through the emulsion, will, by Coulombic

interaction, eject electrons from their sites in the face centered silver bromide crystal; many crystals along the path of the traversing radiation are thus affected, and in each of these affected crystals, or grains, holes and electrons are formed when the valence electron of Br^- is removed; these free electrons now diffuse to the surface of the crystal, where silver nuclei are surrounded by fewer bromine nuclei and the electrons are captured by silver ions, which are transformed into silver atoms. These neutral atoms are initially dispersed on the surface, and they later form an aggregate at a crystal imperfection. This process is known as the formation of the latent image. At this point, the emulsion, which may be as thick as 1mm, is completely opaque and has a white or yellowish appearance due to the presence of the silver salt. The recording process completed, the emulsion is now placed in a reducing solution, otherwise known as developer, which transforms the grains with a latent image into metallic silver. Their size is of the order of one wavelength of light. These islands of metallic silver are not yet visible due to the overwhelming presence of undeveloped silver bromide crystals. All of the remaining silver salts are then removed by dissolving them in a fixing solution. When fixation is complete, the emulsion has become transparent, with myriads of silver granules forming the final and permanent image.

1.1.2. Ionization and Track Formation

There are two main mechanisms for the energy loss of radiation passing through matter which are of importance in emulsion work: elastic nuclear scattering (i.e. Rutherford scattering) and loss due to ionization. The ionization, or specifically the collisions with atomic electrons, accounts for the greatest energy loss by far. The Bethe–Bloch formula for the total rate of ionization energy loss per gcm^{-2} traversed is given by

$$\frac{dE}{dx} = -4\pi\eta r_e^2 m_e c^2 \frac{Z^2}{\beta^2} \ln\left(\frac{2m_e c^2 \beta^2}{I(1-\beta^2)} - \beta^2\right) \qquad (1.1)$$

where

η = # of electrons/cm^3

r_e = classical electron radius

Z = charge of the radiation

I = ionization potential of the medium

For composite media such as emulsion, two factors must be modified: η and I. Here η may be alternately written as

$$\eta = \sum_i N_A \frac{Z_i}{A_i} \eta_i \qquad (1.2)$$

where N_A = Avogadro's number

η_i = density of element i in the medium

Z_i & A_i refer to the ith element

and I must be replaced by I_i , as each summation term is added.

It can be seen that the rate of energy loss may be simply written as

$$\frac{dE}{dx} = - \frac{Z^2}{\beta^2} f(\beta) = -Z^2 g(\beta) \qquad (1.3)$$

which is independent of the mass of the incident radiation. When plotted as a function of energy, the function has the form shown in fig 1.1.

In an emulsion of normal composition, the minimum ionization rate for a singly charged particle is approximately 5.5 MeV/cm. The minimum ionizing particle has a β of .95.

As a particle passes through the emulsion, it loses energy to some of the silver bromide crystals.

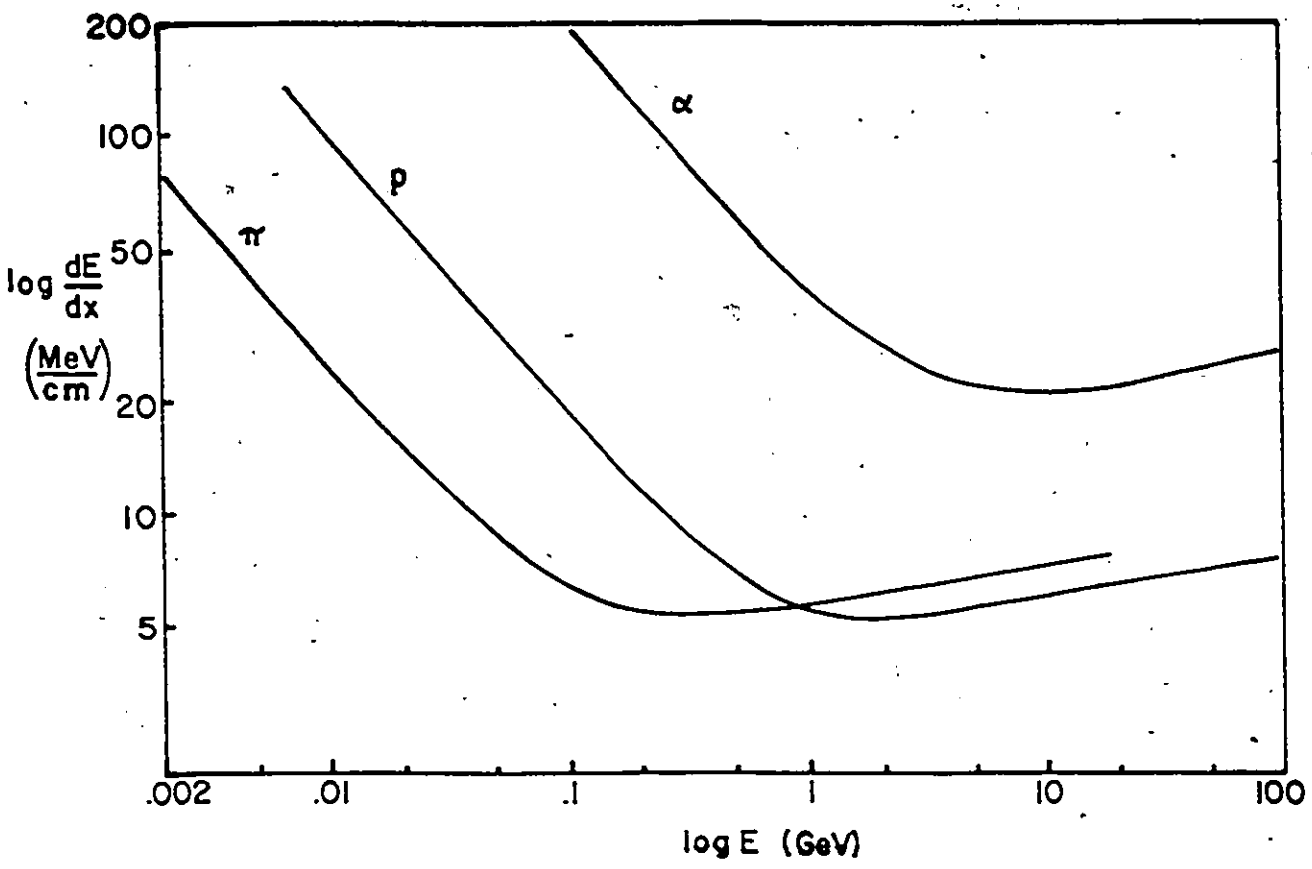

FIG. 1-1: Logarithmic Variation of dE/dx vs log E. The curve has the same shape for all particles. The minimum of ionization occurs when the kinetic energy is roughly twice the rest mass, and the levelling off when the kinetic energy is roughly eight times the rest mass. As the charge increases, i.e. for an α particle, the ionization goes up as the square of the charge.

This eventually results in a series of grains, the number

being a function of the ionization. As the particle slows down, it becomes more ionizing, and this increases the linear grain density of the track. Due to the finite size of the grains, the track will appear solid once the particle has slowed down sufficiently. A particle of high enough charge will also cause this effect, even if it is relativistic. Thus the measure of ionization in emulsion, that is the number of grains per unit distance, gives an indication of the charge and velocity of the particle, and hence the energy if the mass is known or vice versa.

1.1.3. Classification of Tracks

The classification is made in terms of the 'blackness' of the track. The grain density g depends not only on the ionization, but also on the emulsion sensitivity and the degree of development. These factors therefore determine a value g_0 which is the minimum linear grain density due to the passage of a singly charged minimum ionizing particle. All other grain densities are measured relative to this minimum value. This minimum may vary in any one emulsion, and one must account for this by measuring g_0 in the vicinity of the tracks of interest. This variation is caused by non uniform development.

Three categories are usually defined in emulsion

measurements according to grain density. These are N_s, N_g and N_b. A fourth category is often used and this is N_h which is the sum of N_b and N_g.

N_s symbolizes the # of shower (or minimum) tracks

N_g symbolizes the # of grey tracks

N_b symbolizes the # of black tracks

N_h symbolizes the # of heavy (or dark) tracks

The categories are usually taken to mean the following:

In N_s will be included any track whose g value lies between 1.0 to 1.4 - 2.0 g_0. Similarly, N_g is the number of tracks with g between 1.4 - 2.0 g_0 to 4.0 - 8.0 g_0. N_b represents all remaining tracks.

The subscripts shower, grey and black refer to the appearance of the tracks under a microscope. The specific limits on each category are determined by the particular requirements of specific experiments, as far as energy cutoffs etc. are concerned.

Track classifications used in the present investigation are listed in the following table, along with equivalent energy cutoffs for various particles.

TABLE 1-1: Track Classifications, Energies and Velocities

TYPE	IONIZATION CUTOFFS
N_s	$1.8\ g_0 > g$
N_g	$1.8\ g_0 < g < 8\ g_0$
N_b	$g > 8\ g_0$

TYPE /PART.	PION		PROTON		ALPHA	
	E_k (MeV)	Vel.	E_k (MeV)	Vel.	E_k (MeV)	Vel.
N_s	E>40	β>.62	E>250	β>.62	-	-
N_g	40>E>5	.62>β>.25	250>E>30	.62>β>.25	E>860	β>.6
N_b	E<5	β<.25	E<30	β<.25	E<860	β<.6

The cut-off for N_s at $1.8\ g_0$ is a fairly standard one in emulsion experiments, but the choice of $8\ g_0$ as the dividing line between N_g and N_b was selected because of the particular character of relativistic heavy ion interactions. When a charged particle traverses the emulsion, it causes a track to appear by ionizing the media, and in addition to this, a charged particle sometimes enters into a collision with a nucleus in the emulsion with a sufficiently small distance between the nuclear centers (impact parameter b) to

cause either one or both the target (stationary) and the projectile to be transformed. This gives rise to what is called a star in the emulsion, as the collision appears as a number of tracks emerging from a common center. If the projectile is itself a Z>2 nucleus, the track it produces will be a non minimum track due to the Z^2 variation of ionization, regardless of beta. When this nucleus breaks up into particles with Z=1,2,3 or more after a collision, these particles of lower charge will each produce a track. If the beta of the incident nucleus was highly relativistic (>.9), its original constituent parts will not be slowed down to any great extent by the interaction due to relativistic kinematics. It is also possible for only part of the incident nucleus to be involved in the collision, when the impact parameter is large. This means that fragments may emerge as: protons which are N_s tracks; alpha particles which will be N_g tracks ($g_{min} = Z^2 g_0$); particles with Z = 3 or more having $g_{min} > 9\ g_0$. For this reason the categorization chosen will include all relativistic singly charged particles in N_s, all doubly charged relativistic particles and slower singly charged particles in N_g, and all relativistic particles with Z > 2 and slow singly and doubly charged particles in N_b.

1.2. Other Measurements Related to Ionization

The measurement of grain density is a technical resourse of the greatest importance for values of beta between .4 and .9, for singly charged particles. However, when beta lies below these values, or when one is dealing with highly ionizing particles of multiple charge, grain counting runs into difficulties. This happens because the grain density becomes too large to resolve individual grains. The maximum discernable grain count is a function of two factors: the specific ionization governing the number of grains and the particular emulsion characteristics which determine the grain size as well as the grain density. Of course whether or not two grains are determined to be contiguous or not depends on the optical conditions of observation, such as magnifying power, resolution, diffraction around neighbouring impurities, etc. Another very important factor is the angle between the track and the plane of the emulsion, known as the dip angle. A large dip angle has a very marked effect on the grain counting since there will be overshadowing of one grain by its neighbour.

As a typical example, Ilford G-5 emulsion has an undeveloped grain size of approximately 0.3 um and a developed grain size of about 0.7 um. A grain is therefore about the size of one wavelength of visible light. A minimum

ionizing particle causes 18 grains per 100 um to develop, and the maximum number is about 150 grains per 100 um: a range of 8 to 1, which is a fairly limited 'dynamic' range. When the ionization is high, individual grains form into groups or blobs. These blobs then form a dark track interspaced with gaps of varying length. One may thus count the blob or gap density of a given track. The gaps vary in length, and the length distribution is exponential and is given by

$$N(>L) = N_T e^{-L/\langle L \rangle} \qquad (1.4)$$

where $N(>L)$ is the number of gaps of length greater than L

N_T is the total number of gaps

$\langle L \rangle$ is the mean length

Thus, for a specific charge, the measurement of the ratio of the mean gap length of a minimun ionizing particle to the mean gap length of a specific track, that is,

$$\frac{\langle L_{min} \rangle}{\langle L \rangle}$$

provides a satisfactory measurement of the ionization. This relationship is illustrated in Fig. 1.2.

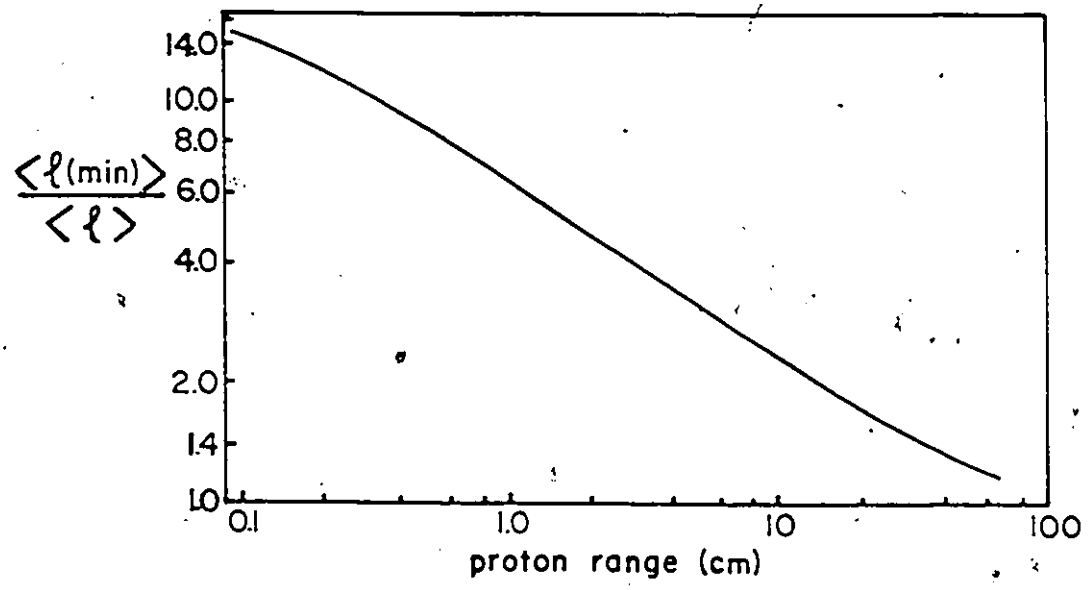

FIG. 1-2: Ratio of Gap Lengths vs Proton Range in Emulsion.

Although no actual gap counting was done in the present experiment, it was always used in a non qualitative fashion when observing tracks of slow protons and alpha particles.

Before discussing the final measurement directly related to ionization, it should be pointed out that as in gap counting, the determination of grain density does not always require an actual measurement in the emulsion for a trained observer. Using standardized observation conditions, it is possible for the scanner to learn to distinguish between shower, grey and black tracks. The process is to first begin by making many actual measurements of grain density, and classify the tracks accordingly. Then the

scanner attempts to classify tracks by eye, and verifies that this classification agrees with the classification obtained by direct measurement. This is continued iteratively until it is no longer necessary to perform grain counts to properly separate the various types of tracks, unless a very high accuracy is required. The simple observation method is very reliable for conscientious scanners, and typically shows better than 95% consistency for a single scanner, and better than 90% consistency for two separate observers. This is periodically verified by recalibration of the 'observers', along with double or triple measurement of specific single events. Large stars are always measured more than once to insure a sufficient degree of accuracy. The great advantage of classification by eye is that the time required per event is reduced by at least a factor of ten. However, this assumes that the consistency of development has been checked within a single emulsion plate as well as from plate to plate in any given batch, since development and emulsion characteristics may vary.

1.3. δ-rays

δ-rays are formed when a Coulombic interaction ejects a single electron from an atom in emulsion with sufficient energy for it to form a track. These may be very short, 2 or

3 grains, or may be up to 100 um in length.

Rutherford's classical formula for the scattering of electrons by nuclei may be transposed, and one obtains the number of delta rays with kinetic energy between E and E + dE produced per unit range along the track of an ionizing particle.

$$N_\delta(E)dE = \frac{2\pi n e^4 Z^2 \, dE}{m_e c^2 \beta^2 E^2} \qquad (1.5)$$

where n is the number of free electrons per unit volume

Z is the charge of the incident particle

Upon integration, one obtains the number of delta rays per unit range.

$$N_\delta = k \frac{Z_i^2}{\beta_i^2} \left(\frac{1}{E_{min}} - \frac{1}{E_{max}} \right) \qquad (1.6)$$

where k is a constant

i is the index referring to the incident particle

E_{max} is given by the maximum amount of energy transferable to an electron by the incident particle.

$$E_{max} = m_e c^2 \frac{2\beta^2}{(1-\beta^2)} \qquad (1.7)$$

For an incident particle with a beta of 0.7, this corresponds to an energy of the electron approximately equal to 1 MeV, and represents a highly relativistic electron (β = 0.95), which will have a minimum grain density track. Because of the difficulty of separating this type of track from the background grains inherent in emulsion, a cut-off is introduced at E_{min} equal to 75 keV, corresponding to a β of 0.5 for the knocked out electron. The value of E_{min} is determined by the requirement for the delta ray to have enough energy to escape the grain from which it was produced, and then to form an observable track, i.e. having three or more grains. Such an electron needs a minimum energy of 15 keV with a corresponding β of 0.25.

It follows from equation 1.6 that the form of the delta ray energy spectrum is the same for all incident particles with $\beta > 0.7$. Variation of E_{max} of the delta ray as a function of the β_i of the incident particle will only lead to a few delta rays of high energy as β_i increases above 0.7. A relativistic particle of unit charge will have a value of $N_d = N_\delta(min)$ which is a mechanism similar to that which yields a certain minimum number of grains for a fast particle. The value of $N_\delta(min)$ in G5 emulsion is very low, rendering the

measurement impractical for most situations. It is however practical to measure the charge of relativistic particles with $Z > 2$, since $N_\delta = Z^2 N_\delta(\min)$, where $N_\delta(\min)$ need not be determined from a singly charged particle. Rather, one uses a relativistic heavy ion of known charge, which for the present investigation is an argon nucleus with $Z = 18$. Using the same convention of measurement for all tracks, one needs only to find the ratio of N_δ of a given track to that of a calibration track (argon) to determine the charge of the said track. This method is insensitive to background grains when the charge is high, as the number of delta rays for a relativistic $Z = 14$ nucleus is roughly 25 per 100 um, well above the background level of 0.1 to 0.5 per 100 um. Another important aspect brought about by the increase in the delta ray density for heavy nuclei is the thickening of the core of the track. Delta rays give a track a rough, grainy like appearance. When enough low energy delta rays are present, which are not countable individually, the core of the track is thickened. Being sensitive to variations in Z^2, the thickness as well as the density of the track make a very good indicator for detecting any change in the charge of a heavy ion due to a nuclear interaction. As an example, it is possible to easily detect changes of one charge for a heavy ion of $Z = 10$, if there is a single proton (or $Z=1$) lost in a peripheral collision. This allows emulsion exposures to heavy

ion beams to be scanned by the 'along the track' method, a method which is far more expedient than scanning given volumes of emulsion.

1.4. Range Considerations Particular to Emulsion

As a direct result of the energy loss of charged particles traversing emulsion, particles will be stopped whithin a certain range. Recalling the basic range equation for a particle of initial kinetic energy E_k.

$$R = \int_0^{E_k} \frac{dE}{(dE/dx)} \qquad (1.8)$$

This has the form shown in Fig. 1.3.

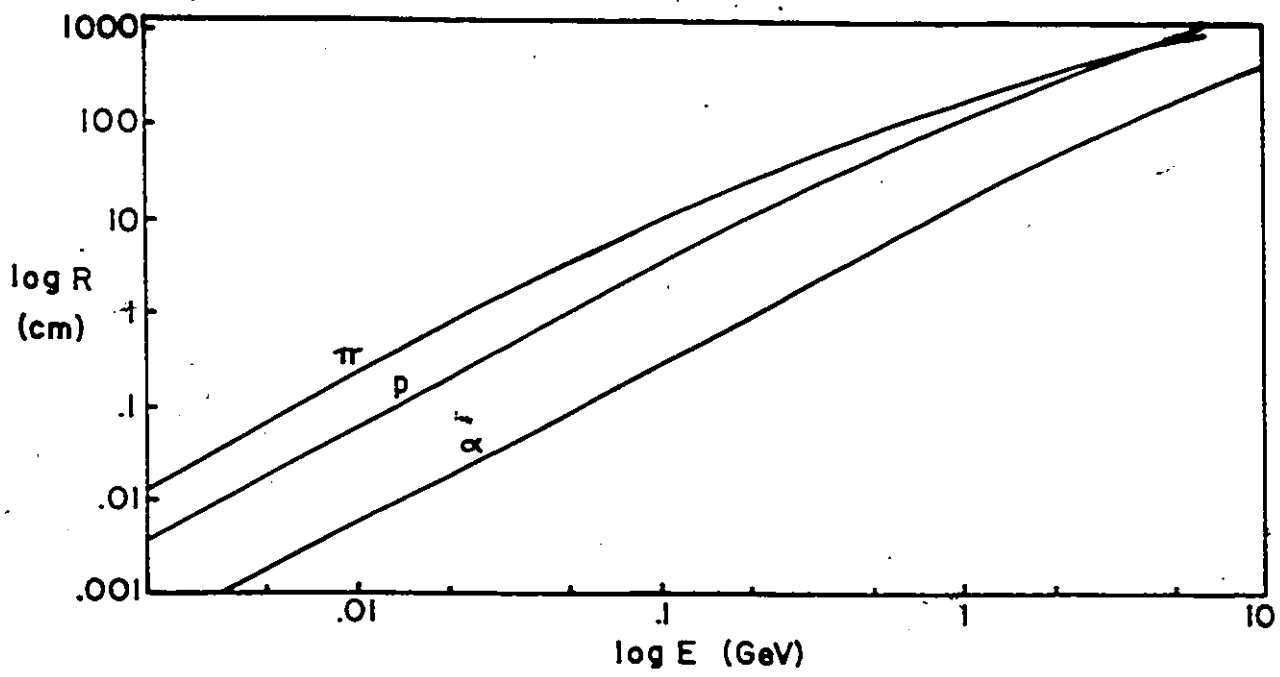

FIG. 1-3: Range vs Energy in Emulsion.

The range energy relation may also be represented by an empirical formula, valid for the straight line portion of Fig. 1.3 (i.e. $R < 10^5$ um), for singly charged particles, given by $E = kR^n$, where E is the kinetic energy, and k and n are constants obtained from measurement. The relationship for other particles may be derived as follows.

Empirical formula	Theoretical formula
$E = kR^n$	$\frac{dE}{dR} = z^2 a(\beta)$

From the kinematics

$$E = (\gamma - 1)m = m f(\beta)$$

Therefore,

$$\frac{dE}{dR} = \frac{d}{dR}\, m\, f(\beta) = m\, f'(\beta)\, \frac{d\beta}{dR} = Z^2\, g(\beta) \qquad (1.9)$$

Gathering terms in β and integrating

$$\frac{f'(\beta)}{g(\beta)}\, d\beta = \frac{Z^2}{m}\, dR = F(\beta) = \frac{Z^2}{m}\, R$$

Or, for a given β, $\frac{Z^2}{m} R$ is a constant.

i.e. $$\frac{Z_1^2 R_1}{m_1} = \frac{Z_2^2 R_2}{m_2}$$

$$R_1 = \left(\frac{Z_2}{Z_1}\right)^2 \frac{m_1}{m_2} R^2 \longrightarrow R_1^n = \left(\frac{Z_2}{Z_1}\right)^{2n} \left(\frac{m_1}{m_2}\right)^n R_2^n$$

Since $E = kR_1^n$

then $$E = k \left(\frac{Z_2}{Z_1}\right)^{2n} \left(\frac{m_1}{m_2}\right)^n R_2^n \qquad (1.10)$$

where Z_1 = proton charge and M_1 = proton mass

We now have the general relationship for any particle.

$$E = kZ^{2n} m^{1-n} R^{n}$$ with Z in proton charges and m in proton masses

For standard emulsion (see section 2.1), $k = 0.251$ and $n = 0.581$ such that

$$E(MeV) = .251\ Z^{1.16}\ m^{0.42}\ R^{.58}\ (um) \qquad (1.11)$$

When a particle stops in emulsion, its range may be measured giving information about the energy of the particle, if both its mass and charge are known. A 20 MeV proton has a range of 2 mm in emulsion. Unless tracks have dip angles near zero, one is limited to range measurements of the order of 1 cm. When many emulsion pellicles are exposed as a stack, it is possible to follow tracks from plate to plate if the dip angle is not near zero.

1.5. Scattering

One of the very serious limitations of ionization measurements is the need to know one or two of the following three quantities: mass, velocity or charge. As no measurement related strictly to ionization determines any one of these

quantities independantly, it is necessary to have recourse to other methods.

Due to the small dimension of an emulsion detector, magnetic fields are very impractical as a means of obtaining momentum information, since extremely large magnetic fields are required to cause sufficient bending for it to be visible in a microscopic observation. There is however a force strong enough to cause adequate deviation of a track in emulsion and this is simply the electronic repulsion between charges. This in effect continuously changes the direction of a particle as it passes through the emulsion, in an amount determined by the mass, velocity and charge of the particle. Scattering decreases with increasing velocity and increases with increasing charge and decreasing mass.

Pions, which make up the greatest proportion of created particles in nuclear interactions, can thus be easily distinguished from protons if their beta is low, by the crookedness of their tracks. Electrons are so light that their tracks may be crooked even if they are minimum ionizing.

The average angular deviation $\langle\phi\rangle$ of a particle of charge Z gives a measure of the quantity $p\beta$, with a relation of the form

$$\langle\phi\rangle = KZ \frac{C^{1/2}}{p\beta}$$

where C is the cell length over which $\langle\phi\rangle$ is measured and is typically between 25 and 10,000 um.

k is a constant and a function of C

Therefore for two particles with the same grain density and hence velocity, the ratio of the scattering angles gives the ratio of the masses of two particles if their charges are identical. Scattering measurements are laborious and require extremely accurate microscope stages due to mechanical noise etc. When the β of particles approaches 1, the scattering angle becomes too small for it to be measured reliably on a normal microscope, and thus it is impractical to separate between a relativistic pion and proton in normal emulsion experiments.

1.6. Beam Exposure

We are indebted to Dr. Heckman from Lawrence Berkeley Laboratory for the loan of 3 plates from a stack of Ilford G5 emulsion exposed to the Bevatron-Bevelac beam of ^{40}Ar ions at a rigidity of 5.7 GeV corresponding to a kinetic energy of 1.8 GeV/A. This emulsion is electron sensitive and yields a

grain density of 18 grains per 100 um. Consequently, all fragmentation products, irrespective of charge and velocity are detectable. All pellicles of these stacks were processed at the accelerator facility, and had very uniform development. The direction of the beam was along the length of the pellicle (referred to as horizontal exposure). Dimensions of the pellicles are as follows: 12 cm long X 7.3 cm wide X 600 um thick (before processing).

1.7. Scanning and Measurement

All scanning was done by the along the track method in order to avoid the biases inherent in volume scanning, especially when the large stars from heavy ions are encountered. In the method selected, all scanning commenced at the edge of the plate where the beam entered. Tracks from the argon beam are selected at random, and then followed one at a time up to a predetermined path length or until an interaction occurs. These tracks will be subsequently referred to as primary tracks, and any interactions caused by the incident beam will be referred to as primary events or stars. Interactions caused by fragmentation products of primary events will be labelled as secondary stars and so on.

A Leitz microscope was used and the tracks were observed with a 25X air objective and a pair of 10X oculars.

Under these observation conditions, 'white' stars (interactions with no produced grey or black tracks) could easily be detected.

1.8. Track Counting

Once events had been located, they were each observed under a 53X or 100X oil immersion objective and 10X oculars. The total number of tracks was counted, starting with the black tracks, by observing at a short distance from the event center in order to ensure that only one track was being counted at a time. For the grey and shower tracks, it was often found necessary to do the counting at points quite removed from the center, due to the kinematics of the break-up of the incident ion, or projectile. Protons and alpha particles fragment off the projectile with low transverse momenta, often accompanied by heavier fragments from the argon nucleus, and all of these form a cluster of tracks emanating from the interaction region. Because of this, projectile related tracks were often counted at distances of up to 1000 μm away from the stars, corresponding to about ten fields of view. Since very high multiplicity events were encountered (in fact a certain group of 25 events had an average multiplicity of 55), the counting often had to be

repeated several times and was checked by different observers. Counting was repeated until consistent results were obtained.

1.9. Separation of Tracks

As the interactions involve two complex nuclei, the target and projectile, there is a dual process occuring when a star is produced. The struck nucleus is broken up partially in the collision, and subsequently breaks up more or less completely in a process referred to as nuclear evaporation. Nuclear evaporation is an isotropic process, and produces mostly black tracks, i.e. slow protons and alphas, and some grey tracks which are medium energy protons. Here the terms proton and alpha are used somewhat loosely to designate $Z = 1$ and $Z = 2$ particles (for deuterons, tritons etc.). Since the target is at rest in the laboratory frame, the evaporation tracks are observed as having no preferred direction about the center of the star. This release of energy by emission (evaporation) of particles occurs in less than 10^{-18} sec.[7] A similar process occurs within the projectile nucleus. At the moment of impact, protons and alpha particles are sheared off, leaving a nucleus of lesser charge travelling in the beam direction (often referred to as abrasion). Abrasion occurs in the time for the two interacting nuclei to traverse

each other, which is of the order of 10^{-22} sec. In certain collisions, the projectile breaks up into more than one heavy fragment with Z > 2. All these constituent parts have most of their momentum in a direction parallel to the beam, and are thus confined to a forward pointing cone subtending an angle less than 15 deg. for protons and less than 5 deg. for alphas, when observed in the laboratory. These tracks will all be at their respective minimum of ionization, with protons as shower tracks, alphas as grey tracks and Z > 2 secondaries as black tracks.

The predominant particle produced in relativistic nucleon-nucleon or nucleus-nucleus collisions is the pion, with approximately equal numbers of positive, negative and neutral pions. Neutral pions are of course unobservable. Created pions may or may not be minimum ionizing, and will travel in directions which depend upon the type of interaction. The problem which arises is the near impossibility of separating the created pions from the projectile related Z = 1 secondaries. Since the particles may only be separated by scattering measurements, and only those with low transverse momenta, there remains a definite ambiguity as to the identity of the shower tracks. It was thus decided to use a separation technique to remove a part of this ambiguity.

In this experiment, the total multiplicity of each event was determined; then the charge of any heavy fragment was obtained from delta ray measurements, and this charge was subsequently subtracted from the original 18 charges of the projectile. Grey tracks with very low scattering found along the beam direction were subtracted from the remaining charge as Z = 2 particles; at larger angles, grey tracks were followed to identify those which originated from the argon nucleus from their low scattering, and the charge of the appropriate (Z = 2) grey tracks was also removed from the original 18. Along the beam shower tracks were then subtracted as Z = 1 particles. Here along the beam is defined as a 0.5 deg. cone. Any remaining charge was assumed to be due to wide angle protons, and a number equal to the remaining charge was subtracted from the total number of shower tracks, without any specific geometric assignment due to the pion-proton ambiguity. By this process, one removes all the projectile related tracks from the total multiplicity of each event.

One thus obtains three different multiplicities for each event: the total multiplicity, the target and created particle multiplicity as well as the projectile multiplicity. When all tracks are included for the total multiplicity, the count was labelled AR. The track count required to recover the incident particle's initial charges, or projectile

multiplicity, was labelled AR-AC. By taking the difference between these two counts, one is left with the count of target related tracks as well as the number of created secondaries. This count or multiplicity was labelled AC, as it represents the 'corrected' track count, where the projectile's charges have been accounted for and removed. An example of this is as follows.

COUNT TYPE	PLATE #	STAR #	N_s	N_g	N_b	N_h
AR	2	45	42	24	11	35
AR-AC	2	45	16	1	0	1
AC	2	45	26	23	11	34

This example shows an argon nucleus breaking up into 16 protons and 1 alpha particle with no heavy fragments remaining. There was a total charge multiplicity N_{ch} equal to 77, of which 26 were charged mesons, 16 were projectile protons, 1 a projectile alpha particle and 34 slow tracks mostly emitted from the struck target nucleus. It was the highest multiplicity event observed.

1.10. Measurement of the Angular Distributions

When multiplicity measurements were completed, the

angular distributions of the shower tracks were obtained using a 53X oil immersion objective. Each ocular was replaced with a micrometer eyepiece to determine the azimuthal angle of each shower track. Measurements were performed at an average distance of 100 um from the center of the event, and included a measurement of depth and local emulsion thickness to determine the dip angle. The direction of the beam tracks was also determined, in relation to the motion of the eyepiece micrometers, which allowed the true space angle of the shower tracks to be obtained. An added benefit of the angular measurements was that it allowed a further verification of the shower track multiplicity.

2. CHAPTER 2. EXPERIMENTAL RESULTS

2.1. Inelastic Mean Free Path

A total of 330 primary events were found by scanning a track length of 3168 cm, giving a mean free path of 9.60 $\pm$ 0.53 cm. Here the error is simply taken as $n^{-1/2}$ x 100%, where n is the number of events. A simple expression known as the Bradt-Peters [8] formula exists for the geometrical cross section and is given by

$$\sigma_{BT} = \pi (R_B + R_T - dR)^2$$

where B refers to the beam and T refers to the target

with

$$R_{B,T} = r_o A_{B,T}^{1/3}$$

and

$$dR = r_o b$$

where dR is the overlap of R_B & R_T for which no interaction occurs. It is of the order of the range of the nuclear force.

thus one obtains

$$\sigma_{BT} = \pi r_o^2 (A_B^{1/3} + A_T^{1/3} - b)^2 \qquad (2.1)$$

The mean free path λ may now be found as

$$\lambda = (n(T)\sigma_{BT})^{-1}$$

where n(T) is the number of nuclei T per cm^3

Introduction of the term b into one of the previous expressions is a crude way to account for the diffuseness of the nuclear surface. (More sophisticated expressions may be used in certain models for particle production, but these are not required to account for observed inelastic cross sections.) For a composite media such as an emulsion, there are a variety of targets T_i, each with their own concentrations and nuclear radii.

For composite targets, λ now becomes

$$\lambda = \sum_{i=1} (n_i(T)\sigma_{BTi})^{-1} \qquad (2.2)$$

with the sum being taken over all the elements contained in emulsion. Table 2.1 shows calculated cross sections for the various elements. Silver salts form 82% of emulsion by weight, CNO accounts for 16%, hydrogen for 1.5% and sulphur and iodine for 0.5%. The number of interactions occurring in one type or another of the constituent nuclei of emulsion is of course a function of their atomic number and concentration. However, the geometric cross section

increases only as a function of $(A_B^{1/3} + A_T^{1/3})^2$, and due to the presence of the constant $A_{40}^{1/3}$, (i.e. $(40)^{1/3}$), the cross section changes relatively little as A_T increases, compared with the increase in A_T itself. This means that the cross section for hydrogen is only 5 times smaller than that for silver (A = 108). Although hydrogen accounts for only 1.5% of the weight of the emulsion, it accounts for 40% of the number of atoms per cm^3. When summing the mean free path due to the different target nuclei, one finds that hydrogen accounts for 18% of the interactions, CNO for 31% and silver salts for 51%. One must take this fact into account when searching for the interactions as, proportionately, there are more small (low N_h) events occurring than when the atomic number of the beam is low, due to the increasing presence of hydrogen and light nuclei events.

From the observed mean free path, and taking r_o as 1.41 fermi, b is found to be equal to 1.40. The parameter r_o and b cannot be determined independently using data from unidentified targets. Unpublished data by Lindstrom et al [9] have found $r_o = 1.29$, and b to be a function of the lowest mass number involved, that is $b = 1 - 0.28\ A_{min}(A_B, A_T)$.

TABLE 2-1: Emulsion Composition (Ilford G-5)

Element	Z_i	A_i	N_i ($\times 10^{20}/cm^3$)	σ_{Ar-T} (barns)
Ag	47	108	101	2.87
Br	35	80	101	2.50
H	1	1	320	0.57
C	6	12	139	1.16
O	8	16	94	1.29
N	7	14	32	1.23
S	16	32	1	1.68
I	53	127	0.5	3.10

A later report by Westfall et al [10] for collisions of ^{56}Fe with various targets showed $r_o = 1.47$, $b = 1.12$, somewhat in conflict with the variability of the impact parameter b as indicated in [9]. In fact, according to the first paper, b would be equal to zero for $A_{min} = 36$. However, the raw data from both papers was used to recalculate the parameters b and r_o, and the new least square fits gave results differing from the published ones. (The authors used some cuts on the data, such as on the hydrogen cross section, which is significant in an emulsion experiment.) It is difficult to justify that r_o should vary in the linear type of equation used for the cross section, and it is felt that this parameter should not

be fitted arbitrarily by chi-squared minimization, as is usually done. If one assigns a value to r_o of the order of the compton wavelength of the pion, $\frac{h}{m_\pi c}$ equal to 1.41 fermis, then b can then be determined from the measured cross section or mean free path. This in essence fixes the slope in equation 2.1, while letting the intercept vary.

For the composition of Ilford G-5 emulsion, and a mean free path of 9.60 cm, a parametric relationship between r_o and b can be found

$$r_o(\lambda = 9.60) = 1.08 + 0.21\ b^{1.19} \text{ fermis} \qquad (2.3)$$

The mean free path equation was transposed to find the average value of A_T for emulsion, when Argon is used as a projectile. One then obtains

$$\langle A_T \rangle = [(\pi r_o^2 n(T) \lambda)^{-1/2} + b - A_B^{1/3}]^3 \qquad (2.4)$$

which then becomes

$$\langle A_T \rangle = [(\pi n(T) \lambda)^{-1/2} (1.08 + .21 b^{1.19})^{-1} + b - A^{1/3}]^3 \qquad (2.5)$$

For $\lambda = 9.60$, $A_B = 40$ and b varying from 0.9 to 1.5, $\langle A_T \rangle$ varies rather smoothly from 17 to 18. This may be

be seen in figure 2.1.

This is in contrast with the mathematical mean of A_T for emulsion which is found to be equal to 29. The reason this weighted $\langle A_T \rangle$ is lower is a direct result of the increased possibility of interactions with light nuclei when using a heavy ion as opposed to a single nucleon as projectile. The concept of an average nuclear target is a useful concept to introduce in order to compare fixed target data (measured with electronic detectors to high accuracies) to emulsion data and its relatively poor statistics.

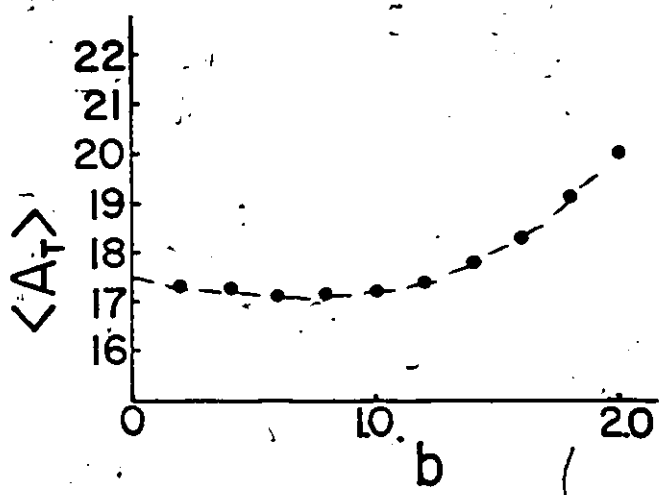

FIG. 2-1: Equivalent Target Nucleus vs b

2.2. Multiplicity Measurements

2.2.1. Slow Particles

The distributions of slow particles, that is black and grey tracks are shown in figure 2.2 and 2.3 .

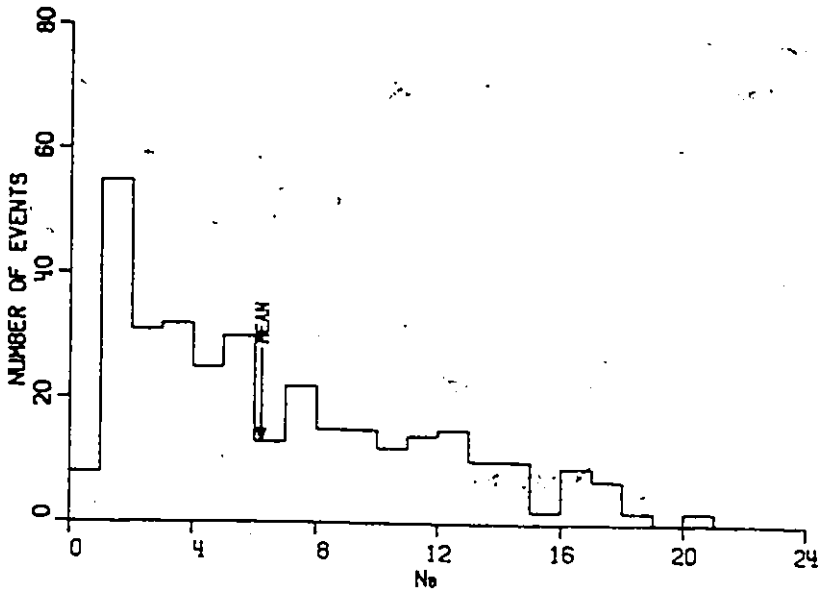

FIG. 2-2: Distribution of Black Tracks

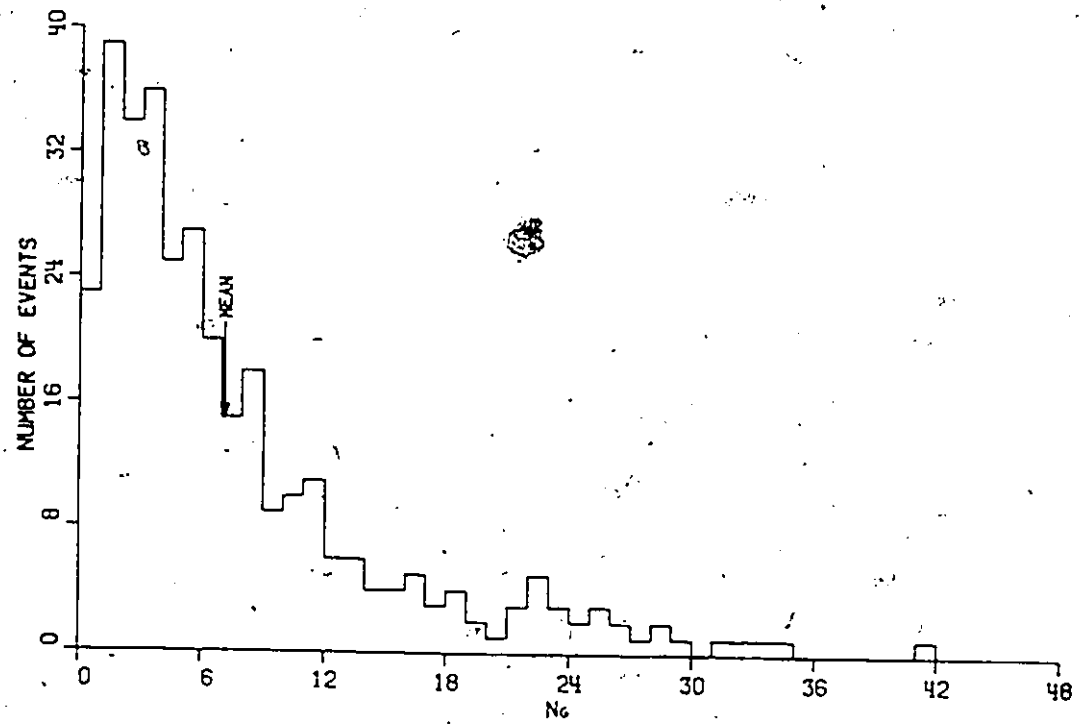

FIG. 2-3: Distribution of Grey Tracks

The average number of black tracks, $\langle N_b \rangle$ is 6.21 $\pm$ 0.26, while the average number of grey tracks $\langle N_g \rangle$ is 7.14 $\pm$ 0.40. The distribution of the sum of $N_b + N_g = N_h$ is shown in figure 2.4, with the average number of slow particles $\langle N_h \rangle$ equal to 13.35 $\pm$ 0.59. Errors given for all multiplicities are the standard errors. The general summary of all mean multiplicities is shown in table 2.2, for both the primary and secondary events, and includes data to be described in this and in following sections.

Grey and black tracks have been labelled as slow particles only in accordance with regular emulsion terminology, which usually deals with fast Z = 1 particles, all others being less than minimum ionizing.

As explained in the previous chapter, included in these multiplicity histograms of so called slow particles are fast, higher than one charged particles. This gives rise to certain complications when one wishes to compare a heavy ion experiment to experiments involving collisions of single hadrons and emulsion.

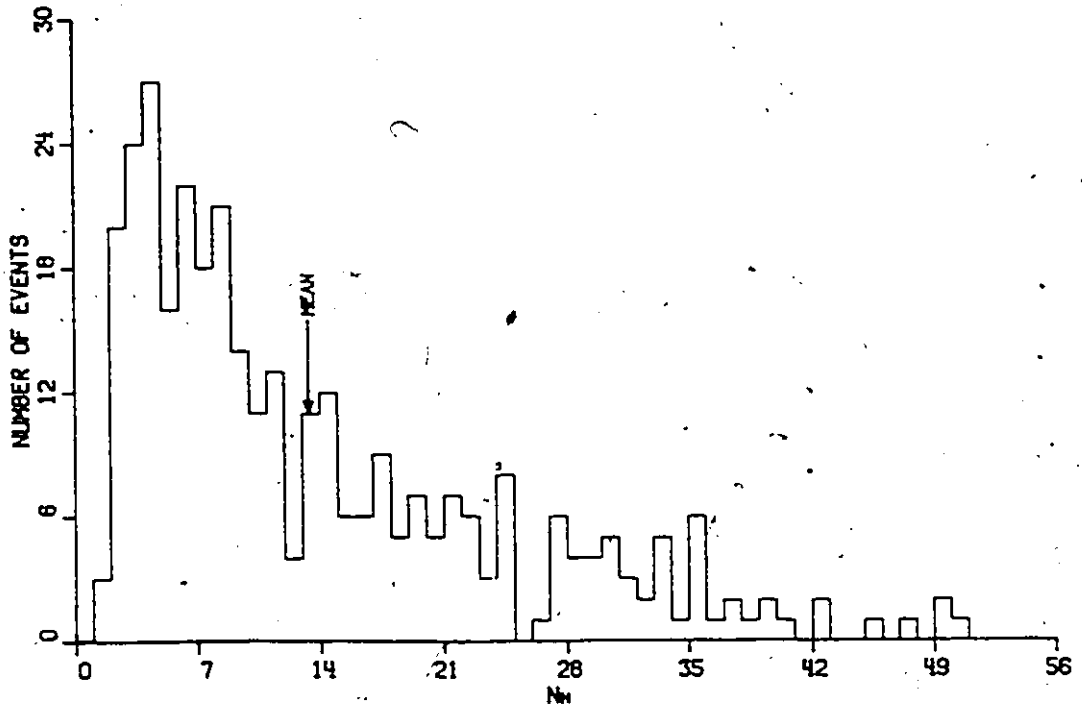

FIG. 2-4: Distribution of Heavy Tracks

In order to alleviate some of the difficulties, these tracks have been removed from the total count presented in all the AR-AC histograms, shown in figures 2.5 and 2.6, for N_b and N_g, and in figure 2.7 for N_h. Here the average values are lowered to $\langle N_b \rangle_c = 5.39 \pm 0.27$. $\langle N_g \rangle_c = 4.93 \pm 0.36$. and $\langle N_h \rangle_c = 10.32 \pm 0.57$. It is these values which are normally measured in emulsion, and are target related tracks.

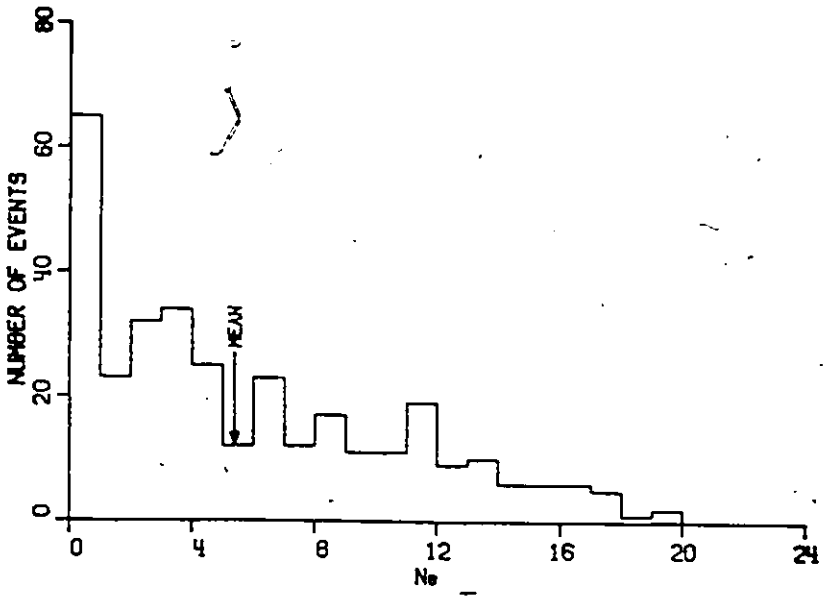

FIG. 2-5: Distribution of 'Corrected' Black Tracks

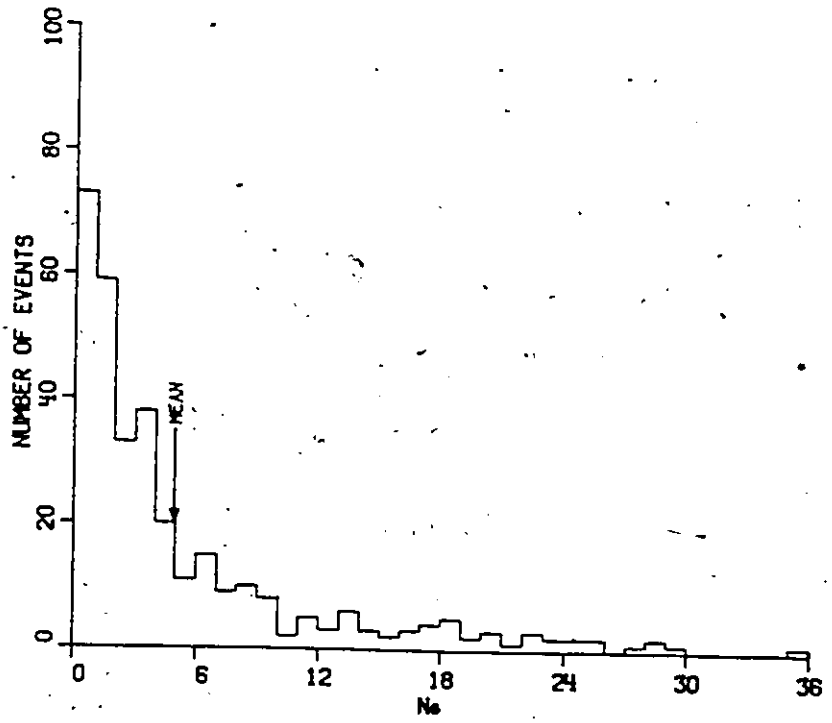

FIG. 2-6: Distribution of 'Corrected' Grey Tracks

As is usual in emulsion interactions, all the distributions are heavily skewed right, and are generally more peaked than a normal distribution, with the exception of the N_b distributions.

The multiplicities are of course lowered in all cases, but less so for the black tracks, since the correction only removes large projectile related fragments, of which there are necessarily few, due to the limited size of the argon nucleus.

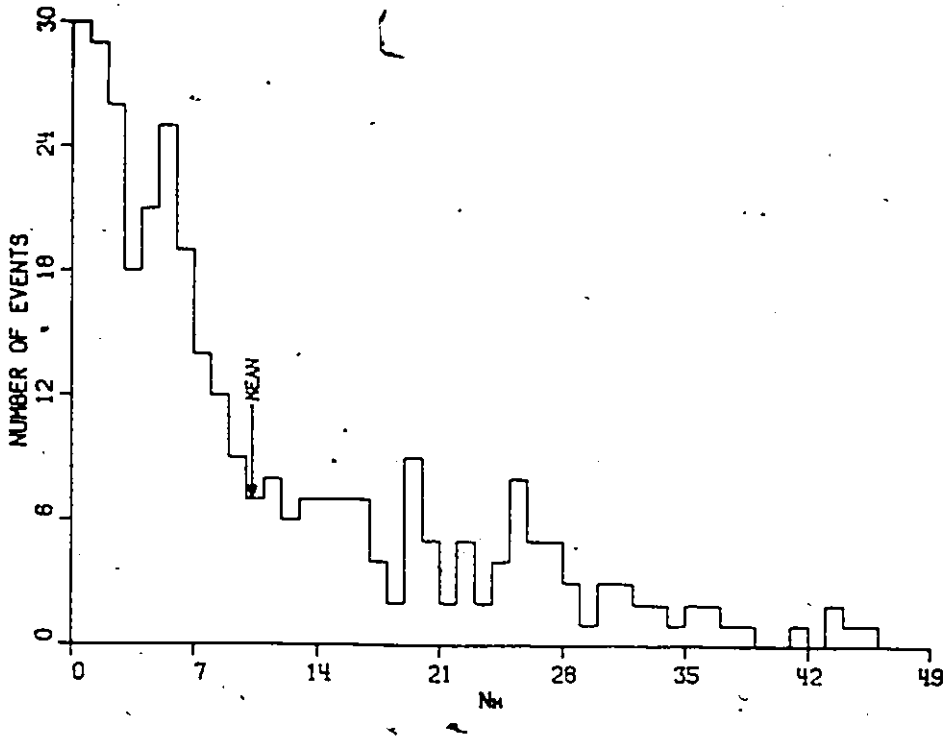

FIG. 2-7: Distribution of 'corrected' Heavy Tracks

2.2.2. Shower Particles

The shower particle distribution is presented in figure 2.8 for primary events, with $\langle N_s \rangle = 9.20 \pm 0.44$. With projectile related protons removed, the distribution of shower particles for events relabelled to AR-AC is shown in figure 2.9. with $\langle N_s \rangle_c = 3.70 \pm 0.25$. This histogram thus shows the number of charged pions produced in all 330 primary events.

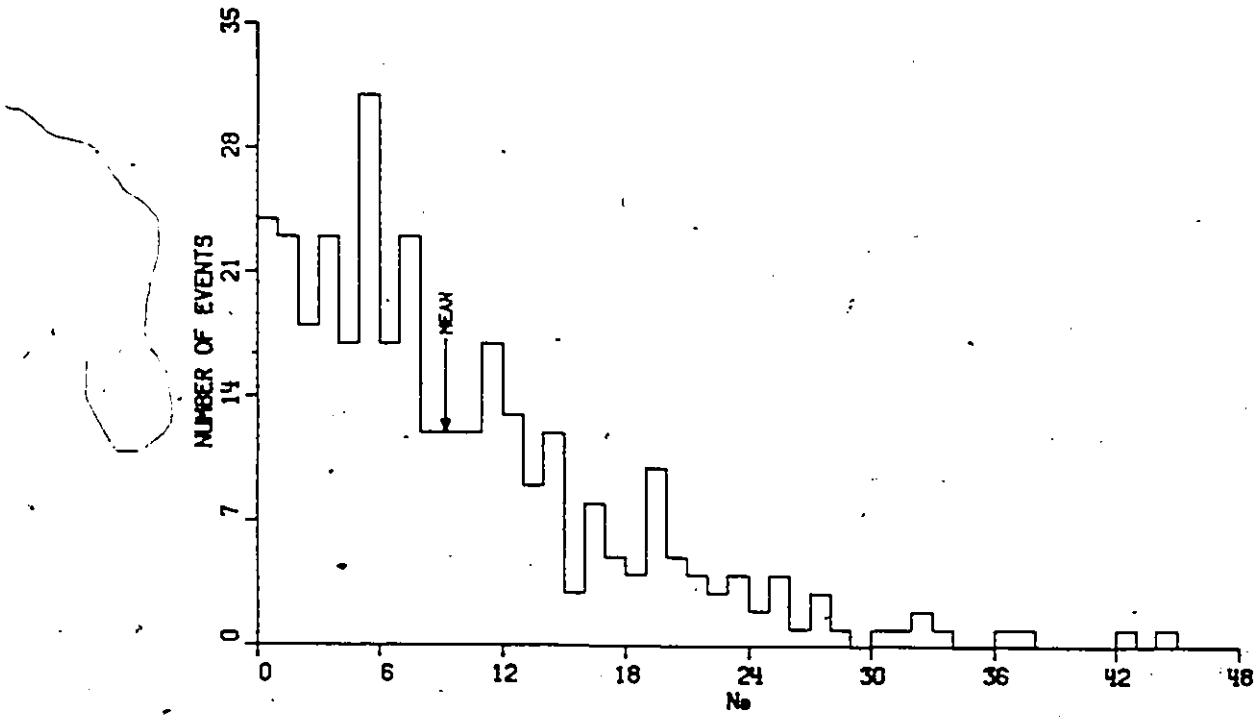

FIG. 2-8: Distribution of Shower Tracks

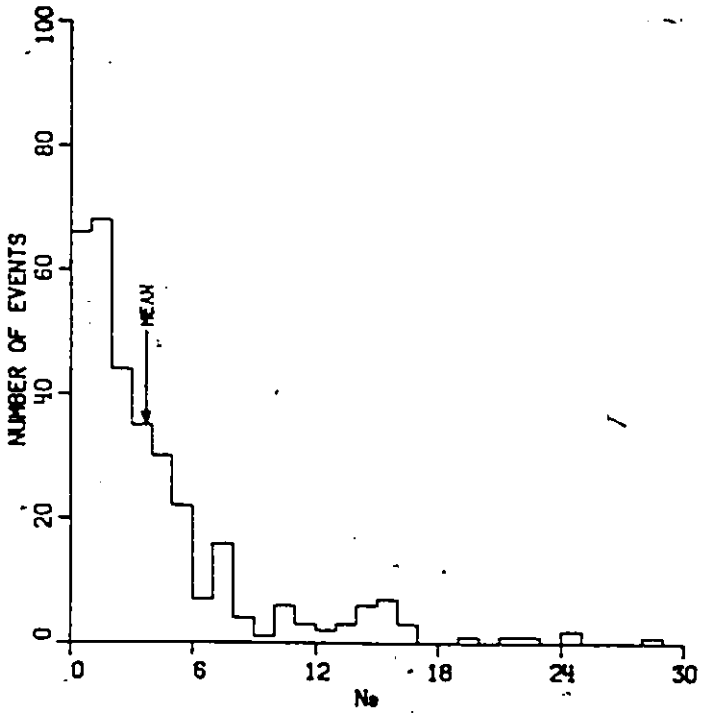

FIG. 2-9: Distribution of 'corrected' Shower Tracks

2.2.3. Projectile Related Fragments

Histograms for the tracks removed from the initial primary events, as being associated with the projectile, are shown in figure 2.10, 2.11, and 2.12 for N_b, N_g, N_s respectively. One thus has the average break up of the argon projectile into protons (N_s), alpha particles (N_g) and heavy fragments of $Z > 2$ (N_b). These graphs are also labelled as AR-AC. There is a marked tendency for the emission of Z=2 particles, showing some of the nuclear structure of the projectile as well as a strong tendency for the emission of

composite particles from the interaction zone.

In terms of the labelling, we refer to Z=1 composites such as deuterons and tritons as 'protons', since the large majority of the particles included in the N_s distribution for the projectile are protons. The same is true for the label 'alpha', where this includes any Z=2 composite nucleus.

It should be noted that in order to obtain these 'corrected' multiplicities, and subsequent projectile breakup, we have assumed no charge exchange reactions occur which would give a $Z_{in} = 18$ and a $Z_{out} = 19$. The cross section for these events has been shown to be of the order of 0.01 of σ_{RT}, the total reaction cross section.

The mean multiplicities for these histograms are referred to as $\langle N_p \rangle_{Ar}$, $\langle N_a \rangle_{Ar}$ for N_s and N_g respectively in table 2.2.

TABLE 2-2: Average Multiplicities in ^{40}Ar & Emulsion Interactions

DATA	PRIMARY EVENTS(330)	SECONDARY EVENTS(53)
$\langle N_s \rangle$	9.20 ± 0.44	9.66 ± 1.40
$\langle N_g \rangle$	7.14 ± 0.40	5.72 ± 1.02
$\langle N_b \rangle$	6.21 ± 0.26	6.04 ± 0.76
$\langle N_h \rangle$	13.35 ± 0.59	11.75 ± 1.58
$\langle N_s \rangle_c$	3.70 ± 0.25	4.77 ± 0.83
$\langle N_g \rangle_c$	4.93 ± 0.36	4.47 ± 0.87
$\langle N_b \rangle_c$	5.39 ± 0.27	5.62 ± 0.80
$\langle N_h \rangle_c$	10.32 ± 0.57	10.09 ± 1.50
$\langle N_p \rangle_{Ar}$	5.50 ± 0.24	4.89 ± 0.70
$\langle N_a \rangle_{Ar}$	2.21 ± 0.69	1.25 ± 0.22
$\langle N_F \rangle_{Ar}$	0.82 ± 0.03	0.42 ± 0.07
$\langle N_a+N_F \rangle_{Ar}$	3.03 ± 0.08	1.66 ± 0.20

$$\langle Z_F \rangle = \frac{Z_{Ar} - [\, \langle N_p \rangle_{Ar} + 2\langle N_a \rangle_{Ar} \,]}{\langle N_F \rangle_{Ar}} \qquad (2.6)$$

$$= \frac{18 - 9.92}{0.82} = 9.85$$

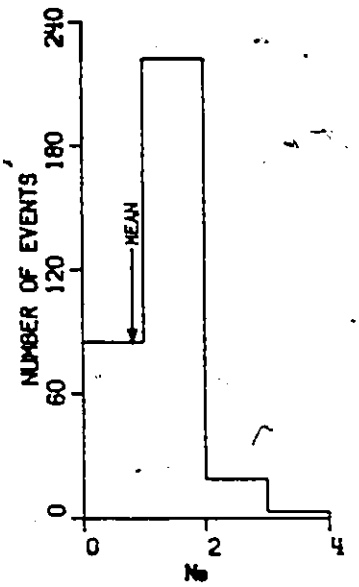

FIG. 2-10: Distribution of Projectile Z>2 Fragments

The histogram for the heavy fragments shows that slightly less than one particle with Z>2 remains intact in the average collision. This value is shown as $\langle N_F \rangle$ in the table, and corresponds to the relativistic black tracks. The equation used to obtain the average charge of the heavy fragment is also given. (We have of course been neglecting the neutrons when we talk of Z = 1 particles, as they are unobservable, but it is understood that they are fragmented off the projectile just as are protons, in the proportion (A-Z)/Z.)

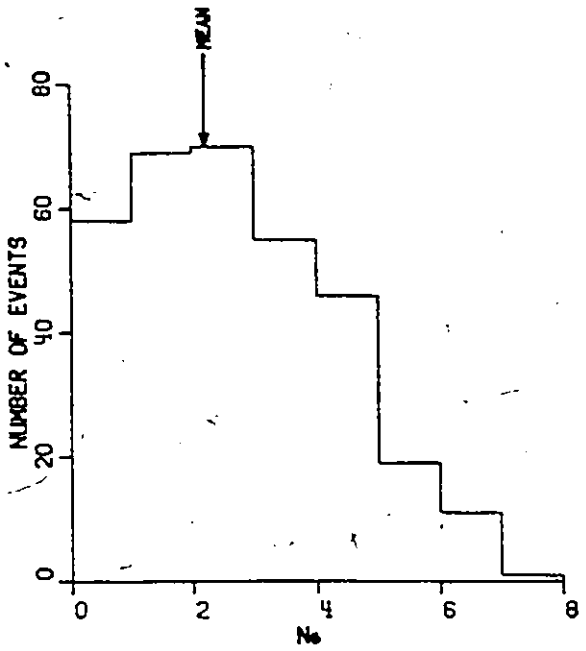

FIG. 2-11: Distribution of Projectile 'alpha' Particles

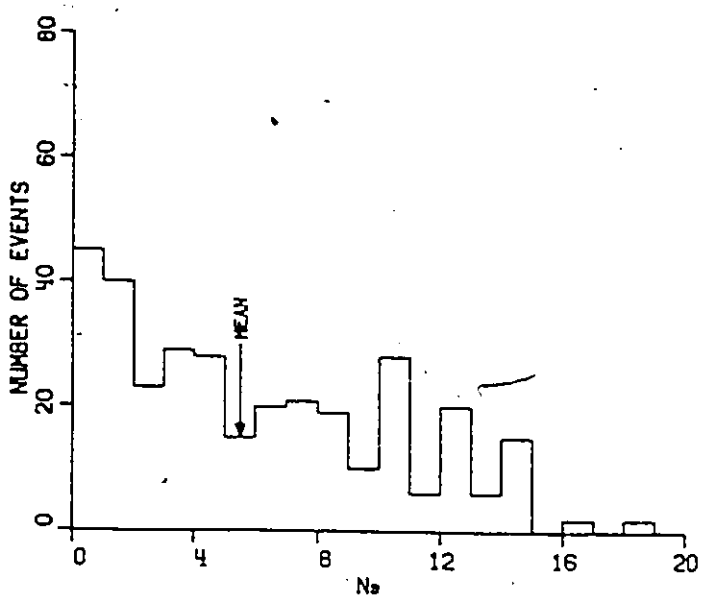

FIG. 2-12: Distribution of Projectile 'protons'

If we consider the reverse process, that is the target break up, we find that according to measurements which have been made [16] for proton bombardment of an emulsion target the ratio of proton to alpha particle emission resulting from the breakup of the target is roughly equal to 2 to 1. Data about the ratio of N_p to N_α for exclusive type of counter experiments involving heavy ions was difficult to obtain. However if we equate the break up of the projectile of this experiment to fixed target evaporation (plus the initial cascade), we see that the emission ratio is also found to be equal to 2 to 1 for a heavy ion collision. Thus the spectator part from the fast projectile behaves as the spectator part from the target nucleus involved in an interaction with a hadron. Observation of the spectator breakup is far easier when it occurs in a reference frame such as that of the Argon projectile, since protons are minimum ionizing while alphas have exactly four times minimum ionization. That the ratios are similar is encouraging from the standpoint of the correct identification of the projectile breakup done in this experiment, for there should not be much difference in between the physical processes which occur in the spectator regions of an interaction, whether the interaction be initiated by a hadron or a heavy ion.

2.3. Comparison with n-N Interactions

Nucleon-nucleus interactions at high energy have been studied in great detail at a variety of energies up to 500 GeV. Emulsion studies [11,12,13] have shown that $\langle N_b \rangle$ reaches a plateau at roughly 5 or 6 for incident nucleons having energies ranging from 6.2 to 400 GeV. The number of shower tracks produced varies from 2.8 to 16.8 respectively, although this number will be reduced by roughly 1.2 [14] due to the fact that the incident hadron plus an average of 0.2 fast recoiling protons per interaction are included in N_s. Therefore, a 6.2 GeV proton produces 1.6 fast charged pions per interaction in emulsion, while a 22.5 GeV proton produces 4.4. In this experiment we have a total kinetic energy of 72 GeV when considering all the incident nucleons of the projectile , and 3.7 fast charged pions are created on the average. We thus have an indication that a good deal of the nucleons are involved in the production process since it would take a proton of about 18 GeV to produce 3.7 fast pions, if the N-N reaction mechanism were similar to that of n-N collisions. As a confirmation of this, it is very interesting to compare the value of $\langle N_g \rangle$ for n-N and N-N interactions. A value of $\langle N_g \rangle$ equal to 2.61 is obtained [14] for n-N interactions at 200 and 300 GeV, when ionization cut-offs similar to ours are used for N_g. This has often [15] been

associated with the number of collisions v occurring inside the nucleus. Babecki [11] gives a parameter fit to the relationship between v and N_g for proton-emulsion interactions as

$$v = a + bN_g + cN_g^2 \qquad (2.7)$$

$$= 1.45 + 0.58\ N_g - 0.015\ N_g^2$$

This corresponds to a value of v equal to 2.86 for an N_g of 2.61. Now v increases to 3.94 for $\langle N_g \rangle_t = 4.93$ which is the value obtained in this experiment. This of course assumes one nucleon making several collisions inside the nucleus, whereas in our case, many nucleons could each be making several collisions inside the nucleus.

It should be noted that the distribution of N_g and the value of $\langle N_g \rangle$ are relatively independent of energy [11] (at least for 6.2 to 400 GeV p-Em interactions). However, they are dependent on the atomic number of the target, and thus the number of collisions inside the nucleus is a function of the geometry of the interaction rather than the energy involved. If one extends this to nucleus-nucleus interactions, one expects to find a much greater number of grey tracks since 2 nuclei interpenatrating each other could

be considered equivalent to many single nucleons traversing one nucleus. We may note that from the cross sections involved for the various constituents of emulsion, there are proportionately many more collisions with hydrogen in N-Em interactions than in p-Em interactions, which results in a larger number of interactions with $N_g min = 1$ (the recoiling hydrogen nucleus) in N-Em than in p-Em. If there were the same proportion of interactions with light (H), medium (C,N,O) and heavy (Ag, Br) nuclei using heavy ions (theoretically one could achieve this by shifting the relative proportions of the various target nuclei to counterbalance the difference in cross sections occurring for Ag-Em and p-Em) it would be found that the number of grey tracks in Argon interactions would be even higher. This would seem to imply an increase in the number of collisions inside the nucleus during an interaction.

The only data found in the literature for p-Em interactions at a comparable energy per nucleon to the one in this experiment is that of Bogdanski et al. [17] with protons of an incident energy of 2.2 GeV. Again, this data showed similarities in the number of heavy tracks, to higher energy p-Em experiments. They found $\langle N_b \rangle = 4.45 \pm 0.22$ and $\langle N_g \rangle = 1.42 \pm 0.12$. Thus it seems that even at this lower energy the target has received a maximum disturbance, and that the

initial cascade, with its associated number of nucleon-nucleon collisions inside the nucleus as indicated by the value of $\langle N_g \rangle$ is the same as at higher energies. A value of $\langle N_s \rangle = 0.95 \pm 0.05$ was found for these interactions, compared with $\langle N_s \rangle = 9.20$ giving $\langle N_s \rangle_c = \langle N_{\pi^\pm} \rangle = 3.70$ for this experiment, with a similar individual nucleon energy. Again one must remove a contribution to the $\langle N_s \rangle$ found by Bogdanski et al. by the incident proton, which then leaves a very feeble production of charged pions. Fully 80% of their events had $N_s = 0$ or 1, and $N_s = 5$ was the maximum. Due to the large number of pions produced, it seems quite obvious that many nucleons are interacting in a nucleus-nucleus collision, and are probably interacting in a collective fashion.

If one considers the energy available in the center of mass for pion production in a nucleon-nucleon collision, one obtains

$$E_{prod} = s^{1/2} - 2m \qquad (2.8)$$

$$= \{ 2[E_{k1}E_{k2} + m(E_{k1} + E_{k2})] + 4m^2$$

$$\pm 2 [(E_{k1}^2 + 2mE_{k1}) (E_{k2}^2 + 2mE_{k2})]^{1/2} \}^{1/2} - 2m$$

where E_{k1} = kinetic energy of the projectile

E_{k2} =kinetic energy of the target nucleon due to Fermi motion

for m= 0.94 GeV, and E_{k1} = 2.2 GeV, one obtains

$$E_{prod} = .91 \pm .20 \text{ GeV}$$

Therefore if all the available energy is used to create pions, of mass = .14 GeV and roughly .04 GeV is taken up as kinetic energy for each pion, it is possible to produce at maximum 6.2 pions, which correlates well with the maximum observed in the data of Bogdanski et al. particularly when one considers that 1/3 of the produced pions are neutral.

For this experiment, a single nucleon-nucleon encounter could produce 4.8 pions at maximum, with 4.2 pions being the average maximum value (i.e. when the Fermi motion is averaged out) assuming the pions only take away .04 GeV of kinetic energy. In order to produce the maximum number of pions (=28) observed in any single event in this experiment would thus

require an absolute minimum of 7 individual nucleon-nucleon collisions, each using up all of the available energy in the c.m. Even more individual collisions would be required if the pion energy is above the very conservative estimate of .04 GeV. This would be extremely unlikely, and one then assumes that many more collisions are involved, or else there is a collective type of interaction where collisions are occurring between groups of nucleons, with proportionately more energy being available in the center of mass.

2.4. Correlations between N_s, N_g, N_b, N_h.

It is customary in emulsion experiments to reproduce graphs showing the correlation between $\langle N \rangle_X$, the average number of track type X evaluated for a particular multiplicity N_Y of another type of track Y and the multiplicity N_Y

Figure 2.13 shows this relationship for $\langle N_b \rangle$ versus N_g. This graph demonstrates an initial linear relationship between the average number of evaporation tracks and the intranuclear cascade tracks N_g. It may be simply represented by the relationship

$$\langle N_b \rangle = 1.98 + 0.98\ N_g. \qquad (\text{for } N_g \lesssim 10)$$

When N_g has risen sufficiently indicating a large number of nuclear collisions, the average value of N_b begins to taper off at a constant value of approximately 11.5.

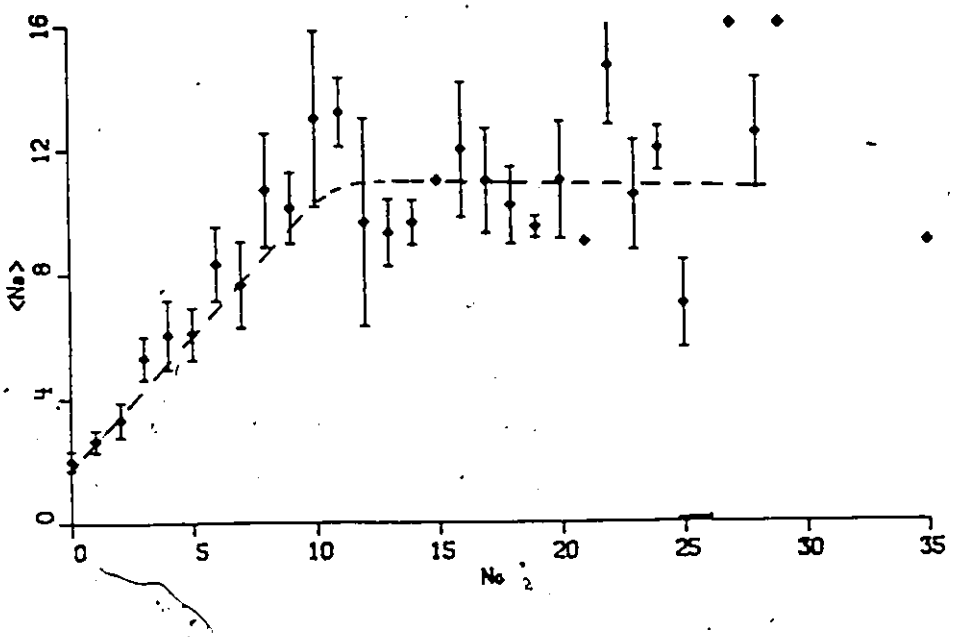

FIG. 2-13: Correlation between $\langle N_b \rangle_c$ and N_{gc}

We thus have an indication that at that point the target nucleus has received enough energy to be broken up completely, and that further energy is not required to evaporate the target. An almost identical relationship [15] is obtained in p-Em interactions, over an energy range of 6.2 to 400 GeV, with the same initial linear rise of $\langle N_b \rangle$ with N_g and then tapering off at $\langle N_b \rangle$ 12.5 when N_g reaches 10. The fact that such close agreement is obtained from two very

different types of interactions should not seem fortuitous, since there are only so many nucleons in any target, and only so much energy is required to completely evaporate the target, which then produces a maximum number of black tracks.

It also does not matter how many pions are produced, from 6.2 to 400 GeV p-Em, as the $\langle N_b \rangle$ vs. N_g correlations are the same. This says that even though the number of pions increases significantly, the pions do not transfer any significant amount of their energy to the target while traversing it, since the correlation equation does not change.

However, there is one significant difference between the p-Em and ^{40}Ar-Em correlations, and this is the extension of the graph to values of $N_g > 30$. Whereas the p-Em graph essentially stops at $N_g = 16$. If the number of grey tracks is a good indication of the number of nucleon-nucleon collisions, we obtain further evidence of a great many possible collisions in nucleus-nucleus interactions. With such high values of N_g, one might expect the graph to go downwards as N_g increases, since there are very few nucleons left inside the target to produce black tracks. It may be noted that in no case does the sum of $N_g + N_b = N_h$ exceed 45, with 47 being the number of protons in a silver nucleus.

Figure 2.14 and 2.15 show correlations between N_s and the average number of N_g and N_h tracks respectively.

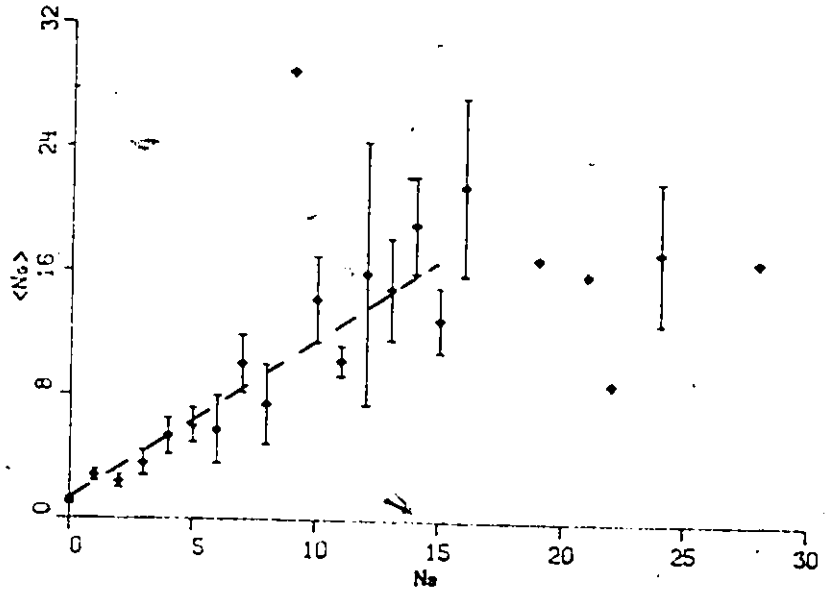

FIG. 2-14: Correlation between $\langle N_g \rangle_c$ and N_{sc}

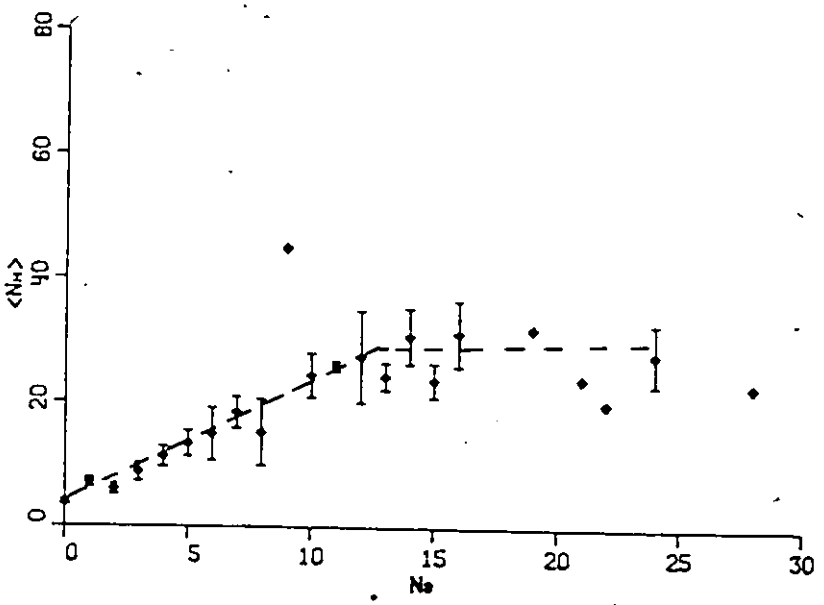

FIG. 2-15: Correlation between $\langle N_h \rangle_c$ and N_{sc}

Here again one obtains a remarkably linear relationship in both graphs for the initial part of the graphs. The $\langle N_g \rangle$ vs. N_s graph may be represented by

$$\langle N_g \rangle = 1.25 + 1.05\ N_s \qquad (\text{for } N_s \leq 15)$$

while for the $\langle N_h \rangle$ vs. N_s graph one obtains

$$\langle N_h \rangle = 4.10 + 1.87\ N_s. \qquad (\text{for } N_s \leq 15)$$

In the first graph, one observes that the number of pions produced increases linearly and very regularly with the average number of grey tracks produced. Here again one sees that the number of created particles is directly related to the number of nucleons involved in the initial cascade. Although the statistics are poor for events with $N_s > 16$, there seems to be a trend for $\langle N_g \rangle$ to reach a limiting value between 17 and 18. However to support this hypothesis one would need more high multiplicity events.

In figure 2.15, it may be seen that the addition of N_b to N_g to get $\langle N_h \rangle$ does not change the form of the relation of the number of pions to target tracks from that of figure 2.14. There is a threshold (average trend only) for pion production at $\langle N_h \rangle = 4$, and then a regular rise in $\langle N_h \rangle$ as a function of N_s. This continues up to the point $N_s = 13$,

where $\langle N_h \rangle$ seems to reach a limiting value of about 29, again with the same statistical problem for high multiplicity events.

The limiting occurs at the same N_s point in both figures 2.14 and 2.15, which indicates that when the maximum average number of collisions has occured, there has also been a sufficient amount of energy deposited in the target to fully evaporate it. From this point on, the number of pions increases as more energy is transferred from the projectile nucleons to the interaction region, in each individual collision, without actually increasing the number of interactions.

2.5. Multiplicities for Light and Heavy Targets

Since the number of black tracks in an event represents evaporation of the target, it is possible to separate interactions with heavy targets from those with light targets. To make the separation completely unambiguous, one has to select events with a corrected track count of $N_hc > 6$. This is so because in the light target group (HCNO) oxygen could give a maximum of eight black tracks. It is, however, very unlikely that at least some of the protons in oxygen would not be involved in the initial cascade, appearing as

grey tracks. One might also expect the struck oxygen nucleons to have an alpha particle in its evaporation products. Thus, the maximum number of black tracks emerging from an encounter with oxygen is not likely to be above 5. By selecting events with $N_h c > 6$, we are selecting encounters with AgBr.

Figures 2.16, 2.17 and 2.18 show the multiplicity distributions for $N_b c$, $N_q c$ and $N_s c$, respectively, for $N_h c > 6$. The number of events involved is 161. This corresponds to 49% of the total number of events. As we expect 50% of all events to be with AgBr, and not all of the events with AgBr have $N_h c > 6$.

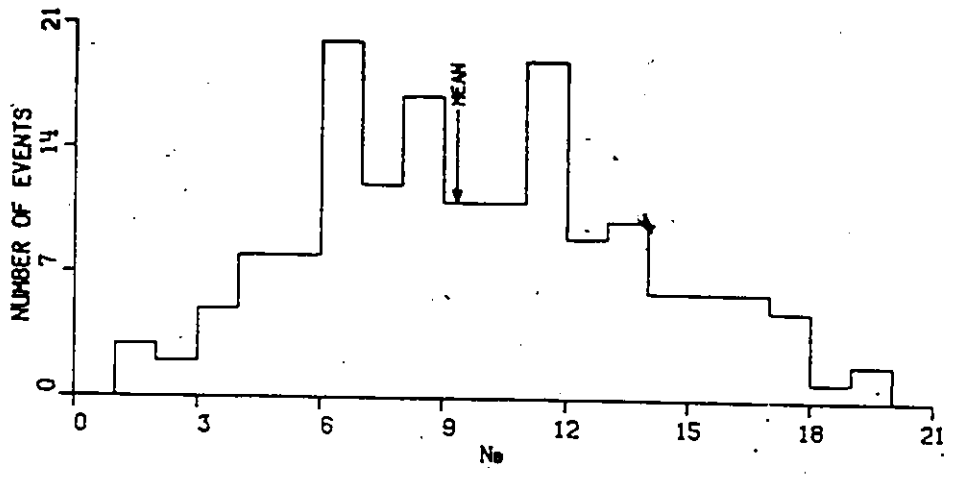

FIG. 2-16: Distribution of $N_b c$ for heavy targets

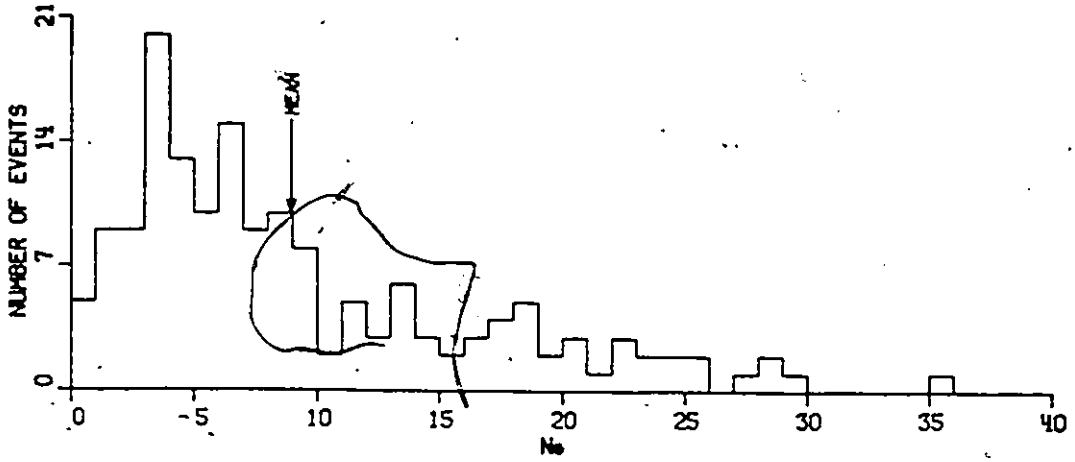

FIG. 2-17: Distribution of $N_g c$ for Heavy Targets

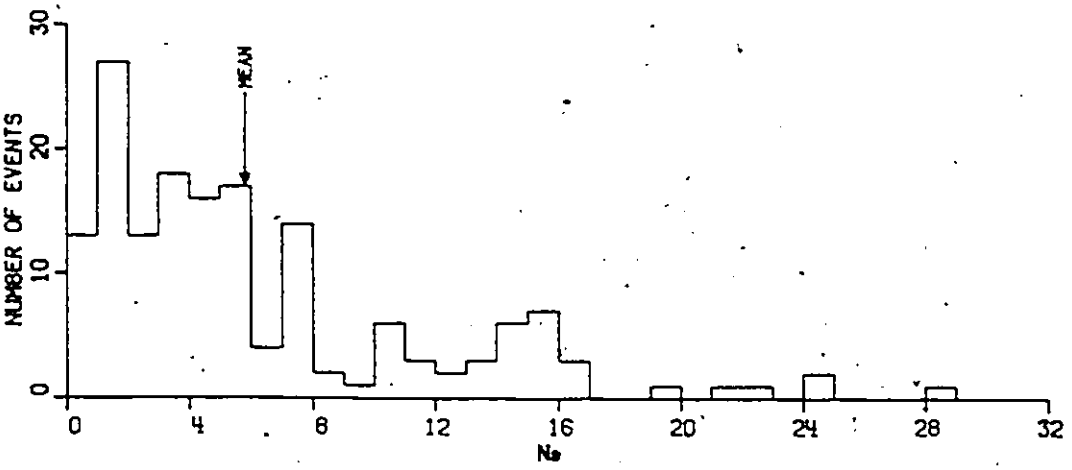

FIG. 2-18: Distribution of $N_s c$ for Heavy Targets

Thus the multiplicity distributions for $N_h c > 6$ involve only the most central collisions with N and O, and any AgBr events not included were peripheral collisions. The latter collisions have large impact parameters, and only a small amount of energy is transferred to the target, which then remains more or less intact; this gives rise to only a small number of heavy tracks.

For the events in figures 2.16, 2.17 and 2.18, one finds a new set of multiplicities for the interactions with heavy targets, as well as those for the events with light targets (HCNO) that have $N_h c < 7$.

TABLE 2-3: Multiplicities for Light and Heavy Groups

DATA	$N_h c < 7$ (169 events)	$N_h c > 6$ (161 events)
$\langle N_s \rangle$	5.36 ± 0.37	13.22 ± 0.68
$\langle N_g \rangle$	2.83 ± 0.17	11.63 ± 0.63
$\langle N_b \rangle$	2.57 ± 0.13	10.01 ± 0.31
$\langle N_h \rangle$	5.40 ± 0.20	21.64 ± 0.77
$\langle N_s \rangle_c$	1.68 ± 0.14	5.80 ± 0.44
$\langle N_g \rangle_c$	1.09 ± 0.09	8.93 ± 0.58
$\langle N_b \rangle_c$	1.65 ± 0.13	9.32 ± 0.32

These values give the corresponding multiplicity ratios as shown in the next table, for various values of the subscript i

TABLE 2-4: Multiplicity Ratios for Various Groups

i	$\frac{\langle N_i \rangle_{Nh(c) > 6}}{\langle N_i \rangle_{all}}$	$\frac{\langle N_i \rangle_{Nh(c) > 6}}{\langle N_i \rangle_{Nh(c) < 7}}$
s	1.44	2.46
g	1.63	4.10
b	1.61	3.89
h	1.62	4.01
s_c	1.57	3.45
g_c	1.81	8.19
b_c	1.73	5.65

From these ratios one may observe that pion production with light targets is very low, especially when one considers that some of the events with $N_hc < 7$ are due to AgBr. The fact that the pion production ratio does not scale the same way as the grey track production ratio for the heavy to light group comparison (i.e. 3.45 vs. 8.19) indicates that pion

production does not increase directly with the number of nucleon-nucleon collisions, assuming the grey track multiplicity is a valid indicator for the number of collisions. Alternately, it is possible that for some of the events with the heavier targets, a number of the grey tracks could be Z = 1 particles emitted in the backward direction from the interaction region, since the interaction region is much larger, and these backward (in the c. of m. of the emitting region) tracks would become more numerous.

2.6. Comparison with N-N Data

Total pion multiplicities are very rarely measured for heavy ion interactions. Instead, double differential cross sections are measured at various lab angles, due to the nature of the detectors normally used. There is, however, one detector besides emulsion where total pion multiplicity may be measured, and that is the streamer chamber. S. Y. Fung et al. [18,19] have measured total pion multiplicity in a triggered streamer chamber for carbon and argon ions incident upon various targets at various energies, as well as for central collisions of argon on a ^{208}Pb target. They found $\langle N_{\pi^-} \rangle$ for ^{40}Ar at 1.8 GeV/n to be 0.97 for interactions with LiH, 1.91 for NaF, 3.27 for BaI_2 and 3.27 for Pb_3O_4. If one makes the assumption that $\langle N_{\pi^-} \rangle / \langle N_{\pi^+} \rangle = (A-Z)/Z = 1.22$,

then the total pion multiplicity $\langle N_\pi \rangle$ is 1.77 for LiH, 3.48 for NaF, and 5.95 for BaI_2 and Pb_3O_4. The results obtained in this experiment are essentially identical. The pion multiplicity is 1.68 for the light (HCNO) group, 3.70 for all the events, and 5.80 for the heavy group (AgBr). The weighted $\langle A \rangle$ for emulsion was found to be equal to 18-19 in section 2.1, and there is an associated mean pion production just slightly more than what Fung et al. found for a NaF target with $\langle A \rangle$ equal to 21.

Emulsion studies [20,21,22,23] have been done for C, N and O projectiles at corresponding projectile energies. More recently, emulsion studies [24,25] have been performed for interactions of ^{56}Fe in emulsion, and comprehensive reviews of inclusive interactions [26,27] for heavy ion interactions give data for a multitude of target-energy combinations. Similar results to ours have been obtained in the emulsion experiments, although some of the data presented in this experiment to describe the overall picture of the interactions is not present in the publications (track separations, light and heavy target multiplicities etc.)

2.7. Angular Distributions of Shower Particles

The angular distribution for the minimum ionizing

particles is shown in Fig. 2.19. It is highly peaked towards the central region ($\theta = 0$) and this is mostly due to the presence of projectile related protons. The sample studied was the first 100 events. with a total of 888 shower tracks. giving an $\langle N_s \rangle = 8.9$ as opposed to $\langle N_s \rangle = 9.2$ for the whole sample.

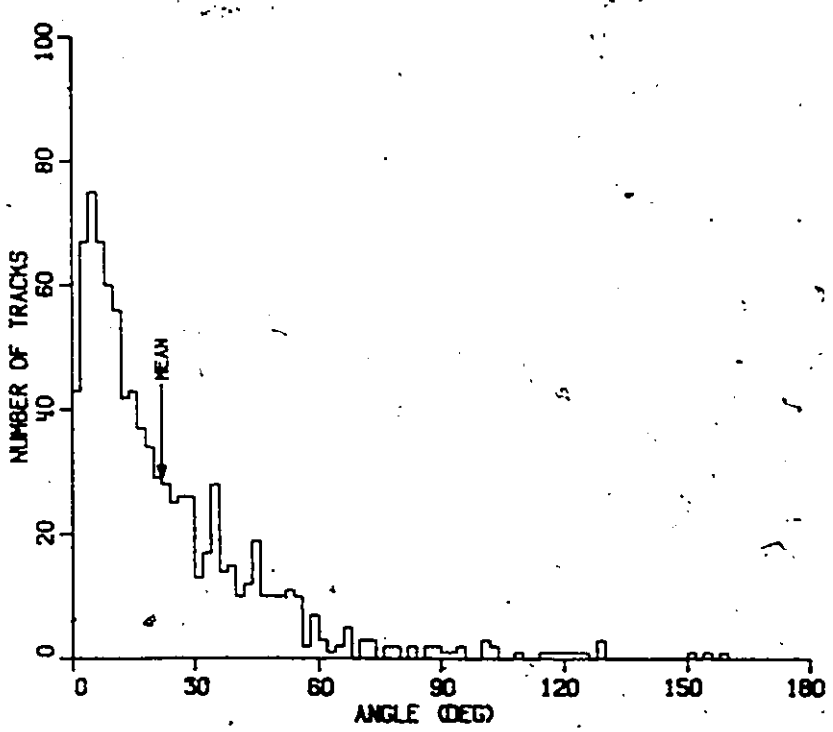

FIG. 2-19: Angular Distribution of Shower Tracks

The values for N_b and N_g for this sample were also very close to that of all the events. If a target proton was given as much as 1 GeV/C of transverse momentum $P_\perp$. and retained its initial parallel momentum $P_{//} = 2.57$ GeV/C. this would form a

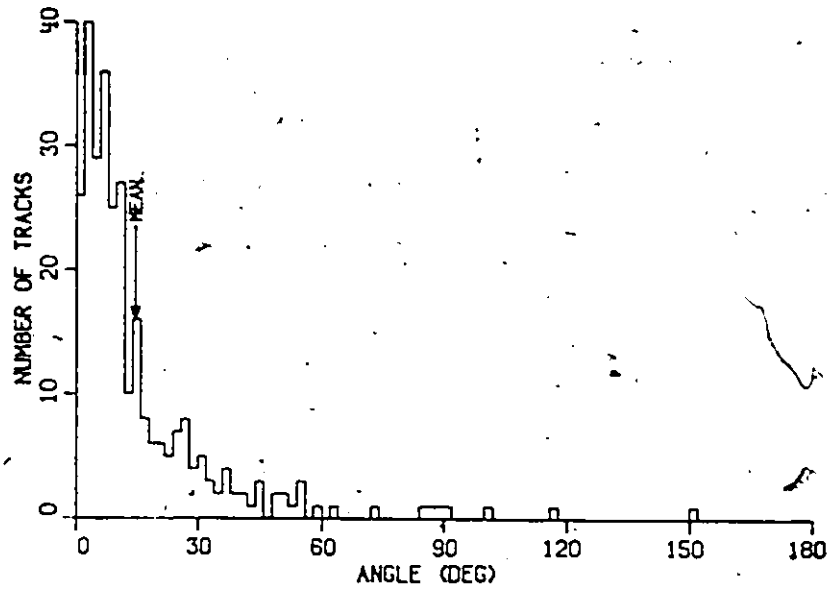

FIG. 2-20: Angular Distribution for the Light Targets

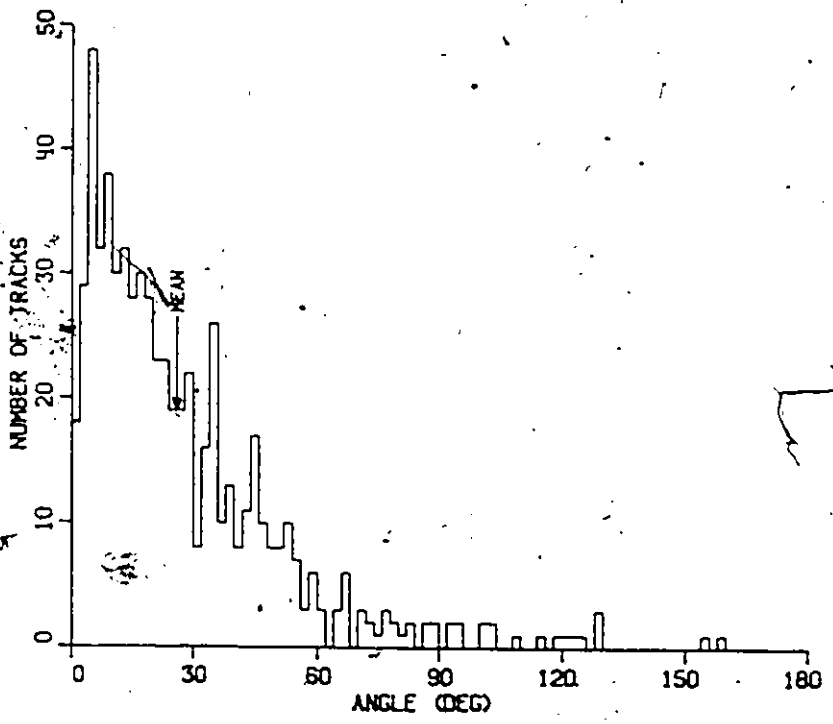

FIG. 2-21: Angular Distribution for the Heavy Targets

space angle in the lab frame of 21°. In a more realistic calculation using evaporation theory and assuming a nuclear temperature of 6 - 8 MeV [61], one obtains a maximum emission energy for protons of the order of 250 MeV. In the rest frame of an excited projectile nucleus, the evaporation will be isotropic, that is a spherical distribution centered on the origin in momentum space. When transforming this distribution into the laboratory, one obtains an ellipsoid which does not enclose the origin, as long as the velocity v_r of particle in the rest frame does not exceed the β of the emitting system in the lab frame of reference. This gives rise to a maximum angle of emission θ_{max}, in the lab system for protons evaporated from the projectile. One then has

$$\tan \theta_{max} = \frac{(1-\beta^2)v_r^2}{(\beta^2-v_r^2)} \qquad (2.9)$$

θ_{max} takes on the value 4.3° for a 20 MeV proton emitted backwards in the projectile frame, when $\beta = 0.94$, 6.9° for a 50 MeV proton and 9.9° for a 100 MeV proton. Therefore almost all protons should be contained within a 10° cone in the lab, if they are emitted in an evaporation process. Projectile related protons emitted from the hotter interaction region may be emitted at substantially larger angles, but will generally be contained with a 30° cone due to the kinematics

involved. Figure 2.19 shows that roughly 670 tracks have $\theta < 30^{\circ}$. As 520 tracks are expected to be projectile related protons, the pion angular distribution must be quite broad.

We show in Fig 2.20 the angular distribution for the light group and that for the heavy group is shown in Fig 2.21. The average angle of emission $\langle\theta\rangle$ of the shower tracks for these distributions are summarized in the table.

TABLE 2-5: Average Emission Angles of Shower Tracks

All stars	Light targets	Heavy targets
21.95 ± 0.77	14.62 ± 1.12	26.02 ± 0.97

One may better observe the anisotropy in a distribution of $\cos\theta$ shown in Fig. 2.22.From Fig. 2.22 one sees that 70% of

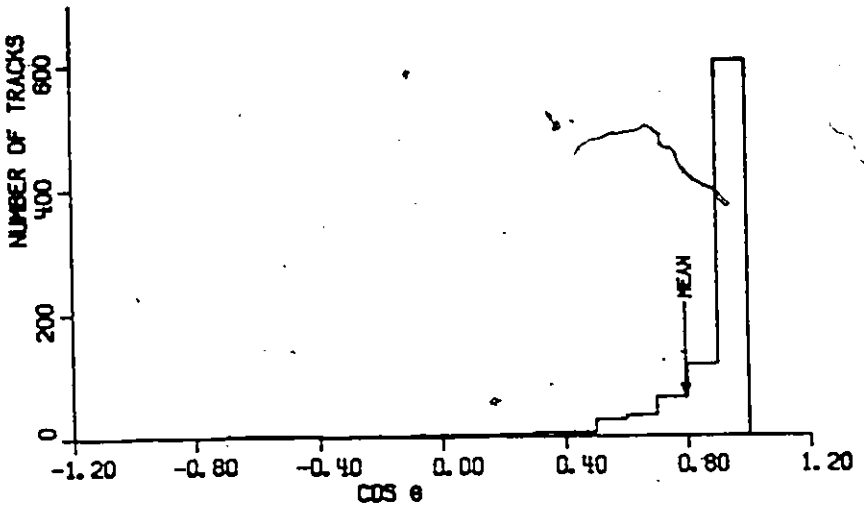

FIG. 2-22: Cos θ Distribution for all Events

the shower tracks are in the region $1.0 > \cos\theta > 0.9$. The proportion of protons in the whole distribution accounts for 60% of the tracks, as $\langle N_p \rangle_{Ar} / \langle N_s \rangle = 0.60$. S. Y. Fung et al.[18] have measured the angular distribution of negative pions emitted from 1.8 GeV/n ^{40}Ar incident on Pb_3O_4 and found $\langle\theta\rangle = 36^{\circ}$. Since their pion multiplicities agreed very well with those found in this experiment, it was decided to fit their distribution to that found for our events with $N_{hc} > 6$, and

thus extract the proton multiplicity by performing a subtraction.

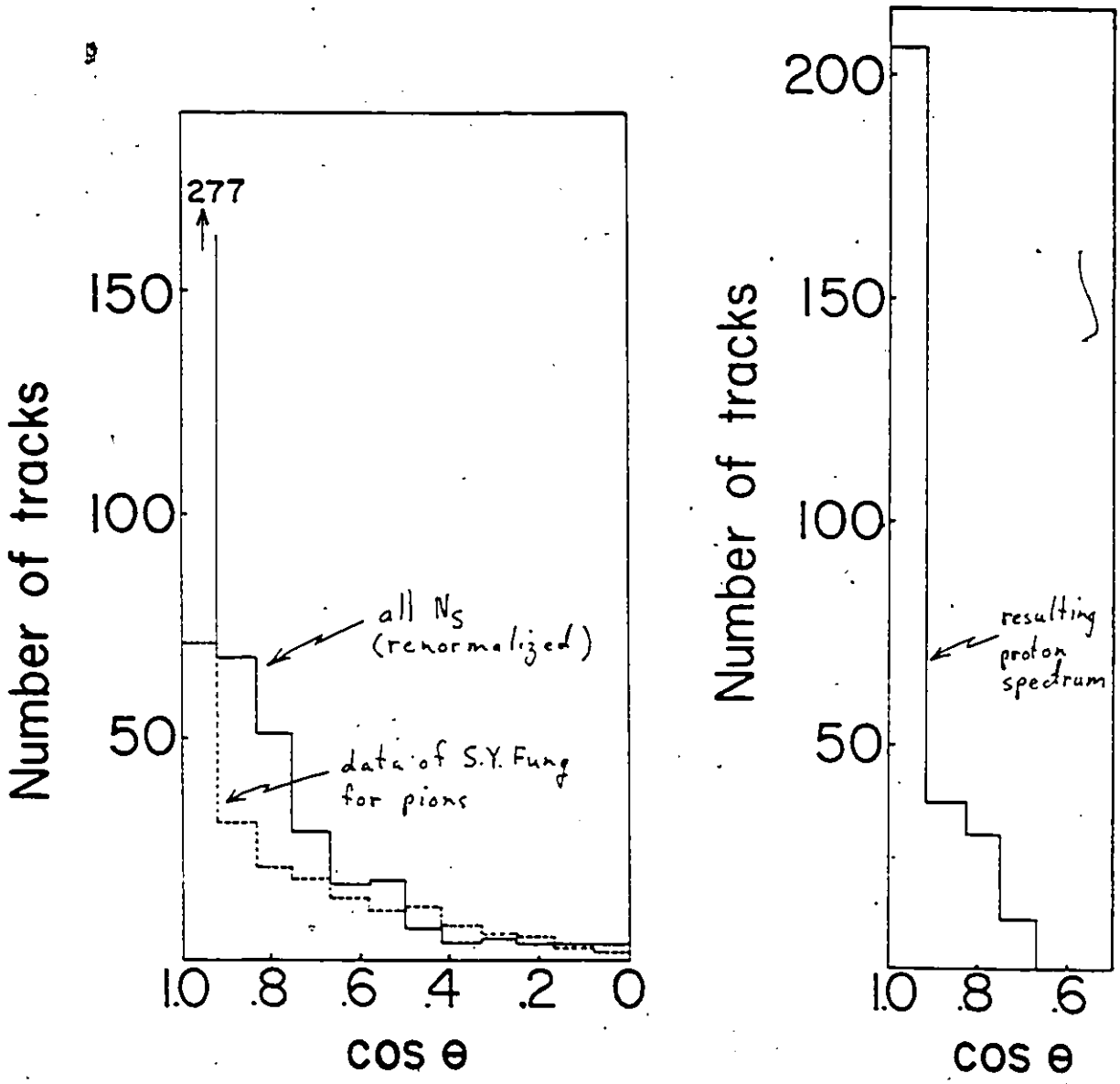

FIG. 2-23: Pion and Proton Dist. for Heavy Targets

Figure 2.23 shows a cos θ distribution for the heavy target group along with the pion distribution (multiplied by

1 + Z/(A-Z))for Ar incident on Pb_3O_4, renormalized such that both distributions contain the same number of tracks above 45^o, which are only pions. The difference between the two histograms accounts for 283 tracks. The total number of pions is 204, giving a ratio of protons to pions equal to 1.39, compared to the expected ratios of $\langle N_p \rangle_{Ar} / \langle N_s \rangle_C = 1.29$ for the heavy group. The resulting proton angular distribution is also shown in figure 2.23, and it may be seen that 86% of the protons are contained within a 30^o cone.

2.8. Pseudo-rapidity Distributions

Angular distribution of shower particles are very often presented in terms of the variable η_L = ln cot /2, known as the pseudo-rapidity. It is related to the longitudinal rapidity $y_L = 1/2 \ln[(E + p_{//})/(E - p_{//})]$. An essential feature of rapidity is that it transforms the relativistic transformation of velocities into a simple addition of rapidities. Rapidity relates 2 longitudinally moving frames by a simple translation along the rapidity axis. Therefore distributions in y_L have Lorentz invariant shapes.

The η_L distributions for all events and those for the light and heavy groups are shown in Fig. 2.24, 2.25 and 2.26 respectively. The right end of the diagrams correspond to the rapidity of the incident ion, while the left end corresponds

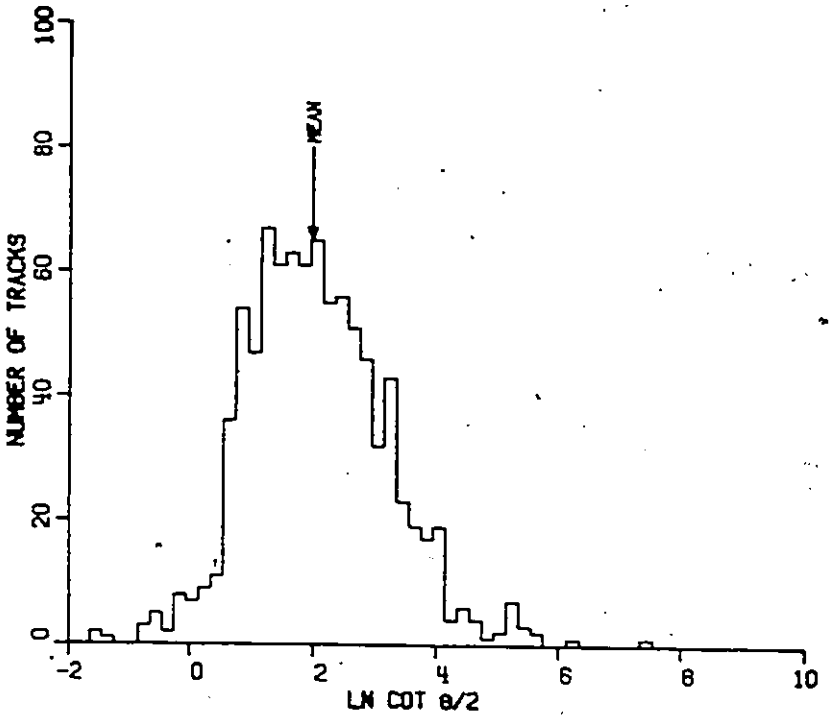

FIG. 2-24: Pseudo-rapidity for all Events

to backward moving tracks. The difference between the histograms is evident. One can see the shift in the centers of the distribution towards high rapidity for small stars and towards low rapidity for large stars, indicating the relative difference in the velocities of the emitting systems in both types of interaction (i.e. when a collision involves many nucleons, the interaction region moves more slowly).

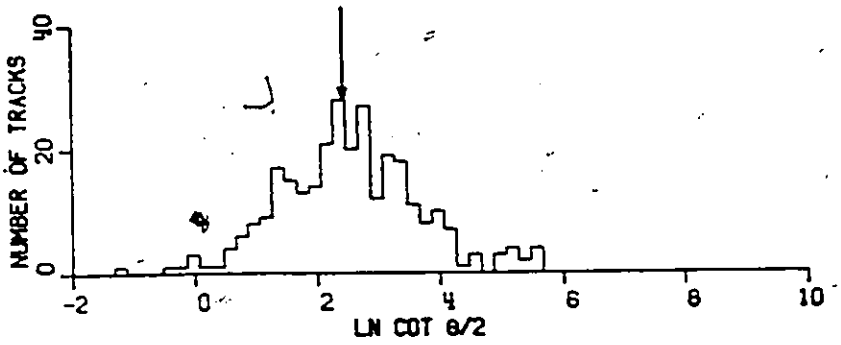

FIG. 2-25: Pseudo-rapidity for Light Targets

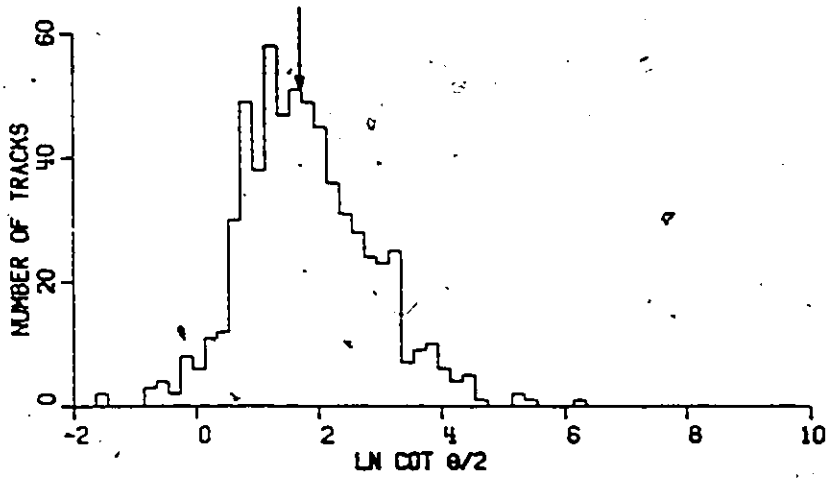

FIG. 2-26: Pseudo-rapidity for Heavy Targets

We have included a further diagram, Fig. 2.27 which compares the rapidity of our highest multiplicity event to that of the whole sample. Thus a highly central and very inelastic collision has an emitting system which moves quite slowly compared to the original velocity of the projectile.

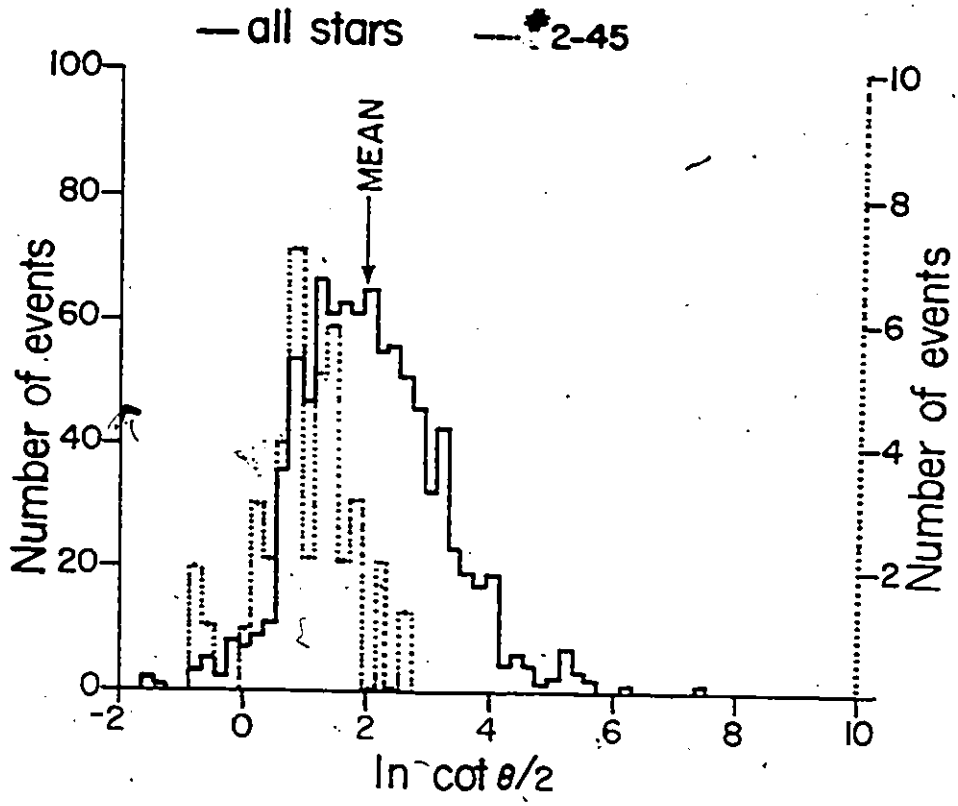

FIG. 2-27: Pseudo-rapidity of a Very Inelastic Event

3. CHAPTER 3. THEORETICAL MODELS

3.1. Model types

The theoretical description of heavy ion reactions should suggest what possible novel effects might occur in hot dense nuclear matter while at the same time provide insight into the general patterns in which the reactions evolve, as well as provide broad and systematic description of various experimental data. It would seem that the best possible solution might be arrived at with a relativistic quantum field theory of nuclear interactions. However any interaction with as many degrees of freedom as a nucleus-nucleus collision generates rather formidable obstacles to the solution of such a model. One generally has to settle for much less, and confine the number of degrees of freedom to those required to determine observables of concern.

With this in mind, several theoreticians have developed groups of various solutions dealing with the prediction of observables and the suggestion of new phenomena. There are thus a multitude of different models for describing relativistic heavy ion collisions, but most of these may be regrouped into three broad classifications. There is the macroscopic type of approach, characterized by the underlying assumption that the fundamental features of heavy ion interactions can be described in terms of parameters which

define the macroscopic properties of general colliding systems. Members of this class are essentially geometric in nature, and are exemplified by the hydrodynamic [28,29] and statistical or thermodynamic [30] types of models, such as the fireball [31,32] and firestreak [33,34] models. Secondly, there is the type of model which exploits the microscopic nature of the constituents involved in the interactions. Here the underlying assumption is that the elastic or inelastic scattering of two fast ions can be related to the scattering of the various constituents out of which these complex objects are made. This type of model is exemplified by the cascade model [35,36], and to some extent by nuclear QCD [37]. Other models belonging to this class are the multiple scattering models such as 'rows on rows' [38] and 'collective tube' models [39], which are essentially dynamical in nature. The last general category is the direct interaction type of model, such as the knock-out [40,41] and hard scattering models [42]. Although similar to the last class, this group considers the individual nucleon-nucleon collisions, and assumes single-scattering. These models really consider the results of heavy ion collisions as being due to the effects of individual nucleon collisions. Some success has also been obtained with classical type models, where the classical equation of motion approach is taken [43,44,45]. These general

types of categories will be further discussed later in this chapter.

While actual experimental data from accelerators of GeV range heavy ion beams have only been available for about a decade, it can be seen that a large number of models has come out to deal with the new physics. One can understand the diversity of the models that have been used and developed because of both the complexity of the interactions, due to the large number of participants, and because of the transfer of several models from particle physics, and their hybridization with nuclear physics models.

The new physics we are dealing with requires the amalgamation of a group of highly complex and compound ideas from other, often seemingly unrelated areas of physics. Relativistic heavy ion beams have allowed us to probe into areas of phase space not previously available. The most prominent theoretical approaches to heavy ion interactions are in general extensions or modifications of models meant to deal with simpler hadron-hadron interactions. A fundamental difference with particle physics is the possibility of depositing large quantities of energy into large volumes, rather than into ever vanishingly small volumes. Heavy ion interactions introduce an extra degree of freedom by allowing the baryon number of both the target and the projectile to vary. This should put additional constraints on the models

and allow one to obtain more information on the nature of hadron-hadron collisions. There is also the possibility that heavy ion interactions will demonstrate nuclear democracy. This has been conjectured by G.F.Chew [46] who said that "whenever the available energy becomes large there should be manifested general strong interaction characteristics that are independent of baryon number B. None of the known hadrons, after all, can be regarded as elementary, the composite nature of any hadron becoming more and more prominent as the energy increases." There are certain experimental distinctions between B= 0 or 1 and B>1 systems such as energy spacings, but Chew maintains that most of the experimentally measured parameters vary rather smoothly with baryon number.

A fundamental difference with nuclear physics is the possibility of compressing nuclear matter to densities comparable to that of neutron stars, or even greater. Because of this, one requires a broad range of models to deal with various aspects of the information obtained from the collisions, each model tuned to a particular aspect being investigated

However, out of all the available models, a few have distinguished themselves by the clear nature of their original hypotheses, their simplicity and their broad range

of coverage of the experimental data. Others, of a more speculative nature, have provided guidance for the type of experiments to be performed, as well as for the new and exciting results which could be obtained. It is in fact one of the speculative models which provided the original impetus for the present experimental investigation. The model in question is that of T. D. Lee and G. C. Wick [5,47].

3.2. The speculative models

3.2.1. Abnormal nuclear states. (ANS)

Several theoreticians have been involved in the ANS models, but foremost it was T.D. Lee's original ideas which gave the initial guidance. A simple quasi-classical model of the nucleus which assumes only the existence of a 0+ isoscalar field, sigma, yields a stability zone at a mass number equal to 400 or more. This meson field ϕ has an associated particle mass m_ϕ, and an expectation value $\langle\phi\rangle = 0$ outside the nucleus, where the nucleon mass appears as m_N. But inside the nucleus, the effective nuclear mass is determined by

$$m_{eff}^2 = [m_N + g\langle\phi\rangle]^2 \qquad (3.1)$$

where $\langle\phi\rangle$ is the expectation value of ϕ inside the nucleus

and $g^2/4\pi \simeq 15$

Thus for certain values of $\langle\phi\rangle$, the effective mass of the nucleon goes to zero inside the nucleus, and the nucleus becomes abnormal.

Using the more specific sigma model for the meson field which is composed of the iso-vector pion field and the iso-scalar sigma field, we have

$$\phi = \pi - (m_N/g) \tag{3.2}$$

The nucleus is assumed to be a degenerate Fermi gas, with top Fermi momentum k_F. We thus have a kinetic energy density U_N given by

$$U_N = 2\pi^{-2} \int k^2 (k^2 + m_{eff}^2)^{1/2} \, dk \tag{3.3}$$

In the simple case where the number of protons and neutrons is equal, we also have k_F related to the nucleon density n by

$$k_F = (3\pi^2 n/2)^{1/3} \tag{3.4}$$

If nuclear matter may be considered an incompressible

fluid (because of a strong repulsive force) then the nucleon density may be fixed, giving the total energy density D of the system as

$$D = U_N + U_\sigma - n m_N \qquad (3.5)$$

where U_σ is the potential energy density of the sigma field

For very large nuclei the surface energy can be neglected. When the energy density is plotted at various fixed densities, starting at $n = 0$, the function has a minimum at $m_{eff} = m_N$. See Fig. 3.1. Increasing the density to $n = n_0 = [(4\pi/3)(1.2\ fm)^3]^{-1}$, corresponding to a unit energy density of 5.2 GeV/nucleon, a local minimum of D appears at $m_{eff} = 0$, and the main minimum decreases to $m_{eff} = 0.8\ m_N$. If the nuclear density can be further increased to exceed a critical value n_c, then the abnormal state becomes the absolute minimum state.

The conditions for the production of such abnormal nuclear states are $N^{1/3} >> 1$ such that surface energy may be neglected and $n > n_c$. It is not exactly known what the value of n_c should be, but it is a function of m_σ and g, neither of which are definitely known. Using a meson mass of 1.15 GeV and the value given previously for g, one expects high energy

heavy ion collisions between large nuclei such as lead on lead at 1/2 GeV/nucleon in the center of mass to approximately double the nucleon density, and possibly

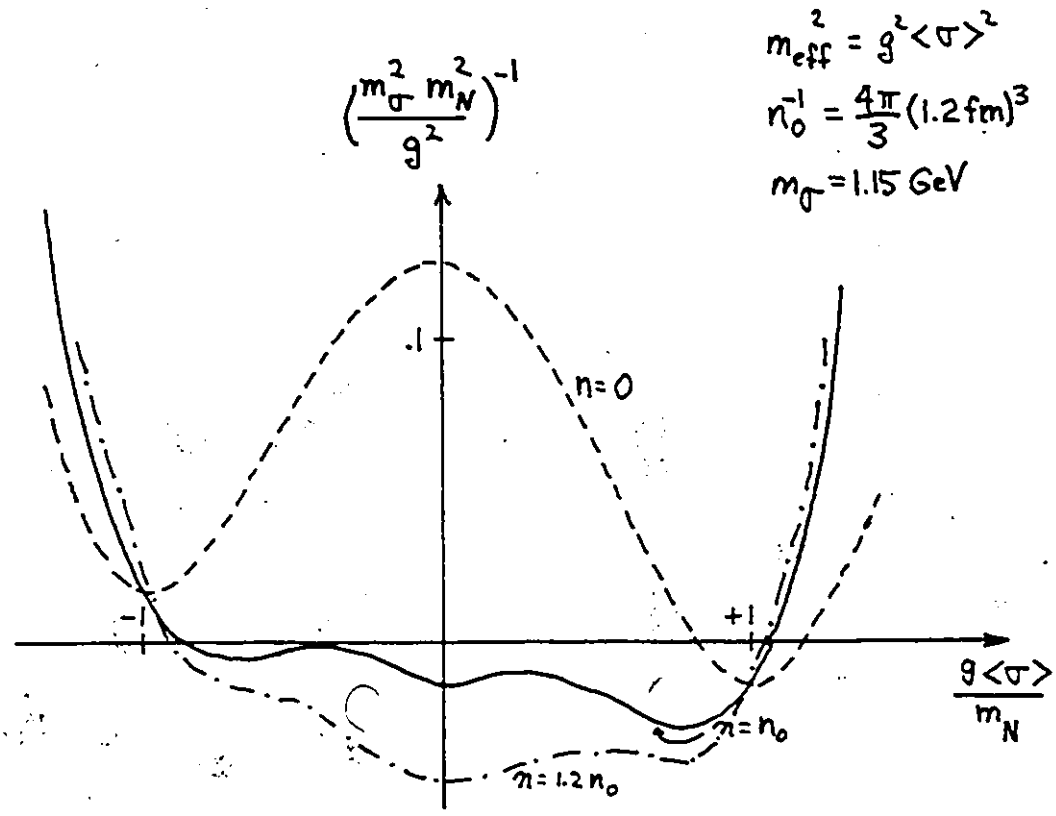

FIG. 3-1: Energy density in the σ model

As n is increased above n_0, the local minimum at $m_{eff} = 0$ becomes the absolute minimum.

produce abnormal nuclear states, at least for a brief period of time, if they are not completely stable. This is providing that the meson mass is not much larger than 1 GeV.

An immediate experimental signature for such an occurrence in emulsion would be a track exiting a collision with more ionization than the track that produced the collision. While it may be fortuitous to expect such a simple and obvious signature for the possible fusion of two very heavy nuclei, one should be on the lookout for certain resonance effects in particle production associated with these types of collisions, which could signal a metastable coupling of two heavy nuclei. The actual conditions for the formation of ANS are certainly far more difficult to achieve than would appear from the simple picture presented above, but it is a good starting point.

Another very interesting possibility is the collision of an ANS with another normal nucleus. Depending upon the type of potential $U(\phi)$, there may be two local minima for this potential, rather than just one for the standard sigma model. Assuming this second local minimum occurs at $\phi = \phi_{vex}$. It is possible that in the collision, a state may be produced with $\langle\phi\rangle = \phi_{vex}$ inside a volume V, and its mass would be given by

$$M_{vex}^2 = [\, V\, U(\phi_{vex}) + \text{surface energy}]^2 \qquad (3.6)$$

The baryon number of this vacuum excitation is zero,

and this whole state may be viewed as a gigantic meson blob, with a linear dimension $V^{1/3}$, much larger than any of the usual microscopic lengths of nuclear physics. Since a large contribution to the mass would come from the surface, these vacuum excitations could decay by contracting their surfaces through meson emission.

Although these are highly speculative proposals, it is possible that if these states can be formed, some of the symmetry properties may be changed inside these ANS, as well as some of the basic forces, notwithstanding changes in the properties of the vacuum itself.

3.2.2. Quark-Gluon Plasma

An alternative but somewhat similar idea comes from quantum chromodynamics (QCD). As was mentioned in the introduction, it is more likely that nucleus-nucleus collisions will allow the deconfinement of quarks and gluons rather than hadron-hadron or hadron-nucleus collisions. If one looks back to the discovery of the nucleus, it was the particles scattered at large angles which gave the most new information about the interaction, in this case Rutherford scattering. These high p_T particles gave information about the 'hard' component in the atom, and defined the structure of the atom. Much more recent experiments at SLAC in the

early 1970's showed an excess component of widely scattered electrons impinging on protons, and this gave rise to the parton model. Objects inside the proton were about a fiftieth of the size of the proton, and this graininess inside the proton could be assumed to cause the observed scattering. While nucleus-nucleus collisions do not look at the structure of individual hadrons, and the graininess of the nucleus is well understood from nuclear physics, similar effects might be expected if the graininess of the nucleus changes from that due to nucleons to that due to quarks.

This phase transition could occur if the nucleons are brought closer together in the nucleus. Such an increase in density might likely occur in a relativistic heavy ion collision. If this density exceeds a certain critical density n_c, where the nucleons are brought so close together that the normal boundaries of the 'bags' which confine the colour force begin to overlap, then the boundaries may disappear, thus liberating the quarks and gluons inside the nuclear volume, forming a quark-gluon plasma [48]. Scattering from such an object would likely have an excess of high p_T components due to the direct interaction with the quarks. Although physicists have had to become comfortable with the idea that quarks are never liberated, we have the possibility of at least deconfining the quarks in a volume much larger than

that of a hadron. The exact conditions under which this happens seem to be at least partly defined: 1. As the projectile nucleus traverses the target nucleus, sequential encounters between the nucleons compress the target by giving its nucleons a velocity v, and in the target's rest frame, the compression $C = \gamma(1 \pm v)$; 2. If one assumes that each of the A nucleons generates pions, then the energy density per nucleon in the rest frame of the target nucleus will be E/N = 3-4 GeV/nucleon, for very heavy nuclei colliding at ISR energies [1,49]. This gives rise to a longitudinal momentum for the target nucleons such that $\gamma = 2$. With a normal nuclear density $n_0 = .15$ GeV/fm^3, one can estimate the energy density e obtained in such a collision

$$e = n_0 \, C \, E/N = 2 \text{ GeV/fm}^3 \qquad (3.7)$$

Such an energy density is expected to produce the phase transition [4,37,50]. 3. It will be possible to obtain this large energy density if the multiplicity of pions is proportional to A, and this is fundamental, for it is the effect of a very large number of pions in a compressed nuclear 'space' which can allow enough heating of the nucleus. The required temperature would be in the range of 150-200 MeV, and this would not be achieved if the pion multiplicity only increases as $A^{2/3}$. In this case, there

would not be sufficient pions to cause a 'freeze-out', which occurs when there is not enough free space in the nucleus to accommodate the volume of all the individual hadrons.

The heating associated with pion production can be easily visualized in rapidity space.

$$y = - \ln (\tan \theta/2) \qquad (3.8)$$

When viewed in the rest frame of the central region, one may compare the y distribution expected for very high energy nucleus-nucleus collisions to that of nucleon-nucleus and nucleon-nucleon collisions, as in the next figure

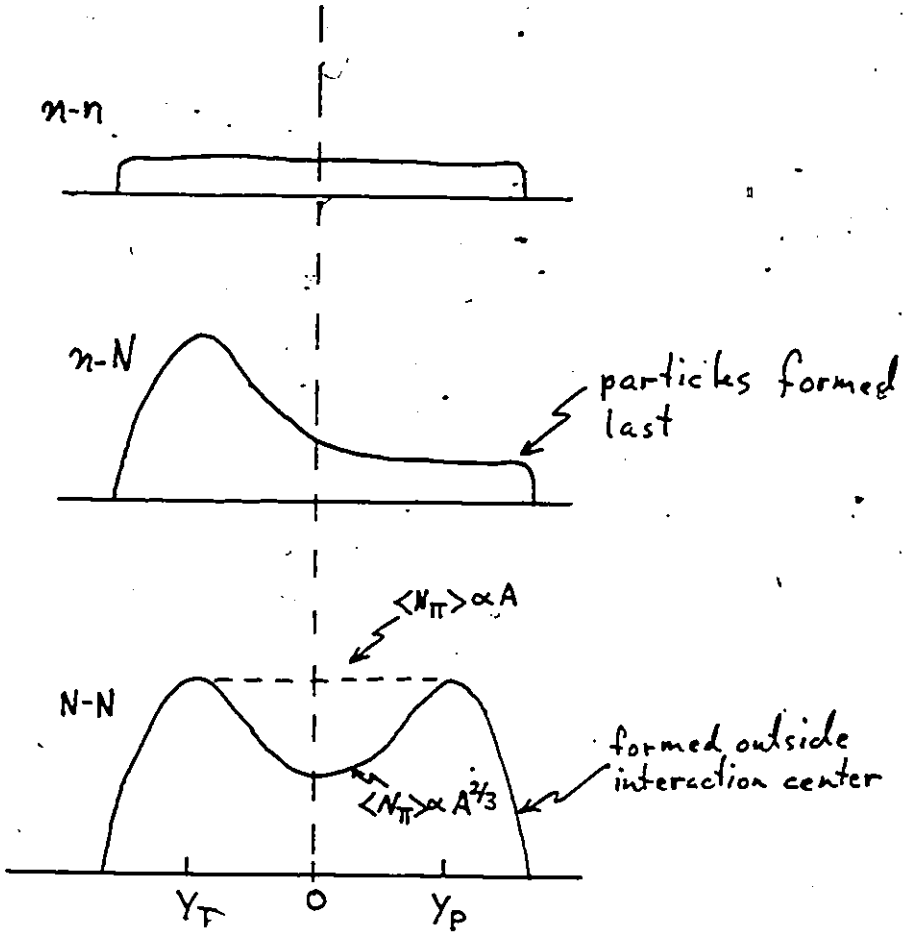

FIG. 3-2: Rapidity distributions of various collisions The top diagram is for a nucleon-nucleon system, which yields a flat y distribution with 2.4 created particles per unit y. The middle figure shows enhancement for the production in the target region in nucleon-nucleus collisions, with evidence of nuclear transparency. This is a consequence of the fast secondaries being produced outside the target. In the last diagram, we have a similar projectile and target distribution in the solid line. Pion production in the central region is expected to be proportional to A. and would be represented by the dashed line, causing substantial heating of the central region. ISR energies are assumed.

Aside from the observation of such rapidity distributions for very high energy nucleus-nucleus (A-A) collisions, one may expect some heavy flavour quark production if a quark-gluon plasma is formed [51]. A signal would be kinks or V's in an emulsion, with a production rate much larger than that normally expected for charmed particle production. Compressed quark matter might also have increased interaction length due to its smaller geometrical cross-section, if it is stable and can travel away from the collision site. There seems to be some experimental evidence for quark matter formation in the cosmic ray experiments of the JACEE collaboration, and possible signals might be observed at the energies involved in our experiment, but this is somewhat unlikely. However, the multiplicity and rapidity distributions, as well as the most inelastic events may yield some insight into the formation of this exotic material.

3.3. Macroscopic models

3.3.1. Hydrodynamic model

Most of the internal degrees of freedom inside dense nuclear matter are difficult to determine from first principles, and hence it becomes attractive to describe nuclear matter as a fluid, and to employ fluid dynamics to

describe the evolution of nuclear matter in collision. One of the first such descriptions was proposed by Landau [52] and has been used with great success in describing hadron-hadron as well as hadron-nucleus collisions [53]. In treating colliding nuclei, two major approaches are used.

A. The first is done using relativistic non-viscous fluid dynamics. Here the colliding nuclei are considered to form an equilibrated single fluid, with the inclusion of some phenomenological parameters. An equation of state is written and experimental data may be related to this equation. Typically, a reaction may be written as

$$A + B \rightarrow W(n,t) + X \qquad (3.9)$$

where n is the density and t is the temperature.

From hydrodynamics one gets the pressure $P = n^2 dW(n,t)/dn$ with the derivative evaluated at constant entropy. Since the form is not known for W(n,t), a comparison is made to experimental data to yield certain constraints, and the Euler equations for various models of W(n,t) are solved. W(n,t) is assumed to be of the form $W_0 + W_T(n,t)$ where the first term is the compression energy per baryon at t = 0 MeV, and the second term represents the thermal energy. This second term is assumed to be for an ideal Fermi gas,

while the compression term is given various forms to study the effects of different compressibilities. Thus the pressure is a sum of a compression and a thermal part. Comparison with experimental data shows very little sensitivity to the forms tried for W_0 for double differential cross sections. Additionally, there remain dicrepansies of the order of 2 to 3 with the data, a problem which is difficult to overcome because of the numerical complications encountered in solving the hydrodynamic equations.

Since at high velocities the constituents cannot instantly share the momentum and energy (between target and projectile), it is unlikely that the one fluid formulation described above will yield valid results for relativistic collisions.

B. Thus a second hydrodynamic approach is used where the two nuclei are treated as two separate fluids coupled together by a frictional drag [54]. The requirement for equilibration is somewhat reduced, but only large nuclei interacting at small impact parameters are likely to share energy in such a way that the non interacting parts in the collision reach equilibrium. In addition to this a third fluid must be added to deal with the mesons. In any case, large technical numerical difficulties remain and there has not been to date very good agreement between this type of

model and the data. It is probable that larger colliding systems such as U + U will provide a closer approximation to equilibration and increase the applicability of the hydrodynamic approach.

3.3.2. Fireball model

Again a geometrical picture of the nuclear collision is invoked, and to this picture one adds statistical thermodynamics. This has been one of the most successful models for predicting the results of processes occurring in the interaction region [30]. Nuclear collisions are treated by dividing the process into the participant and spectator regions, whereby the non-interacting regions of both the target and projectile nuclei are considered spectators to the collision, and are not treated further. To obtain the contribution of these spectator regions to the observed multiplicities, one assumes an increase in the surface energy of the resulting cut spheres, with subsequent evaporation of singly and doubly charged nuclei, at laboratory angles characteristic of the reference frame in which they are emitted. (A narrow cone for the leading projectile and isotropic emission for the stationary target. In effect, at E_k = 1.8 GeV, and for an average internal Fermi momentum P_F = 230 MeV, the projectile like fragments should be limited to less then 5° degrees in the forward direction, and the target

like fragments should have momenta below 230 MeV/c) [55,56].

Participating nucleons from the interaction region are assumed to form one or more fireballs, travelling at velocities intermediate to that of the two spectator regions. In the simplest one fireball model, one estimates the number of participating nucleons from the impact parameter b and the atomic numbers of the two colliding nuclei. This is equivalent to the intersection of a sphere and a cylinder, each with constant density and well defined radius. Typically one gets the number of participant protons or neutrons from the target or projectile by evaluating an equation like

$$N_{prot}(b) = \mathrm{Sum}(Z_i/A_i)N_i(b), \quad i = t,p \tag{3.10}$$

which must be solved by numerical intergration for each combination of target and projectile (t,p) atomic numbers [57]. The initial energy of the system is

$$E_{lab} = E_t + E_p = (m_0 + E_k)N_p + m_0N_t \tag{3.11}$$

And the momentum

$$P_{lab} = N_p(E_k[E_k + 2m_0])^{1/2} \tag{3.12}$$

from which one can calculate the velocity of the center of mass of the participant nucleons as measured in the lab,

$$\beta_{c.m.} = P_{lab}/E_{lab} \qquad (3.13)$$

This gives us the total energy in the center of mass of the fireball

$$E_{c.m.} = (E_{lab}^2 - P_{lab}^2)^{1/2} \qquad (3.14)$$

$$= \gamma_{c.m.}(E_{lab} - \beta_{c.m.}P_{lab})$$

$$= [(N_p + N_t)^2 m_0^2 + 2E_k m_0 N_p N_t]^2$$

For a collision of argon on argon at 0 impact parameter and E_k = 1.80 GeV, one obtains the following quantities

E_{lab} = 146.5 GeV, P_{lab} = 102.7 GeV/c

$\beta_{c.m.}$ = .70 and $E_{c.m.}$ = 104.5 GeV

It is assumed in the model that all of the projectile's participant nucleons transfer all of their momentum to the effective center of mass system of the participants. As at

Bevelac energies the average internal energy is much higher than the average binding energy, all of the nucleons are liberated. Here we have taken m_0 to be 939 MeV - 8 MeV(binding) = 931 MeV.

When the two regions completely fuse, all of the center of mass energy becomes available for thermalization. This fusion region is known as the fireball, and is treated as an equilibrated non-rotating ideal gas with a characteristic temperature T, which then expands isotropically with a Maxwellian distribution of energy. For a relativistic ideal gas of nucleons, the temperature T can be evaluated as [31]

$$E_{c.m.}/(N_p + N_t)T = 3 + mK_1(m/T)/TK_2(m,T) \qquad (3.15)$$

where K is a Macdonald function.

The energy per nucleon e available in the center of mass when considering baryon conservation is given by

$$e = E_{c.m.}/(N_p + N_t) - m \qquad (3.16)$$

and the non relativistic relation between e and T is

$$e = 3/2\ T \qquad (3.17)$$

with values of e = 370 MeV and T = 247 MeV for the last collision example. This is an overestimate, but gives the order of magnitude. However, in the fireball model, one can compute the temperature directly by employing certain conservation laws. From the geometry and kinematics, one knows that

$$E_{c.m.} = E_{prot} + E_{neut} + E_{pion} + ... \qquad (3.18)$$

and the charge Q is

$$Q = N_{prot} + N_{pion^+} - N_{pion^-} + ... \qquad (3.19)$$

with .... representing any other particles included in the calculation.

Baryon conservation is simply

$$N_b = N_{prot} + N_{neut} \qquad (3.20)$$

Assuming thermalization, we have the number of particles of any type

$$dN = \frac{gV}{(2\pi)^3} \frac{1}{e^{(E-u)/T} + 1} p^2 dp d\Omega \qquad (3.21)$$

an ensemble of fermions, with g being a spin degeneracy

factor, E the total energy available in the fireball, and u the chemical potential (Gibbs potential) of the particular type of particle. V is the volume of the fireball and its equivalent size is estimated to be slightly larger than a normal nucleus, since in the fireball model one assumes an initial compression of the nuclear matter, followed by an expansion to a larger volume, , at which point the matter disintegrates. A typical density of 0.12 nucleons/fm^3 is used in the calculations. Since $e^{(E-u)/T} >> 1$, we can use the approximation that

$$dN = e^{u/T} \frac{gV}{(2\pi)^3} e^{-E/T} p^2 dp d\Omega \qquad (3.22)$$

Thus for protons and neutrons, we get

$$N_{prot} = e^{u_p/T} \int \frac{gV}{(2\pi)^3} e^{-E/T} p^2 dp d\Omega \qquad (3.23)$$

$$N_{neut} = e^{u_n/T} \int \frac{gV}{(2\pi)^3} e^{-E/T} p^2 dp d\Omega$$

The energy of the particles in the center of mass is given by an expression like

$$E_{prot} = e^{u_p/T} \int \frac{gV}{(2\pi)^3} E e^{-E/T} p^2 dp d\Omega$$

A similar expression for E_{neut} then gives the total center of mass energy

$$E_{c.m.} = E_{prot} + E_{neut} \tag{3.25}$$

and since the left hand side of these equations is known, it is possible to solve these equations for the three unknowns, u_p , u_n and T. When this is done, the distribution degenerates to a Maxwell-Boltzmann distribution, whereby the resulting number of particle i can be simply represented by

$$N_i = e^{(u_i/T)} Z \tag{3.26}$$

where Z is the partition function for one particle.

Chemical kinetic equations are used to include particle production in the fireball. At Bevelac energies, the only particles of significant importance to include are the pions and the deltas. Using reactions like

$$\begin{aligned} n + p &\rightleftharpoons n + n + \pi^+ \\ n + n &\rightleftharpoons n + p + \pi^- \end{aligned} \tag{3.27}$$

and if one assumes that thermal as well as chemical equilibrium are reached, then the law of chemical equilibrium

defines a set of rules for chemical potentials. (Reif, F. Fundamentals of Statistical and Thermal Physics, p.312) Now at chemical equilibrium, we will have

$$u_n + u_p = u_n + u_n + u_{\pi^+} \qquad (3.28)$$
$$u_n + u_n = u_n + u_p + u_{\pi^-}$$

From which

$$u_{\pi^+} = u_p - u_n \quad \text{and} \quad u_{\pi^-} = u_n - u_p \qquad (3.29)$$
$$u_{\pi^0} = 0$$

The production of pions from the decay of the four delta baryon resonances are included with equations like

$$\Delta^{++} == p + \pi^+ \text{ giving } u_{\Delta^{++}} = 2u_p - u_n \qquad (3.30)$$

Decay of deltas accounts for about one third of the total pion production, and is thus quite significant. In order to obtain the total average multiplicity, <M>, of any given type of particle to compare with an exclusive measurement obtained in emulsion, the particle production must be found at each impact parameter b and the result summed over all impact parameters, such that

$$\langle M \rangle = \frac{\int N(b)\, 2\pi\, b\, db}{\int 2\pi b\, db} \qquad (3.31)$$

Composite particle production may also be included from reaction equations like

$$p + n + N \rightleftarrows d + N \quad \text{giving} \quad u_d = u_p + u_n \qquad (3.33)$$

for deuterons, with similar expressions for tritons and Z=2 composites. Fundamentally, only u_p and u_n need to be known, as well as T, and these can be obtained from the charge Q, the baryon number B and the total energy $E_{c.m.}$.

For counter experiments, which tend to make inclusive type measurements, the model can alternately give inclusive cross-sections, at various angles and momenta. In fact the great versatility of this statistical type of model is that it can simultaneously predict almost any experimental result, and has done so with very good success for certain types of results, notably for composite particle production. Unfortunatly, the model is not very good at predicting pion production, as this model routinely overestimates pion multiplicities by a factor of 2 to 3.

In an attempt to overcome this serious flaw, and some others, a different geometry has been introduced. This is

called the two fireball model, and it assumes that in any nucleus-nucleus collision, two fireballs are formed, each with a different velocity. The first fireball is projectile related, and travels with a high velocity, while the second is target related, and travels with a considerably lower velocity. This new geometry is introduced by recognizing the fact that neither the overlapping part of the target or the projectile loses all of its momentum after a collision, thus forming two fireballs. A new parameter must be introduced, and this is the fraction x of the initial momentum that remains after the collision. Usually, an ad hoc choice is made for x as a function of impact parameter, or data from p-p or p-nucleus collisions are used.

However, not all difficulties are resolved by this modification, since better agreement is obtained for the proton spectra [30] but no improvement is obtained in the pion multiplicity prediction. This overestimation of pion production seems to be a universal feature of statistical thermodynamic models. Certain suggestions have been made such as the fact that thermal equilibrium is likely achieved, but chemical equilibrium is not for the pions. Possibly the pions are generated only at the surface of the fireballs, rather than throughout the entire volume, with subsequently lower multiplicities due to the reduced amount of energy available

for production. A more plausible explanation might be that the assumption of constant energy expansion used in the fireball model might be incorrect. It could very well be that the expansion of the fireball is a constant entropy process, whereby the internal energy of the fireball decreases during the expansion. The internal energy lost during the expansion would appear as some form of collective energy in a hydrodynamic type of model [29]. A similar idea was the factor which allowed the great success of Landau's hydrodynamical model for nucleon-nucleon and nucleon-nucleus collisions. In that model, hydrodynamic considerations give the energy and angular distributions of the particles, while thermodynamic considerations give the number of particles since local equilibrium is assumed, and the number of particles decreases as the volume expands isentropically.

3.3.3. Firestreak model

A model similar to the fireball model in that it is a statistical thermodynamic model, but with a different collision geometry was originally proposed by Myers [34]. Nuclei are considered to interact in a manner such that thermalization occurs, but the regions which are thermalized are a series of streaks of hot nuclear matter. Instead of considering the interaction region as a whole, homogeneous

region, the firestreak model considers the material in the overlap region to be moving with velocities uniformly spread between those of the target and projectile. The material is thus drawn into a streak by the velocity shear across the overlap region. This is equivalent to treating the interaction region as a series of tubes, each with different velocity and number of nucleons contained within it. Diffuse nuclear surface functions can be utilized in this model, as opposed to hard sphere type geometry in the fireball model. Thermodynamic properties and the velocity of the streak depend only on the ratio η,

$$\eta = n_A/(n_A + n_B) \tag{3.34}$$

where n_A and n_B are the numbers of nucleons in the projectile and target respectively involved in the collision to produce the tube. The lab momentum space densities are calculated with the aid of a 'yield' function which essentially contains the geometry of the collisions, and with the Lorentz invariant momentum space density for each particle type produced. This latter function assumes a thermodynamic equilibrium for a Fermi or Bose distribution, with a temperature T and chemical potentials u, as in the fireball model.

Using a substantially different geometry, the model predicts the nucleon, pion and light nucleus inclusive spectra for a wide variety of projectile–target combinations, over a wide energy range [58]. To overcome certain errors in the predictions of proton spectra, different yield functions have been used [33] which incorporate both direct knockout processes and multiple collisions, relating to whether the diffuse surface is involved in the collision (leading to single knock out), or the central core of the nucleus is involved (leading to multiple collisions). However, in common with the fireball model, the firestreak model also overestimates the pion cross sections by a factor of 2.

3.4. Dynamical models

3.4.1. Rows on rows

In an attempt to treat heavy ion collisions in a microscopic way, Hufner and Knoll [38] developed the rows on rows model. It is a model in which the dynamics of the collision are followed microscopically, in a type of one–dimensional cascade. They consider both the projectile and target nuclei to be decomposed into rows of nucleons, with the rows oriented in the beam direction. Nucleons within any given row do not interact with each other. However, where one projectile row comes into contact with a target row, each

nucleon in the corresponding projectile row scatters by each of the nucleons in the colinear target row, thus interacting with each one of the nucleons in its path. Thus a sequential type of interaction is assumed, and this is equivalent to a cascade type of interaction, with the limitation that the cascade is unidimensional. The length of a row (and the number of nucleons within it) depends on the A of the nucleus and on its position within the nucleus.

It is of course a formidable task to follow the evolution of a nuclear collision by this method, especially for large nuclei. But as a nucleon does not really heat up a large nucleus in a n-A collision, and its interaction can be reasonably well described by Glauber [59] theory, it is only natural to extend this multiple scattering formalism to A-A collisions. The rows are therefore introduced, and they are spaced a mean free path $\lambda = \pi \sigma_{nn}$ apart, where σ_{nn} is the section area of each row, obtained from n-n experiments. Each nucleon is then followed through its transformations into various states, with the state of a nucleon at each stage of the reaction described by a momentum distribution function, $W^{P}_{mn}(p,i)$. Here p is the momentum, and n and m refer to the m th projectile nucleon after it has scattered with the first n nucleons in the target row. A corresponding distribution is associated with the target nucleons, i.e. $W^{T}_{mn}(p,i)$. The

label i refers to the inelastic excitations which occur such as the baryonic resonances. The calculation proceeds by taking the previous probability distribution as an input for the next stage of the collision, with the result that the final momentum distribution is obtained at the end of the collision. Thus the cross sections for proton and pion production can be calculated, yielding a typical integrated cross section of

$$\sigma_{\pi} = w_{\pi} (A_P \pi R^2_T + A_T \pi R^2_P) \qquad (3.35)$$

It is assumed in this model that all pion production comes from the decay of delta resonances. The model also does not account for the production of composites, which is a serious limitation. The general result of this model is in reasonable agreement with the data for relativistic collisions, and also the momentum distributions approach Maxwell distributions, equivalent to thermalization, a surprising result from a dynamical calculation.

3.4.2. Collective tube model (CTM)

In a similar fashion to the rows on rows model, the CTM model assumes independent collisions of several tubes of nucleons. Each nucleus is thus decomposed into a series of

tubes, each of radius equal to that of one nucleon and of length depending on its position in the nucleus. The novelty of this model is that it essentially treats the tubes as individual particles, rather than as being composed of individual particles. The authors [39] consider that for relativistic collisions, when observing each of the nuclei in the center of mass frame, they will both appear as Lorentz contracted disks, and that the collisions of colinear disks are equivalent to elementary particle collisions, with each collision independent from the others.

In a collision involving two elementary particles, one could calculate the pion multiplicity from the energy available for production. (i.e. the hydrodynamic model gives the pion multiplicity as $ks^{1/4}$) [60] Thus an evaluation of s, the total center of mass energy, should give us the pion multiplicity in a heavy ion collision. Due to the low energy of present A-A collisions compared to n-n or n-A collisions, one must include the effect of the rest masses, especially since we are grouping several hadrons into one 'elementary' particle. For an n-n collision, the available energy Q is

$$Q = s^{1/2} - (m_1 + m_2) \qquad (3.36)$$

where m_1 and m_2 are the masses of the interacting hadrons. Equivalently, in the CTM model, there are i_1 and i_2 nucleons

in each tube, giving Q as

$$Q = \left(m^2 \left(i_1^2 + i_2^2 \right) + 2mi_1i_2E_k \right)^{1/2} - m\left(i_1 + i_2 \right) \tag{3.37}$$

where E_k is the kinetic energy per nucleon. The multiplicity of pions is now obtained from n-n collisions at this value of Q. Taking an average of the probabilility P(n_,b) of producing n_ pions in a collision with impact parameter b, over all impact parameters, we get Pn_, the probability of producing n_ pions in a nucleus-nucleus collision.

$$Pn_ = \frac{\int d\sigma(b) P(n_,b)}{\int d\sigma(b)} \tag{3.38}$$

For A-A collisions, we have

$$\int d\sigma(b) = \sigma b^2 = \sigma_{PT} \text{ for } b<b_{max}$$
$$= 0 \text{ otherwise} \tag{3.39}$$

Here P and T refer to the projectile and target. We now obtain

$$Pn_ = \frac{\int d\sigma(b) P(n_,b)}{\sigma_{PT}} \tag{3.40}$$

and using Poisson distributions for Pn_-, the average pion multiplicity is found

$$\langle n_- \rangle_{PT} = n_- Pn_- = \frac{\sigma_{pP}\,\sigma_{pT}}{\sigma_{pp}\,\sigma_{PT}} \langle n_-(Q) \rangle_{pp} \qquad (3.41)$$

Using the Bradt-Peters formula for the cross-sections

$\sigma_{xy} = \sigma_{pp}\,(x^{1/3} + y^{1/3} - d)^2$ we get

$$\langle n_- \rangle_{PT} = \frac{P^{2/3}\,T^{2/3}}{(P^{1/3} + T^{1/3} - d)^2} \langle n_-(Q') \rangle_{pp} \qquad (3.42)$$

where $Q' = Q(P^{1/3}, T^{1/3}, E_k)$

Typically, a parametric equation is used for the p-p pion multiplicity, such as

$$\langle n_- \rangle_{pp} = 0.25 + 0.17 \ln Q + 0.25 \ln^2 Q \qquad (3.43)$$

Unfortunately, this model is limited to predicting only particles produced in p-p collisions, but this does not detract from its remarkable agreement with experiment in the prediction of pion multiplicities [39]. It should be remembered that there are no free parameters in this model.

3.5. Summary

While we have described some of the models for heavy ion collisions, we have by no means covered the exhaustive list available. Little mention has been made of knock-out nucleons, cascade or classical types of models, nor of the attempts at quantum mechanical description.

The models we chose to describe are considered to be representative of the most intense activity in the theoretical community. Great similarities exist between some of the models, at least in some of their basic premises (thermodynamics, geometry, etc.) but there are also many differences in detail, which add up to create significant overall differences between the models. The fact that many of these give similar predictions leaves one wanting for a more precise model, but this is just a reflection of the great many degrees of freedom in a nucleus-nucleus collision.

From the standpoint of simplicity, the thermodynamic type of models are the most likely candidates to describe the overall picture, but their assumption that thermalization occurs, whereby the energy is randomized, for systems consisting of only a few nucleons is far from ideal. They do however provide the opportunity of at least calculating almost any observable desired, and this is the main reason for their popularity and extended development.

The largest part of the interest should be reserved for the speculative models, as it is these models which will provide predictions about the phenomena from which we are likely to learn the most.

4. CHAPTER 4. COMPARISON BETWEEN THEORY AND EXPERIMENT

4.1. Introduction

In the previous chapter many of the more common theoretical models for relativistic heavy ion collisions were described, without however presenting many of the theoretical predictions. It is the purpose of the present chapter to present several of the theoretical predictions, in as much as they are related to the present experimental investigation. This will allow us to draw some conclusions related to the validity and applicability of these models, their fortes and weaknesses, while at the same time presenting an analysis of our data. As most of the models have been applied to predicting data for inclusive experiments, especially double differential angular cross sections, much of the literature providing comparisons between data and theory cannot be easily applied to the present case. Where comparisons are made to other types of interactions such as n-A collisions, every effort is made to compare quantities which closely correspond to one another.

Due to the composite nature of the spectra presented in the chapter on experimental results, it is often difficult to relate predictions on specific particle production from well defined projectile-target combinations. Many averages must be performed, since emulsion is composed of several target

nuclei, and we have no concrete momentum information. Different particles are included in most of our multiplicity distributions, necessitating that averages be taken over the production rates of many individual particles. We will rather be concerned with average multiplicities, correlations between these and general angular emission patterns. It is possible to perform some target separation, allowing comparisons with the more common type of theoretical predictions, done invariably for specific target nuclei.

4.2. The CTM Model

Predictions obtained in this model are for the charged pion multiplicity only, as formulated in ref. [39], and the nucleon spectra are not considered; neither for the target, spectator or the interaction region. Here the distinction between the various regions is very clear cut due to the tube geometry involved, and the model is this sense similar to the fireball model, where clean cylindrical cuts are assumed. With its fundamental dependence on the proton-proton cross section, the model gives a very simple framework in which to evaluate the pion multiplicities for any projectile-target combination, at a variety of energies. We present the results of calculations of the various pion multiplicities expected

for our experiment, as a whole for emulsion and for the various groups, in table 4.1. Emulsion may be considered as a composite material with the following ' chemical ' formula using data from table 2.1

$$Em \equiv H_{.41}\ C_{.18}\ N_{.04}\ O_{.12}\ Ag_{.13}\ Br_{.13}$$

By using weighting appropriate to the interaction cross sections of each element contained in emulsion, we can predict the pion production for any group of elements. We have used Eq.(10) from [39] since the inclusion of nuclear density functions obtained in electron scattering changes the results obtained by only 5%, and the error on the proton-proton pion multiplicities used yields an error of the order of 20%. Using the observed multiplicities from tables 2.2 and 2.3, and assuming our separation according to $N_h c$ gives us the multiplicities for HCNO as that for the light group and for AgBr as that for the heavy group, we find remarkable agreement between the model predictions for the total charged pion multiplicity and our results for $\langle N_s \rangle_c$.

TABLE 4-1: CTM Model Predictions and Experimental Results

(^{40}Ar projectile with E_{tot}/nucleon = 2.74 GeV)

Element	$\langle N_{\pi^-} \rangle$	$\langle N_{\pi^\pm} \rangle$	Exp. $\langle N_s \rangle_c$
^{1}H	0.29 ± 0.06	0.53 ± 0.11	
^{12}C	1.23 ± 0.25	2.24 ± 0.45	
^{14}N	1.31 ± 0.26	2.38 ± 0.48	
^{16}O	1.38 ± 0.28	2.51 ± 0.50	
^{80}Br	2.57 ± 0.51	4.68 ± 0.94	
^{108}Ag	2.92 ± 0.58	5.31 ± 1.06	
Em	1.95 ± 0.39	3.55 ± 0.71	3.70 ± 0.25
HCNO	0.96 ± 0.19	1.75 ± 0.35	1.68 ± 0.14
AgBr	2.76 ± 0.55	5.02 ± 1.00	5.80 ± 0.44

In fact the multiplicities are reproduced to within 13% for AgBr and within 4% for both emulsion as a whole and the HCNO group, well within the experimental and theoretical errors. Similar excellent predictions have been obtained for counter experiments [18]. The usefulness of this model for calculating pion multiplicities and spectra for a very wide range of possible collisions is evident from the success of its predictions. It is possible to examine the variation of the multiplicity in terms of the energy in the collision, the atomic number A_T of the target ,and its sensitivity to the expression used for the A_T A_P cross section (namely the value

of d in equation 3.42). A plot of the energy and A_T dependances for an ^{40}Ar projectile is shown in figure 4.1.

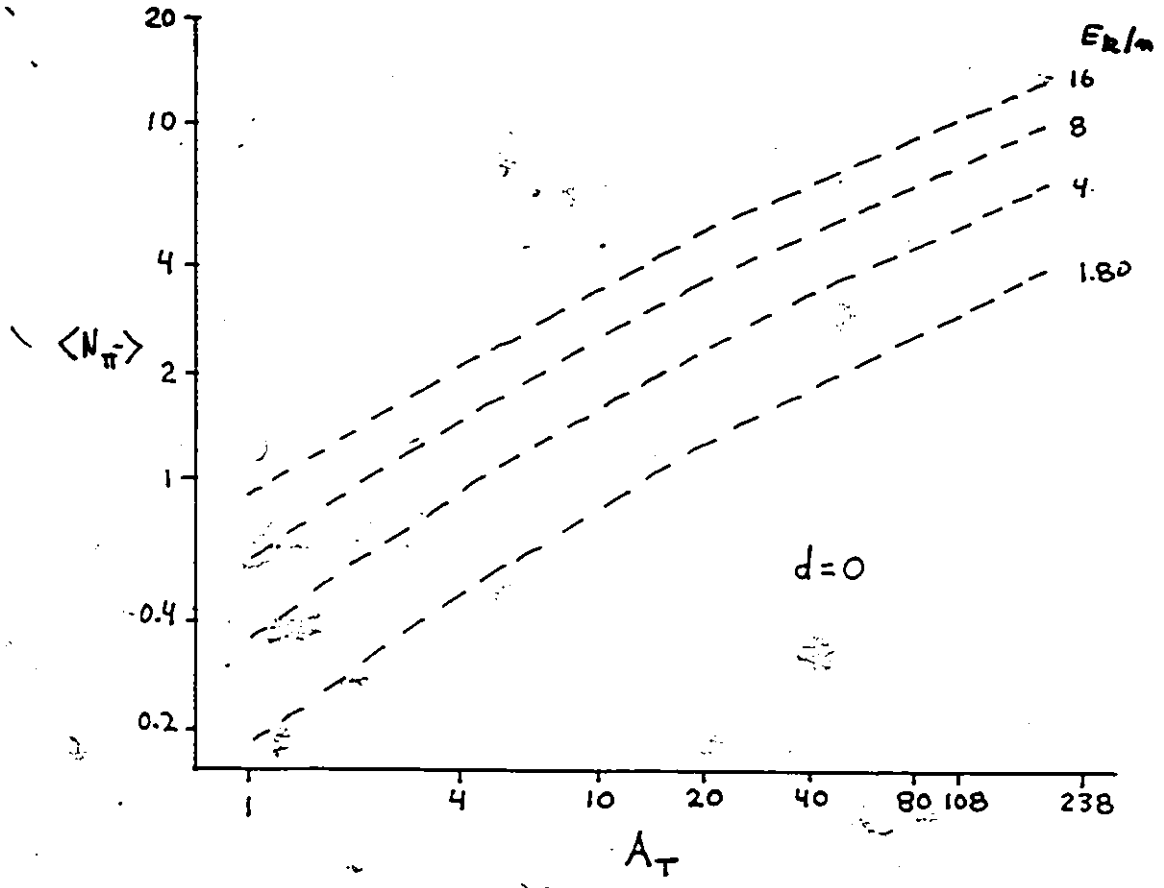

FIG. 4-1: CTM Predictions for various A_T and E_k/n

All the curves for different energies are approximately parallel, showing an almost logarithmic increase in the pion production as the kinetic energy is increased, and a similar power law variation is obtained for A_T. For the particular projectile used, we get an approximate relationship of $\langle N_\pi^- \rangle$ to A_T for $A_T > 10$ as

$$\langle N_{\pi^-} \rangle = 0.42\, E_k^{1/2}\, A_T^{0.38} \qquad \text{using } A_P = 40 \qquad (4.1)$$

This simple relationship holds valid for E_k above 1.8 Gev and provides results generally agreeing with the CTM model to better than 10% in most instances. One of the sensitivities of this model remains and that is the sensitivity to the value of d, the parameter compensating for the lack of interaction in a grazing collision. While the curves shown in fig 4.1 are for d = 0, similar curves are obtained for other values of d, depending on whether a constant value or an expression is used, such as that used in table 4.1

$$d = 1.0 - 0.028\, A_{min}(A_P, A_T) \qquad (4.2)$$
$$= 0 \qquad \text{for } A_{min} > 30 \text{ to } 40$$

This relationship has been plotted in figure 4.2 for an argon projectile of 1.8 GeV/n at various A_T for different values of d. This shows the sensitivity to the A-A cross section used in the geometrical factor for the CTM model.

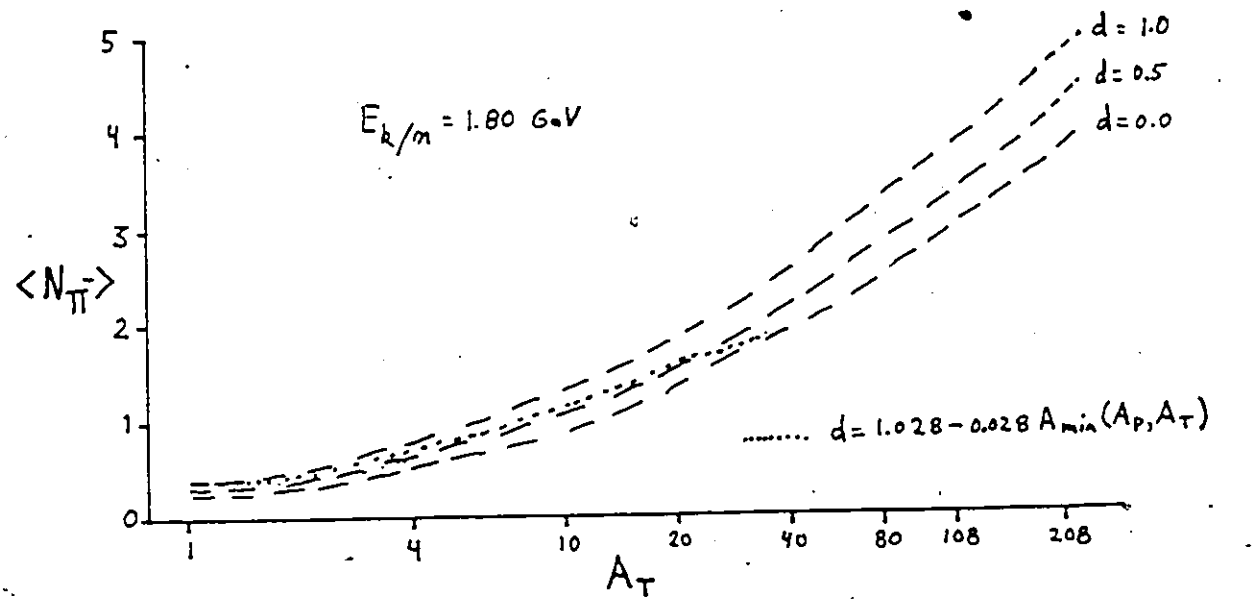

FIG. 4-2: Effect of d on the CTM Predictions

It can be seen that the effect of d is to increase the predicted multiplicity as d increases, particularly for large target nuclei. The increase is of the order of 20% as d varies from 0 to 1. One can thus consider that the choice for the parameter used for the A-A cross section is only of minor importance, and that the results of the model are valid in any case. The model assumes that Poisson distributions can be used to describe the p-p multiplicity distributions, and this is valid up to 70 GeV [62].

Due to the structure of the model, it is not possible to obtain the angular distributions for A-A collisions, but we are confident that our charge and target separations are

consistent, and that further emulsion studies could be carried out using similar techniques.

4.3. Predictions of the Fireball Model

While the previous model obtains its results from a dynamical calculation, using a geometrical factor to differentiate A-A collisions from p-p collisions, the fireball model uses geometry to obtain the available energy, charge and baryon number to yield a statistical description of the interaction process. By this means, the model is far more complete since it treats all particles, not just the mesons.

A calculation of the number of particles generated by the interaction region of the collision has been performed for the present experiment according to the model in ref. [30] for unequal mass ions. The detailed results are presented in table 4.2 for the collisions of ^{40}Ar with ^{12}C and ^{108}Ag, and the general results for the pion multiplicities in table 4.3 are compared to our experimental data. Table 4.3 is presented in a similar fashion to table 4.1, and both sets of results may be compared. The model assumes that the ratio of negative pions to positive pions is the same as the neutron to proton ratio for the interacting system.

TABLE 4-2: Fireball Calculations for ^{12}C and ^{108}Ag targets

(an ^{40}Ar projectile with 1.80 GeV/nucleon is used)

Temperature and velocity of the fireball

	one fireball		two fireball			
A_T	$\langle T \rangle$ (MeV)	$\langle \beta \rangle$	$\langle T_T \rangle$ (MeV)	$\langle \beta_T \rangle$	$\langle T_P \rangle$ (MeV)	$\langle \beta_P \rangle$
^{12}C	106	.77	87	.55	105	.87
^{108}Ag	107	.73	92	.59	107	.84

Multiplicities from the interaction region

one fireball

A_T	$\langle N_{\pi^-} \rangle$	$\langle N_{\pi^+} \rangle$	$\langle N_p \rangle$	$\langle N_d \rangle$	$\langle N_t \rangle$	$\langle N_{Z=2} \rangle$
^{12}C	2.04	1.85	3.21	0.70	0.05	0.05
^{108}Ag	6.52	5.35	9.39	2.10	0.15	0.14

two fireball

A_T	$\langle N_{\pi^-} \rangle$	$\langle N_{\pi^+} \rangle$	$\langle N_p \rangle$	$\langle N_d \rangle$	$\langle N_t \rangle$	$\langle N_{Z=2} \rangle$
^{12}C	1.75	1.59	3.24	0.78	0.05	0.05
^{108}Ag	6.14	5.01	9.41	2.20	0.16	0.16

Pion production from deltas is included. These resonances subsequently decay to nucleons and pions, accounting for about 45% of the total pion multiplicity. The production of composites (d,t,He) accounts for 20% of the produced hadrons and this agrees well with experimental data. This is one of the strengths the fireball model has over the firestreak model, since the latter does not account for the production of composites.

TABLE 4-3: Fireball Model and Experimental Results

ELEMENT	$\langle N_{\pi^-} \rangle$	$\langle N_{\pi^\pm} \rangle$	Exp. $\langle N_s \rangle_c$
H	0.50	0.95	
C	1.75	3.34	
N	1.94	3.70	
O	2.10	4.01	
Br	4.96	9.00	
Ag	6.14	11.15	
Em		6.73	3.70 ± 0.25
HCNO		2.73	1.68 ± 0.14
AgBr		10.14	5.80 ± 0.44

From table 4.2, we observe that the velocity of the emitting system is relatively constant for a one fireball system and equal to 0.75 c, while in the two fireball formulation, the target fireball has a velocity of 0.57 c and the projectile fireball a velocity of .87 c. The mean nuclear temperatures achieved in the interaction zone range from 90 to 110 MeV, a value lower by more than a factor of two than that obtained using the somewhat naive classical approximation of equation 3.17. Nonetheless, these temperatures are close to those required to form a quark-gluon plasma, and if the energy density could be increased, the proper conditions should be achieved in the near future (when heavier ions are available).

Nucleon spectra are often well reproduced by the fireball model, but pion spectra are not [30]. It can be seen in table 4.3 that our pion multiplicities in all cases are lower than those predicted by the two fireball model by a factor of two. (We have used the two fireball model calculation, since it is expected to be more accurate for the nucleon spectra, and yields lower multiplicities for the pions.) Our results are thus consistent with those of inclusive experiments [27], since the fireball model regularly overestimates the pion production. This dilemma has not yet been resolved [63], as there seems to be no logical scheme for incorporating a feature into the model which would make it

agree with the observed multiplicities. From a slight asymmetry in the angular distribution of the target related black tracks, we know [61] that the target is moving with a velocity of 0.015 c, a fact relatively insensitive to the atomic number or energy of the projectile. The resulting kinematic picture is a projectile spectator with a velocity equal to that of the beam, 0.94 c, decaying by evaporation, with a participant region consisting of two fireballs travelling at approximately 0.6 and 0.85 c, generating pions and nucleons, and a spectator target region also decaying by evaporation, with a mean temperature of 6-7 MeV and travelling at 0.015 c. The last region is solely responsible for the N_b spectra, and all that will be said about these black tracks is that they represent no new information in that the shape of the distribution and the average multiplicity obtained in this experiment is the same as in other emulsion experiments, whether one uses a hadron or a nucleus as a projectile. These tracks simply represent the fact that maximum target excitation for the spectator is achieved, and the target forgets the nature of the disturbance. Since no preferential emission direction has been observed for these tracks, the formation of a shock wave is unlikely. The two most forward regions in the interaction provide contributions to both the N_s and N_g spectra: pions

from the fireball, nucleons and composites from the fireball and protons and deuterons from the projectile spectator contribute to the N_s distribution, while nucleons and deuterons from the fireballs and some low energy pions form most of the N_gc distributions. The fireball model gives us the number of Z=1 nucleons for the various targets in emulsion, with an equivalent $N_{Z=1}$ of 7.34 for emulsion, 3.12 for the HCNO group and 10.94 for the AgBr group. A comparison of these numbers can be made to the total number of medium and ~~fast~~ velocity secondaries which are not pions. This number can be estimated for our experiment as the sum of the target associated protons, $\langle N_p \rangle_{Ar}$, and the corrected grey tracks, $\langle N_g \rangle_c$. We obtain 10.43 for emulsion in general, 4.77 for the HCNO group and 16.35 for the AgBr group. This result gives us the mean number of non participating Z=1 baryons by taking the difference between the two values, whereby we obtain 3.09, 1.65 and 5.41 projectile evaporated protons (and deuterons) for Em, HCNO and AgBr respectively. This appears to be in agreement with projectile fragmentation experiments, and we see that the projectile evaporates in the same fashion as the target.

4.4. General Trends of the Pion Production

There is some experimental evidence [27] that pions are

not produced throughout the entire interaction volume, as assumed in the fireball model, but that they are rather preferentially produced at the surface rather than in the core of the interaction volume. A parametrization which fits the data well is

$$\langle N_{\pi} \rangle = c\, P^{2/3} \tag{4.3}$$

where c is a constant and P is the average number of participant nucleons. P is obtained from Glauber theory [64] and is given by

$$P = \frac{A_T A_P^{2/3} + A_T A_P^{2/3}}{(A_P^{1/3} + A_T^{1/3})^2} \tag{4.4}$$

We can compare the number of pions produced to the average number of charges involved in the participant region. As reported in ref. [65], the ratio of the negative pion multiplicity $\langle m_{\pi^-} \rangle$ to the multiplicity of charged nuclear fragments $\langle m_Z \rangle$ depends only on the incident kinetic energy per nucleon, and not on the geometry of the collision, for equal mass nuclei. The ratio found is equal to 0.20 for $E_k \simeq$ 1.8 GeV. Similarly, our data can be compared and an equivalent ratio can be calculated. Our estimate of the pion

multiplicity $\langle N_s \rangle_c$ can be divided by 1.82 to give the negative pion multiplicity of 2.03, while the average number of charged nuclear fragments is obtained by summing the number of projectile protons $\langle N_p \rangle_{Ar}$ and the corrected number of grey tracks $\langle N_g \rangle_c$ which gives us a value of $\langle m_Z \rangle$ = 10.43. The ratio of the two quantities is 0.19, a value very close to that of the inclusive and streamer chamber experiments. It is also possible to evaluate this ratio for the light and heavy group of targets, and the ratios found using the data from tables 2.3 are equal to 0.19 and 0.35. While emulsion as a whole and the light group of targets behave as the data in [65], there is an increase in the pion production for heavy targets, indicating a collective behavior in the production of charged mesons.

We may also compare our multiplicity correlations in figures 2.13 to 2.15 with data from Ar + KCl collisions [66], which give a completely linear relationship between m and m_Z. Since our data also shows this type of relationship, we would suggest a P^1 dependence for the pion production. Additional confirmation of this is obtained if we plot the values obtained for P and $\langle N_s \rangle_c$ for emulsion as a whole and for the light and heavy groups. In order to obtain meaningful values for P, a weighted sum of the P calculated for each target nucleus in emulsion was performed, and this gave P = 8.53 for the light group, 20.58 for emulsion as a

whole and 30.38 for the AgBr group. The results are shown in figure 4.3

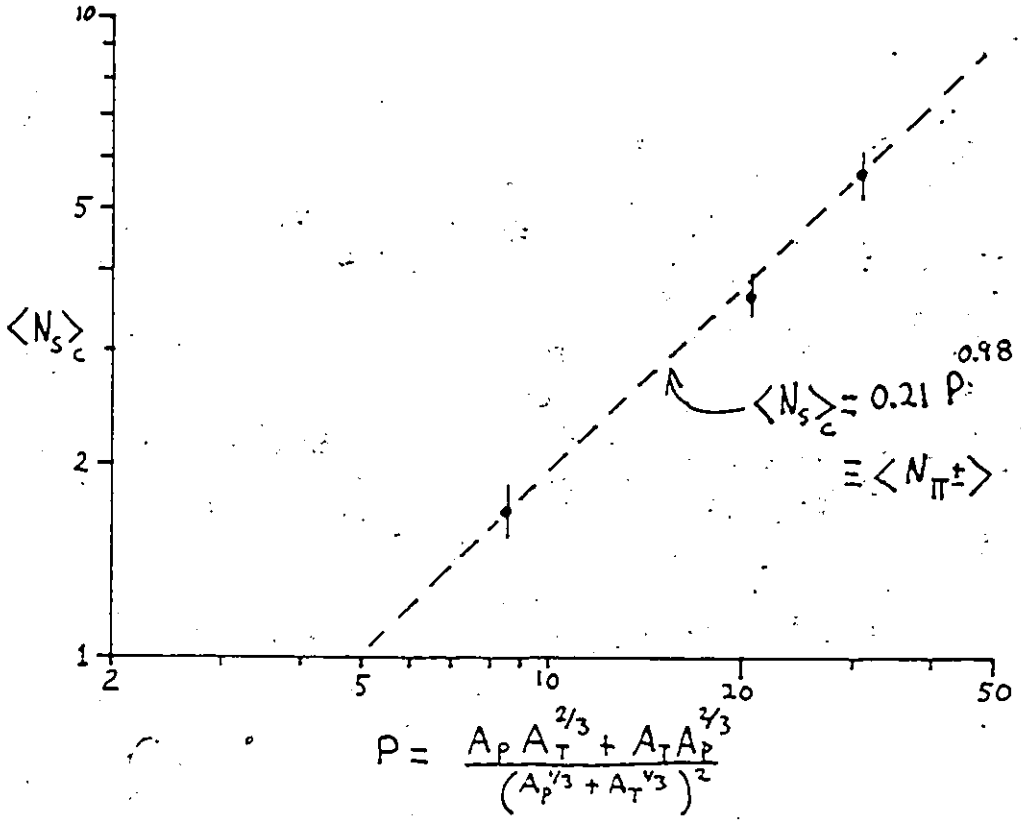

FIG. 4-3: Average Nucleon Number P vs $\langle N_s \rangle_c$

A very definite linear relationship is obtained, and is consistent with that observed in [66], but is inconsistent with equation 4.3 and data from ref [67], where equal mass ions are used. A possible explanation for this effect is that in emulsion, as in the most general projectile-target combinations, the asymmetry of A_T/A_P yields a larger piece of

cold spectator matter in an average collision, which remains to absorb pions. The larger the asymmetry, the greater the amount of pions which can be absorbed. Thus the pions may be produced by the surface of the participant region, as in equation 4.4, valid for equal A collisions, but in most general systems the pion absorption masks this effect. Certainly, any theoretical model should consider pion absorption, and this might be one of the reasons for the overestimate obtained in the statistical thermodynamic models such as the fireball and firestreak descriptions.

4.5. Angular Distributions

As presented in figures 2.19 to 2.22, the shower track angular distributions contain two components: the forward proton component and a broader pion component. We were able to obtain an approximate separation of these two components (as in figures 2.23 and 2.24) by comparing our data to an experiment for pion production only, from approximately equivalent targets. Pseudo-rapidity distributions for the heavy targets and for emulsion as a whole display peaks located below the mean value, and show preferential emission at the target rapidity. The distribution for the light target group shown in fig. 2.25 is more symmetric in shape, and

shows a rapidity characteristic of the projectile.

A quantum mechanical model was developed [68] by Lepore and Riddell, which uses sudden approximation with shell model wave functions to obtain the width of the projectile spectator proton and alpha particle distributions. A Gaussian distribution has been found from this model, and fits the projectile fragmentation data quite well. An expression for the angular distribution is

$$N(\theta) = Ce^{-\theta^2/2\sigma^2} \qquad (4.5)$$

Strict projectile fragmentation events provide the type of events from which to obtain the appropriate angular width for the emission of Z = 1 particles not participating in the interaction. Our closest approximation to this is in the light target angular distribution of figure 2.20. By using a two component fit, with one curve for the proton and one for the pion spectra we can fit our data. This results in a value of $\sigma = 10^{\circ}$ for the proton component, and a best value of 30° for the pion spectra. This fit is shown in fig 4.4. The fit is not very good for the pion spectra, since the wide angle tail is not well reproduced, and this would become worse when attempting to fit the angular distributions for the interactions with the heavy targets. Thus our angular spectra for the pions does not seem consistent with a Gaussian

distribution, due to the wide angle tail, and Poisson distributions for the pions seem more appropriate.

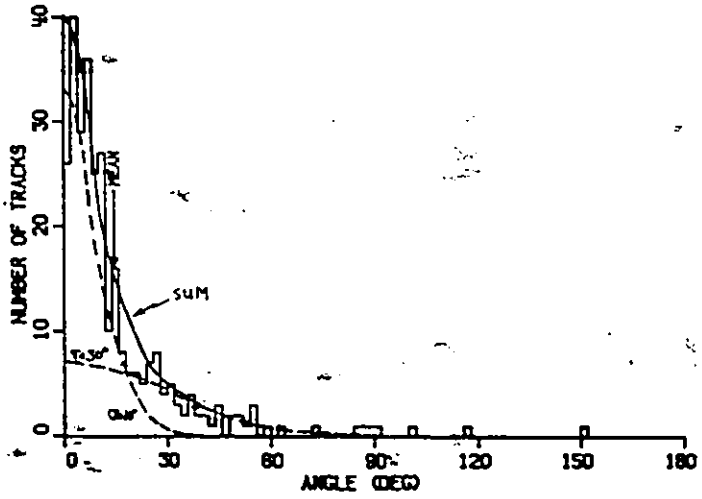

FIG. 4-4: Gaussian fits to the Light Target Angular Dist.

4.6. Effect of the Atomic Number of the Projectile

Other emulsion experiments have found the particle production for lighter beams [17,22], while data has been reported for ^{56}Fe in ref [69]. In table 4.3 we present a comparison of all these data, where it may be seen that our emulsion data for ^{40}Ar fits in with the others.

TABLE 4-4: Multiplicities for various Projectiles

Ion:	p	^{14}N	^{40}Ar	^{56}Fe
$\langle N_s \rangle$	0.95	8.85	9.20	14.07
$\langle N_{ch} \rangle$	7.82	19.69	22.55	27.19
$\langle N_b \rangle_c$	4.45	4.57	5.39	4.40
$\langle N_g \rangle_c$	2.42	5.29	4.93	9.10
$\langle N_h \rangle_c$	6.87	9.86	10.32	13.50

Although not all the data is directly comparable since different ionization cut-offs are used, the increase in total multiplicity (which is comparable for different exp. as long as all events are found) is rather smooth with increasing A of the projectile.

An expression for the average total multiplicity is given in [69] as

$$\langle N_{ch} \rangle = 2 \, (A_P A_T)^{0.357} \qquad (4.6)$$

where the results for ^{56}Fe on AgBr targets gives 39.9 and 42.6 for the values of $\langle N_{ch} \rangle$ from exp. and the above equation respectively. Similarly, for our exp., we have a value of $\langle N_{ch} \rangle$ = 34.86 for the AgBr group, and the equation gives

37.69, in remarkable agreement. Since the value of the black tracks does not go up, the main contribution to the increase in N_{ch} comes from the shower and grey tracks. The increase in these multiplicities thus appears to be a smoothly varying function of the projectile 's mass number.

4.7. Exotic Production

None of our events has provided a direct signature for the production of exotic nuclei. We do not see any evidence for copious pion production, and the spectra are rather smooth for both the grey and shower tracks. This indicates that the processes going on in the collisions are not giving rise to new matter states, or at least they are hidden in the general observed trends. As we mentioned earlier, many of the features of our interactions such as the high grey track multiplicity and extension of the multiplicity diagrams to values much larger than those observed in similar n-A interactions indicate that some form of collective behavior is occurring in a few of the events. Sub threshold pion production has been observed at E_k = 80 MeV/n, requiring that eight nucleons share their energy to produce a pion. While our experiment is at an energy well above the threshold for meson production, many of the events leading to catastrophic

destruction of both the projectile and target must be creating nuclear densities and/or temperatures approaching that for the production of exotic nuclei. In a careful analysis, we selected 10 of the events with the highest total charge multiplicities N_{ch}, in order that any peculiar phenomena might be observed. Two of these events possess a track with a subsequent decay occurring within a few 10 's of microns from the interaction center. Only one of these decays can be studied in some detail due to the loss of tracks at the surface of the emulsion. Francois Lamarche from our laboratory has performed a preliminary analysis of a two prong decay in event AR 2 45, and found evidence for the production of a kaon; this could represent a charmed decay, and might be a signal that in the most inelastic collisions, the conditions for the production of a quark-gluon plasma are being approached [51].

CONCLUSION

The important features that emerge from these studies on relativistic heavy ion collisions are: 1) Particle production in A-A interactions varies smoothly with the atomic number of the target and projectile. 2) while thermal equilibrium is reached in these collisions, the pion spectra have components which are not strictly thermal. 3) There are no obvious nuclear phase transitions occurring at a projectile energy of 72 GeV and total mass of projectile and target equal to 148. 4) Nuclear geometry plays a fundamental role in these events and is essential in explaining any of the several features of the reactions.

Considering the first conclusion, we can say that it does not matter whether a light or heavy projectile is used, there is no step or bump in the production cross sections of any particle in emulsion, for beams up to ^{56}Fe. Both the shape of the multiplicity distributions and the mean of these distributions can be directly related to the product of the atomic mass numbers of the nuclei involved, at any given energy. Rather simple criteria can be used to separate interactions with various targets in emulsion, as exemplified by the agreement of our data with that obtained for several other beams, and it is unlikely that much more complicated selection schemes would yield different results. While we

have not investigated the interactions of heavy ions at other energies, it is probable that as energy goes up when new machines come on line, the initial characteristics of the interactions will vary smoothly with energy, as they do with the mass number.

We have investigated the pion production in detail for the Argon interactions, and found that the mean multiplicity is a function of P^1, where P is the average number of nucleons involved in the collision, and not $P^{2/3}$, as has been observed [67] for some equal mass collisions at an equivalent energy. While the pions are only produced in the participant region, it would seem that the spectator region is important in terms of the pion absorption. We note here that the mean free path of nucleons in normal matter is 2 fm, while for pions it is only .5-1 fm, and this may contribute significantly to the absorption in the spectator region.

A dynamical model fits our pion data very well, while a thermal model does not. The dynamical model assumes some form of collective behavior for the nucleons by grouping them into contracted tubes of nucleons, but assumes only straight line trajectories, and predicts the observed spectra using only data from p-p collisions. Thermodynamic description on the other hand assumes randomization of the energy, and reproduces the trend for our baryon data, but is in difficulty when it comes to the pion spectra. This confirms

the observations of others, and the result is that the specific physics or dynamics in heavy ion collisions is confined to a factor of 2 modification of the overall spectra predicted by the statistical models.

In all the fits to our data, geometrical factors play a crucial role. The interaction cross sections cannot be factored nor can the production cross sections. The interacting system must be treated as a whole and cannot be separated into contributions from different parts. We found total charge multiplicities to be consistent with the form $C(A_T A_P)^x$, and pion multiplicities and interaction cross sections with the form $(A_T^y + A_P^y)^2$. It is also obvious that more sophisticated models are required to treat the data as a whole, and a good possibility lies in the detailed cascade calculations which include both the geometry, phase space and quantum mechanics or the reaction.

Until now, there has been no observation of the production of exotic nuclei, except for some signals present in very high energy cosmic ray events. The high multiplicity, central collisions studied in this experiment may also be a good place to look for a phase transition of nuclear matter. Events with no heavy fragments, wide angle shower tracks accompanied by high multiplicity warrant further investigation. Even if the phase transitions are metastable,

several signals for their formation are available, and they will likely be found in these types of catastrophic events. The search for strange particle production, some from decays of interaction products, is really only possible in a high resolution detector such as emulsion.

APPENDIX: SECONDARY INTERACTIONS

In addition to the measurement of the primary interactions caused by the relativistic argon beam, we have performed a study of the secondary interactions caused by the high charge fragments left over from the primary collisions. These data are presented as an appendix since our statistical basis is not solid enough to draw any real conclusions. We therefore present these data as a point of information.

The table 2.2 which listed the average multiplicities for our entire sample of events also lists the multiplicities obtained from a group of 53 secondary interactions. These interactions were found by along the track scanning of the fragments with charge $Z \geq 3$. Such fragments are the largest surviving part of the projectile spectator, and can be considered as the remnants of the collision. Motivation to find these events came from the fact that the interactions of these fragments seemed to occur quite frequently, often at distances very close to the interaction. (One striking example was a first and second generation event separated by only 5 um, with both events showing copious pion production.) Such an observation automatically leads one to assume that some very unusual phenomenon is occurring. In general, the data which has emerged from relativistic heavy ion collisions has been devoid of any spectacular new phenomena, and it is

just these phenomena one hopes to find, whether predicted by theory or not.

Several investigations were performed to look at the seemingly anomalously short mean free path, two examples of which may be found in references [70,71]. These emulsion experiments are very difficult, since to obtain a sufficient amount of statistics on the interaction mean free path of fragments of each possible charge, a great many primary events must be found and their fragments followed and identified. To obtain sufficient statistical accuracy requires that several thousand primary interactions be investigated. Failing this, the results from several different species of secondaries can be binned, with the hope that the result be equivalent to that which would be obtained from analysis of a very large number of events. The need for this large number of events can be seen with the following argument: assuming that each charge Z is equally probable for the secondary fragments from an argon collision (not true but a reasonable approximation for the purpose of the demonstration), then there are 16 possible values of $Z \geq 3$; to determine the mean free path of each charge to an accuracy of 5% requires the analysis of more than 6000 secondary interactions, which would arise from nearly 8000 primary events. The Jaipur-Jamma-Lund collaboration has performed an analysis of this magnitude in emulsion, and their results

show [25] no anomalous mean free path for the secondary fragments.

A method which had been used for grouping the results from several charges was to parametrize the mean free path using the following formula

$$\lambda(Z) = \lambda_0 Z^{-b} \qquad (A.1)$$

At Z = 1, this should give the value of the mean free path of singly charged particles in emulsion. Unfortunately, several researchers have found that different values of were required to fit their data, since not everyone defines an interaction in the same manner, and this leads to 10% variations even when 1500 events are grouped using A.1. The parameter b was also different in the various studies.

What has lead to such a controversy about the interaction mean free paths of the secondaries is that the parameter λ_0 seemed to vary with distance. When the data was separated according to distance from the primary vertex, the value of λ_0 was lower than the value at large distances (> 5 cm) by a factor of 25% . This anomalous mean free path could be explained by the addition of a 6% component with interaction cross sections of ten times the normal value, or a 20% component with a cross section of four times the normal value. A variation with distance also implied a lifetime of

10^{-10} s, and no decays via a charged channel was observed in our or any one else's data. In our opinion, there has been no satisfactory theoretical model capable of explaining and even less predicting such anomalous cross sections or lifetimes; a few examples from the many models proposed are toroidal or spinning longitudinal nuclei and pion-nucleon composites.

Our data for the mean free path of about 100 secondary interactions emanating from all our primary interactions gives the following results, when the data points are grouped two charges to a bin

Z of fragment	mean free path
3-4	34 ± 19
5-6	4 ± 3
7-8	21 ± 15
9-10	10 ± 7
11-12	8.6 ± 4
13-14	3.9 ± 1
15-16	6.1 ± 2
17-18	7.5 ± 3

Since we have data from such a limited number of events, the errors are extremely large, but we definitely see a trend for the mean free path to be lower in all cases than that which would be observed if one were scanning for primary

interactions. An explanation for this result comes from a statistical argument [72] which says that a bias is introduced by the use of equation A.1 when the parameter is evaluated at different distances from the primary interaction when the number of events is low (typically less than 1000). This evaluation using a Monte Carlo technique represents the trend of our data, especially when one considers the limited length of our emulsion plates which only allowed us to scan at short distances from the primary interactions.

While we certainly cannot draw any conclusions from our very limited data, (it was decided not to pursue this direction in our investigation, since we could not possibly hope to get good enough statistics) there have been some recent experiments which rule out the anomalous effect with a 95% confidence limit [73] to less than 1 cm from the primary interaction for at most a 2% anomalon component. We believe that if there is any effect, it must be contained within the first few mm from the primary interactions.

Returning to the data for the secondary events presented in table 2.2, we see that the black track multiplicity is the same as for the primary interactions at about 5.6, and the grey track multiplicity is also the same and equal to 4.5. The latter is somewhat surprising, since there are less nucleons available in the secondary interactions due to the reduced atomic number of the

projectile. As one would expect, this high grey track multiplicity is accompanied with a large pion production equal to 4.8, larger in fact than that observed in the entire sample of the primary interactions. We have no other explanation for this large pion multiplicity except that our sample of events selected for multiplicity counts was biased towards the more spectacular events, since the event selection was not completely random due to the order in which they were found. The lower multiplicity events were found later when the secondary fragments were followed more carefully to estimate the mean free path, but these events were only located and not measured.

BIBLIOGRAPHY

1. L. McLerran, 5th High Energy Heavy Ion Study, LBL-12652, 133 (1981)

2. W. Willis, 5th High Energy Heavy Ion Study, LBL-12652, 476 (1981)

3. A. Chodos *et al.*, Phys. Rev. D 9, 3471 (1974)

4. E. V. Shuryak, Physics Repts 61, 71 (1980)

5. T. D. Lee, Rev. of Mod. Phys. 47, 267 (1975)

6. A. B. Migdal, Physics Lett. 52B, 264 (1974)

7. J. D. Bowman, W. J. Swiatecki, C. F. Tsang, LBL-2908 (1978)

8. H. L. Bradt, B. Peters, Phys. Rev. 77, 54 (1950)

9. L. Lindstrom *et al*, LBL-3650 (1975)

10. G. D. Westfall *et al*, LBL-7162 (1978)

11. J. Babecki *et al*, Acta Phys. Pol. B9, 495 (1978)

12. J. Hebert *et al*, Phys. Lett. B48, 467 (1974)

13. H. Winzeler, Nucl. Phys. 69, 661 (1965)

14. H. Areti, PhD thesis, Univ. of Ottawa (1976)

15. I. Otterlund *et al*, Nucl. Phys. B142, 445 (1978)

16. E. Stenlund, I. Otterlund, CERN-EP 182-42 (1982)

17. M. Bogdanski, E. Jeannet, C. Metzner, Helv. Phys. Acta 42, 485 (1969)

18. S. Y. Fung *et al*, Phys. Rev. Lett. 40, 292 (1978)

19. J. J. Lu *et al*, Phys. Rev. Lett. 46, 898 (1981)

20. H. H. Heckman *et al*, Proc. 14th Int. Conf. Cosmic Rays, Munich, 2319 (1975)

21. B. Jackobsson, R. Kullberg, I. Otterlund, Zeit. f. Phys. A272, 159 (1975)

22. G. M. Chernov *et al*, Nucl. Phys. A280, 478 (1977)

23. B. Jackobsson *et al*, Lund Univ. Rep. LUIP 7708 (1977); also Lund Univ. Rep. CR-75-14 (1975)

24. K. B. Bhalla *et al*, LUND Univ. Rep. LUIP 7809 (1978)

25. S. Lokanathan, Jaipur-Jammu-Lund Collaboration, private communication (1983); K. B. Bhalla *et al*, Nucl. Phys. A367, 446 (1981)

26. S. Nagamiya, M. Gyulassy, LBL Report 14035 (1982)

27. S. Nagamiya, 5th High Energy Heavy Ion Study, LBL-12652, 141 (1981)

28. A. A. Amsden *et al*, Phys. Rev. Lett. 35, 905 (1975); Phys. Rev. C 17, 2080 (1980)

29. P. J. Seimens, J. D. Rasmussen, Phys. Rev. Lett. 42, 880 (1980)

30. S. Das Gupta, A. Z. Mekjian, Phys. Repts 72, 131 (1981)

31. J. Gosset *et al*, Phys. Rev. C 16, 629 (1977)

32. G. D. Westfall *et al*, Phys. Rev. Lett. 37, 1202 (1976)

33. N. Mobed, S. Das Gupta, B. K. Jennings, Phys. Rev. C 27, 1526 (1983)

34. W. D. Myers, Nucl. Phys. A296, 177 (1978)

35. A. A. Amsden *et al*, Phys. Rev. Lett. 38, 1055 (1977)

36. J. P. Bondorf *et al*, Phys. Lett. B65, 217 (1976)

37. F. Halzen, Contemporary Phys. 24, 591 (1983)

38. J. Hufner, J. Knoll, Nucl. Phys. A290, 460 (1977)

39. Y. Afek, G. Berlad, A. Dar, E. Eilam, Phys. Rev. Lett. 41, 849 (1978)

40. S. E. Koonin, Phys. Rev. Lett. 39, 680 (1977)

41. I. A. Schmidt, R. Blackenbecker, Phys. Rev. D 15, 3321 (1977)

42. R. L. Hatch, S. E. Koonin, Phys. Lett. B81, 1 (1979)

43. A. R. Bodmer, C. N. Panos, Phys. Rev. C 15, 1342 (1979); Nucl. Phys. A356, 517 (1981)

44. J. D. Stevenson, Phys. Rev. Lett. 41, 1702 (1978)

45. G. F. Bertsch, H. Kruse, S. Das Gupta, Phys. Rev. C 29, 673 (1984)

46. G. F. Chew, High Energy Physics Conf., Munich (1975)

47. T. D. Lee, G. C. Wick, Phys. Rev. D 9, 2291 (1974)

48. M. Jacob, H. Satz, (editors), Proc. of the Bielefeld Workshop (1982)

49. R. Anishetty, P. Koehler, L. McLerran, Phys. Rev. D 22, 2793 (1980)

50. H. Satz, 5th High Energy Heavy Ion Study, LBL-12652, 499 (1981)

51. J. Cleymans *et al*, Zeit. f. Phys. C 17, 341 (1983)

52. L. D. Landau, Izv. Akad. Nauk. SSSR 17, 51 (1953)

53. P. Carruthers, Ann. New York Acad. of Sc. 229, 91 (1974)

54. A. A. Amsden *et al*, Phys. Rev. C 17, 2080 (1978)

55. J. Hufner *et al*, Phys. Rev. C 12, 1888 (1975)

56. A. Abul-Magd *et al*, Phys. Lett. B60, 327 (1976); Zeit. f. Phys. A 277, 379 (1976)

57. L. D. Landau, l. Lifshitz, Statistical Physics

58. J. Gosset, J. Kapusta, G. D. Westfall, Phys. Rev. C 18, 844 (1978)

59. R. Glauber, Lectures in Theoretical Physics 1, 315 (1959)

60. P. Carruthers, 5th High Energy Heavy Ion Study, LBL-12652, 499 (1981)

61. H. H. Heckman *et al*, Phys. Rev. C 17, 1651 (1978)

62. Z. Koba, H. B. Nielson, P. Olsen, Nucl. Phys. B40, 317 (1972)

63. S. Das Gupta, private communication (1984)

64. S. Nagamiya, Nucl. Phys. A335, 517 (1980); R. J. Glauber, G. Matthiae, Nucl. Phys. B21, 135 (1970)

65. S. Nagamiya, M. Gyulassy, Adv. in Nucl. Phys. 13, 201 (1984)

66. A. Sandoval *et al*, Phys. Rev. Lett. 45, 874 (1980)

67. S. Nagamiya *et al*, Phys. Rev. C 24, 971 (1981)

68. J. V. Lepore, R. J. Riddell, LBL-3086 (1974)

69. A. Antonchik *et al*, Sov. J. Nucl. Phys. 32, 164 (1980); ibid 33, 558 (1981); ibid 35, 645 (1982)

70. E. M. Friedlander *et al*, Phys. Rev. C 27, 1489 (1983)

71. P. L. Jain, G. Das, Phys. Rev. Lett. 48, 305 (1982)

72. E. S. Pshenin, V. G. Voinov, Phys. Lett. B128, 133 (1983)

73. J. D. Stevenson, J. A. Musser, S. W. Barwick, Phys. Rev. Lett. 52, 515 (1984); T. J. Symons *et al*, Phys. Rev. Lett. 52, 982 (1984)